FINITE ELEMENT ANALYSIS OF EFFECT OF PRECIPITATE ASPECT RATIO ON THE ACCOMMODATION ENERGIES DURING SOLID STATE HYDROGEN TRANSFORMATION

A Thesis Submitted
in Partial Fulfillment of the Requirements
for the Degree of

MASTER OF TECHNOLOGY

by

R. K. SAJIKUMAR

to the

DEPARTMENT OF
MATERILAS AND METALLURGICAL ENGINEERING
INDIAN INSTITUTE OF TECHNOLOGY KANPUR

JULY , 1996

Dedicated to

My beloved Parents

CERTIFICATE

This is to certify that the work on "FINITE ELEMENT ANALYSIS OF EFFECT OF PRECIPITATE ASPECT RATIO ON THE ACCOMMODATION ENERGIES DURING SOLID STATE HYDROGEN TRANSFORMATIONS " *has been carried out by* Mr.R. K. Sajikumar *under my supervision and that it has not been submitted elsewhere for a degree.*

(R.BALASUBRAMANIAM)

ASSISTANT PROFESSOR

Department of Materials

and

Metallurgical Engineering

Indian Institute of Technology

Kanpur

July, 1996

ACKNOWLEDGEMENTS

I acknowledge with sincerity and deep sense o gratitude the expert guidance and continuous encouragemen provided by my thesis supervisor Dr. R. Balasubramaniam throughou the course of this thesis.

I wish to express my sincere appreciation of valuabl help and suggestions obtained from Dr. N. N. Kishore during thi work.

I cherish the affection showered on me by my dear frien Paddy. Cooperation and help received from Dr. M. N. Mungole an Mr. U. S. Dixit are thankfully acknowledged.

I am thankful to my brothers, Raghavan and Jayan fo their encouragement for higher studies.

I owe my fruitful stay in campus to all my classmate and Keralite friends.

At the end I am thankful to all those who helped m directly or indirectly during my stay at IIT Kanpur.

R. K. Sajikumar.

CONTENTS

ABSTRACT

The process of hydrogen transformations in metal-hydrogen systems has been simulated using the finite element method (FEM). The aim of the finite element evaluation was to calculate the accommodation energies as a function of progress of hydrogen transformations. The α-β transformation in the niobium-hydrogen system has been specifically addressed. The accommodation energies during the phase transformation has been evaluated by assuming both linear elastic and elasto-plastic behaviour of the system. In elasto-plastic analysis NbH is assumed to be elastic and Nb is assumed to be undergoing plastic deformation following the linear strain hardening law. In the finite system considered, the transformation progress from the centre of the system outwards and from the surface of the system inwards have been addressed. Accommodation energies have been evaluated for both $\alpha \rightarrow \beta$ (Nb$\rightarrow$NbH) and $\beta \rightarrow \alpha$ (NbH$\rightarrow$Nb) transformations using plane stress and axisymmetric formulations. The effect of changing the aspect ratio of a disk shaped and prolate spheroidal precipitate on the accommodation energy has been investigated. The results obtained in elastic analysis indicates that the total accommodation energy decreases with increasing aspect ratio, for all the transformation cases considered. Moreover, most of the energy is accommodated in the outer phase which surrounds the inner phase in the elastic analyses. The accommodation energies

obtained in the plane stress case are lower than that in the axisymmetric case because of the constraint against the free expansion is lower. The finite element elasto-plastic analysis of the hydrogen transformations revealed that plastic deformation of Nb results in lowering of the elastic energy of the system. The variation of this plastic energy for all the transformations has been discussed as a function of the aspect ratio.

LIST OF FIGURES

LIST OF TABLES

CHAPTER 1
INTRODUCTION

1.1 GENERAL INTRODUCTION

Hydrogen transformation refers to the class of transformations in which the new phase precipitates essentially due to the diffusion of only hydrogen [1]. Hydrogen transformation can be further classified in to two broad groups. In forward hydrogen transformation, the hydride precipitates from the metallic matrix. This is generally observed in metal-hydrogen systems at low temperatures where the metal atoms in the lattice are relatively immobile and hydrogen diffuses with ease in the metallic matrix. The subsequent ordering of these mobile hydrogen atoms on certain fixed subsets of interstitial sites in the parent matrix leads to the formation of hydride phase in the matrix. Reverse hydrogen transformation, i.e. involving hydride decomposition can be visualized to occur when hydrogen is removed from the hydride phase which leads either to the transformation of a hydride to a hydrogen free structure or to the transformation of hydride of higher hydrogen concentration to a hydride of lower hydrogen concentration.

In metal-hydrogen systems, the precipitation of a solid second phase from a solid matrix results in the creation of strain energy in the system [2]. This strain energy arises because the

transformation strains cannot be relaxed in the case of solid state phase transformations. Transformation strains are present in solid state transformations due to molar volume differences between the precipitating phase and the matrix. The transformation strain energy or accommodation energy controls several features of the transformation. The kinetics of transformation and precipitate morphological characteristics are governed by its magnitude [3]. The free energy changes of solid state transformations are affected by the strain energy contribution [3]. Repeated formation and decomposition of hydrides in metal-hydrogen energy storage systems result in hysteresis losses [4]. This hysteresis loss has to be minimized while developing commercial hydrogen storage materials, because it leads to a loss in useful available energy. Moreover, accommodation energies determine the embrittling effects of hydrogen in many commercially important nuclear materials [5].

There is a volume increase upon precipitation of hydride from a metallic matrix, which has been observed in the Nb-H [6],V-H [7], Zr-H [8] and Ti-H [9] systems. In metal-hydrogen systems, the molar volume of the hydride phase is generally 20 to 25% greater than that of the matrix from which it forms. Therefore, during hydride formation, the free expansion of the hydride is restricted by the presence of the surrounding matrix. This creates compressive normal stresses at the precipitate-matrix interface. In a reverse hydrogen transformation, tensile normal

stresses develop. The presence of these stresses during the forward and reverse hydrogen transformations creates strain energy in the system. For the purely elastic case, neglecting the strain energy due to hydrogen solution, which occurs before the beginning and after the end of hydrogen transformations, the system is stress-free at the beginning and end of the hydrogen transformation. The energy associated with the volume change upon transformation is stored as elastic energy in the matrix and the precipitate. If the metal or hydride phase yields during the transformation, the strain energies are relaxed to lower values due to irreversible plastic deformation [1].

The transformation strain energy has been previously related to elastic [10], plastic [11] and elasto-plastic [1] strain energy changes over the entire cycle of the hydrogen transformation. Most of the earlier strain energy calculations during solid state transformations have been performed assuming an infinite system size under isotropic continuum conditions. An infinite continuum is rarely encountered in practice. Moreover, isotropic conditions rarely prevail in the matrix or the precipitate. In the case of practical metal-hydrogen systems, the finite particle size leads to relaxation of energies due to the presence of free external surfaces. No satisfactory theory exists to model this effect; although, the effect of the surfaces has been conventionally treated using an extra 'image' stress field [3]. Recently, the finite element method has been used to model

the phase transformation in metal-hydrogen system, in which the effect of the free surface is also considered. In a pioneering work, Sen et al developed an elastic [12,13] and elasto-plastic [14] finite element model to calculate the accommodation energies during forward and reverse hydrogen transformations as a function of progress of transformation in the Nb-H system. The precipitate was considered as both a solid and hollow sphere. However hydrides in general tend to have ellipsoidal or plate-like shapes rather than spherical shape [15].

1.2 OBJECTIVE OF THE WORK

The main objective of the present work is to develop a finite element model for calculating the accommodation energies during solid state hydrogen transformation, where the shape of the precipitate is a general ellipsoid. The finite element method is selected for the calculation because it is a versatile method and it is possible to predict, with sufficient accuracy, the distribution of stress, strain etc. for a complicated problem. It is intended to prepare a displacement-based finite element program employing the initial strain method. It is proposed to carry out a comprehensive investigation of the effect of changing the aspect ratio on the accommodation energies of the precipitate and the matrix. Both elastic and elasto-plastic analysis are undertaken for the plane stress as well as axisymmetric cases. The hydride transformations Nb-NbH and Pd-PdH have been addressed in this thesis.

1.3 THESIS ORGANIZATION

Chapter 2 of this thesis contains the literature review. Theoretical solid-solid transformation models proposed by earlier workers have been discussed here. The concepts of the finite flement method (FEM), and the models developed using FEM have been discussed in detail in Chapter 3. The results obtained using the FEM models and their comparison with other mathematical models and experimental observations have been presented and discussed in chapter 4. The conclusions are drawn and the scope for further study are presented in Chapter 5. The Appendix A provides the results for the Pd-H system.

CHAPTER 2
LITERATURE REVIEW

2.1 SOLID STATE PHASE TRANSFORMATION

2.1.1 Introduction

The free energy change (ΔG°) of phase transformation is a balance between the reduction in the volume free energy of the transformation and the increase in surface free energy due to the precipitation of a new phase during the transformation. If the transformation takes place in a stress free condition, and the nucleation of a spherical precipitate is considered, the free energy change of the transformation is given by [16]

$$\Delta G^{\circ} = \frac{4}{3} \Pi a^3 \Delta G_v + 4 \Pi a^2 \Delta\sigma \qquad ..2.1$$

where, ΔG_v is the the volume free energy change associated with nucleation free energy change per unit volume, $\Delta\sigma$ is the free energy change per unit surface area created and a is the radius of the spherical precipitate nucleus. The variation of the two energy terms with the size of the precipitate (a) are shown schematically in Figure 1 [16]. The above expression holds good for phase transformations involving at least one non-rigid phase so that it takes place under unconstrained conditions. However, in phase transformations involving the precipitation of a solid phase in a

solid matrix, the transformation involves development of stresses within the system [3] because the specific molar volumes of the matrix and the precipitate (which forms from it) are normally different. The free energy expression then needs modification to account for the transformation stresses.

In solid state transformation, the strain energy term (W) has to be incorporated in the relation expressing free energy. The transformation free energy (ΔG°) is then expressed as [17]

$$\Delta G^{\circ} = \frac{4}{3}\Pi a^{3}\beta[\Delta G_{v}+W]+\Pi a^{2}\Delta\sigma[2+g(\beta)] \qquad ..2.2$$

where , W is the elastic strain energy per unit volume, β is the aspect ratio of the precipitate, $\Delta\sigma$ is the nucleus/matrix interfacial energy, and the function $g(\beta)$ is given by hyperbolic functions for $\beta<1$ or $\beta>1$. For $\beta=1$, $g(\beta)=2$. For the formation of the critical nucleus, the required conditions are

$$[\delta(\Delta G^{\circ})/\delta a]_{\beta} = 0 \qquad ..2.3$$

and

$$[\delta(\Delta G^{\circ})/\delta\beta]_{a} = 0 \qquad ..2.4$$

From equations 2, 3 and 4, the critical nucleus size (a^{*}) for stable nucleus formation is given as

$$a^{*} = -\frac{\sigma\ [2+g(\beta)]}{2\ \beta\ [\Delta G_{v}+W]} \qquad ..2.5$$

From equations 2.2 and 2.5, the activation energy for the formation of a stable embryo (ΔG^{*}) for a spherical nucleus is given by

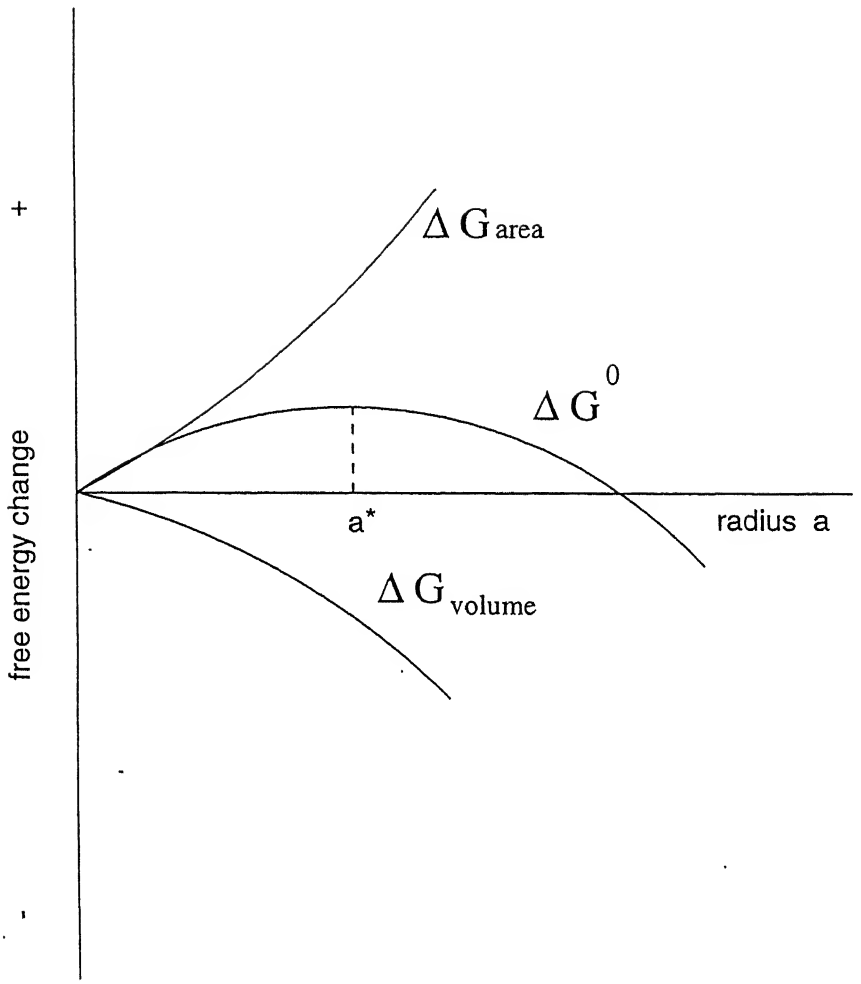

Figure 1. Variation of free energy of transformation as a function of nucleus radius without the strain energy contribution.

$$\Delta G^{*} = \frac{\Pi \sigma^{3} [2 + g(\beta)]^{3}}{12 \beta^{2} [\Delta G_{v} + W]^{2}} \quad ..2.6$$

or,

$$\Delta G^{*}/\Delta G_{h}^{*} = \frac{[2 + g(\beta)]^{3}}{[8 \beta (1 + W/\Delta G_{v}]^{2}} \quad ..2.7$$

where, ΔG_{h}^{*} is $(16 \Pi \sigma^{3}/3 \Delta G_{v}^{2})$, the free energy for the formation of a spherical nucleus in the absence of strain energy. The above equations have been formulated for homogeneous nucleation and have to be slightly modified to account for heterogeneous nucleation.

2.1.2 Continuum mechanics models

Many models have been earlier evolved to evaluate the stresses, strains and strain energies involved during solid state transformations. They are discussed briefly below.

2.1.2.1 Elastic models.

Most of the earlier models have assumed a purely elastic continuum. The first study of the elastic strain problem were conducted by Eshelby [2] whose work has since become a classic. The elastic strain energy induced by the coherent ellipsoidal inclusion in an elastic isotropic medium was calculated on the assumption that both the phases have the same elastic moduli. The general theory of strain energy was proposed by Khachaturyan [18], in which The exact equation for strain energy and the fourier transform of the elastic displacements in an arbitrary two-phase coherent matrix were derived. Sass, Mura and Cohen [19] expressed

the displacement field associated with a cuboidal precipitate in the form of a fourier series. Favier [20] proposed the exact solution for inclusions having the shape of rectangular parallelepiped. Sankaran and Laird [21] calculated the deformation field associated with a square inclusion. All these calculations have been carried out for elastic strain field in the limiting case of isotropic elasticity and homogeneous moduli. Lee and Johnson [22] evaluated the strain energy of a coherent cuboidal precipitate in an anisotropic matrix. In the following paragraphs, the Eshelby method as elucidated by Khachaturyan [3] would be presented.

The formation of a multi phase alloy has been considered and the following assumptions have been made:

1. The parent and transformed phase particles have the same elastic moduli (the homogeneous moduli approximation).

2. The average length dimension of the precipitate and the average distance between the nearest precipitates are small compared with the typical length dimensions of the crystal.

3. External boundaries of the multiphase mixture are stress free.

The stress-free strain tensors

$$\varepsilon^{\circ}_{ij}(1),\ \varepsilon^{\circ}_{ij}(2),\ldots,\ \varepsilon^{\circ}_{ij}(p),\ldots,\ \varepsilon^{\circ}_{ij}(\nu) \qquad ..2.8$$

describe the macroscopic shape deformation of the parent phase

caused by crystal lattice re-arrangements of the 1^{st}, 2^{nd}, ..., p^{th}, ..., ν^{th} kinds associated with the phase transformation in the stress-free state.

The transformation to the multiphase mixture from the parent matrix is modelled to involve six successive steps (Figure 2).

Step 1 : A small group of clusters is chosen in the parent phase crystal, and cut out of it. If the clusters are large enough to ignore the surface effects, the energy of the system remains unaffected in this step.

Step 2 : Each cluster is allowed to transform to a new phase corresponding to one of the crystal lattice re-arrangements under stress-free conditions. The clusters are thus transformed into a set of new phase precipitates. The associated expansion of clusters involves no strain energy change since clusters are stress-free. The expansion is described by strain tensors $\varepsilon^{\circ}_{ij}(p)$ ($p = 1, 2, ..., \nu$) associated with the macroscopic shape deformation in the stress-free state.

Step 3 : Surface traction is applied to each cluster to restore the shape it had before the transformation. The restoration of the shape of the p^{th} kind particle requires the homogeneous strain

$$\varepsilon_{ij} = -\varepsilon^{\circ}_{ij}(p) \qquad ..2.9$$

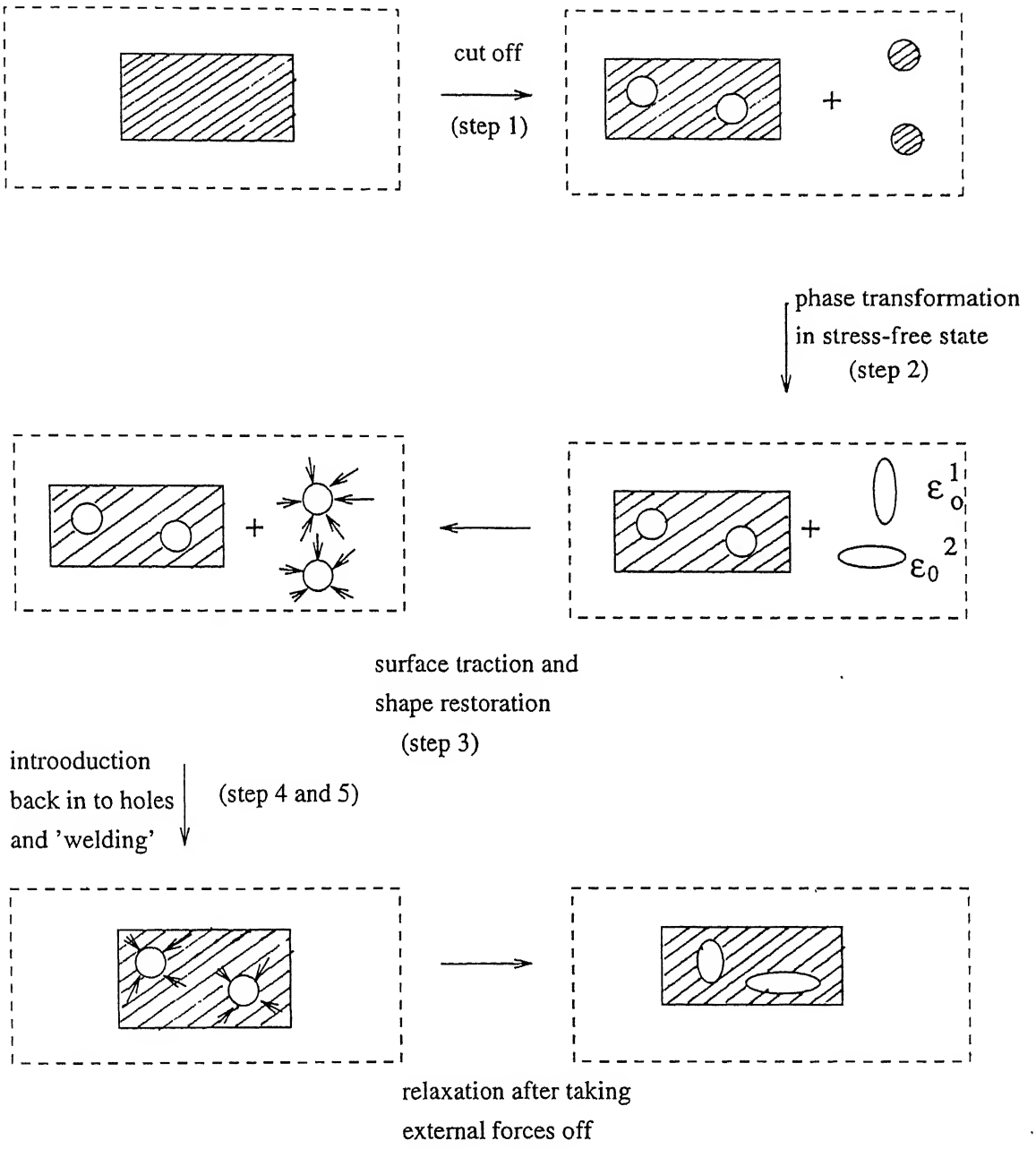

Figure 2. Successive steps to form coherent new phase inclusion [3].

According to Hooke's law the internal stress induced by surface traction is

$$\sigma_{ij} = \lambda_{ijkl}(-\varepsilon^{\circ}_{ij}(p)) \qquad ..2.10$$

where λ_{ijkl} is the elastic modulus tensor. Since the final homogeneous strain within a p^{th} kind particle is determined by equation 9, the mechanical energy changes by

$$\Delta E_{self}(p) = \frac{1}{2} v_p \lambda_{ijkl} \varepsilon^{\circ}_{ij}(p) \varepsilon^{\circ}_{kl}(p) \qquad ..2.11$$

where v_p is the volume of a particle of the p^{th} kind. The total energy change of all p^{th} kind particles is

$$N_p \Delta E_{self}(p) = \frac{1}{2} N_p v_p \lambda_{ijkl} \varepsilon^{\circ}_{ij}(p) \varepsilon^{\circ}_{kl}(p)$$

$$= \frac{1}{2} V_p \lambda_{ijkl} \varepsilon^{\circ}_{ij}(p) \varepsilon^{\circ}_{kl}(p) \qquad ..2.12$$

where N_p is the number of all p^{th} kind particles, $V_p = N_p v_p$ is the total volume of the p_{th} kind particle. Finally, the total energy change associated with the shape restoration of all particles is the sum of the energy changes given by equation 2.12, and is written as

$$\Delta E_3 = \frac{1}{2} \sum_p V_p \lambda_{ijkl} \varepsilon^{\circ}_{ij}(p) \varepsilon^{\circ}_{kl}(p) \qquad ..2.13$$

Step 4 : The particles (p= 1, 2,...,ν) are re-introduced back into their holes left in the parent crystal after their removal. Since after step 3 each particle just fits into the space

from which it was removed, the insertion does not give rise to any energy change:

$$\Delta E_4 = 0 \qquad ..2.14$$

Step 5 : The particles are now welded to the parent phase (matrix).

Step 6 : Finally, the particles relax by introducing the equilibrium elastic strain into the lattice. During relaxation, each particle will initiate crystal lattice displacements in its vicinity. The displacement is opposed by elastic resistance of the lattices. The associated relaxation energy per unit volume $f_{relax}(\mathbf{r})$ may therefore be presented as power series in the deformations $\varepsilon_{ij}(\mathbf{r})$. Truncation after the square term yields

$$f_{relax}(\mathbf{r}) = -\sigma^{\circ}_{ij}(\mathbf{r})\ \varepsilon_{ij} + \frac{1}{2}\ \lambda_{ijkl}\ \varepsilon_{ij}\ \varepsilon_{kl} \qquad ..2.15$$

where $\sigma^{\circ}_{ij}(\mathbf{r})$ and λ_{ijkl} are the first- and second-order expansion coefficients. The total relaxation energy is given as integral of equation 2.15 over the system volume V

$$\Delta E_{relax} = \int [-\sigma^{\circ}_{ij}(\mathbf{r})\ \varepsilon_{ij} + \frac{1}{2}\ \lambda_{ijkl}\ \varepsilon_{ij}\ \varepsilon_{kl}]\ dV \qquad ..2.16$$

Since the elastic relaxation is a spontaneous process,

$$\Delta E_{relax} \leq 0 \qquad ..2.17$$

Physically, the effect of relaxation is to remove a part of the elastic distortion energy introduced in step 3 when transformed clusters were deformed to fit properly into the parent phase body.

Summation of the contributions to strain energy from all steps gives the total elastic strain energy:

$$E_{elastic} = \Delta E_3 + \Delta E_{relax}$$
$$= \frac{1}{2} \sum_p V_p \lambda_{ijkl} \varepsilon^{\circ}_{ij}(p) \varepsilon^{\circ}_{kl}(p) +$$
$$\int [-\sigma^{\circ}_{ij}(\mathbf{r}) \varepsilon_{ij} + \frac{1}{2} \lambda_{ijkl} \varepsilon_{ij} \varepsilon_{kl}] \, dV \quad ..2.18$$

Linear terms in ε_{ij} appear in equations 2.15, 2.16 and 2.18 because a multi-connected heterogeneous medium is being considered. Unlike the usual case of homogeneous media, the systems under consideration are strained in the stress-free state. In other words, if $\sigma_{ij}(\mathbf{r}) \equiv 0$, we have $\varepsilon_{ij}(\mathbf{r}) \not\equiv 0$ (σ_{ij} is the stress tensor).

Let the strain tensor of a stress-free state ($\sigma_{ij}(\mathbf{r}) \equiv 0$) be $\varepsilon^{\circ}_{ij}(\mathbf{r})$. Using the notation of equation 8, we have

$$\varepsilon_{ij}(\mathbf{r}) = \begin{cases} \varepsilon^{\circ}_{ij}(1) & \text{if } \mathbf{r} \text{ is inside any first-type particle} \\ \varepsilon^{\circ}_{ij}(p) & \text{if } \mathbf{r} \text{ is inside any } p^{th} \text{ type particle} \\ \varepsilon^{\circ}_{ij}(\nu) & \text{if } \mathbf{r} \text{ is inside any } \nu^{th} \text{ type particle} \\ 0 & \text{otherwise} \end{cases} \quad ..2.19$$

The condition 2.19 may be written in the condensed form:

$$\varepsilon^{\circ}_{ij}(\mathbf{r}) = \sum_{p=1}^{\nu} \tilde{\theta}_p(\mathbf{r}) \varepsilon^{\circ}_{ij}(p) \quad ..2.20$$

where $\tilde{\theta}_p(\mathbf{r})$ is the shape function of particles of type p equal to

unity inside a particle and zero outside it. The shape function $\tilde{\theta}_p(\mathbf{r})$ is in general a multi connected function and may describe an arbitrary set of particles of the p^{th} type.

According to the usual relation of elasticity, the elastic stress is related to the elastic strain as

$$\sigma_{ij}(\mathbf{r}) = \frac{\delta E_{elastic}}{\delta \varepsilon_{ij}(\mathbf{r})} = -\sigma^{\circ}_{ij}(\mathbf{r}) + \lambda_{ijkl}\,\varepsilon_{kl} \qquad ..2.21$$

The strain, $\varepsilon^{\circ}_{ij}(\mathbf{r})$, corresponding to the stress-free state may be found from equation 2.21 by setting $\sigma_{ij}(\mathbf{r}) \equiv 0$

$$-\sigma^{\circ}_{ij}(\mathbf{r}) + \lambda_{ijkl}\,\varepsilon_{kl} = 0 \qquad ..2.22$$

Substituting equation 2.20 into equation 2.22 yields the definition of the function $\sigma^{\circ}_{ij}(\mathbf{r})$:

$$\sigma^{\circ}_{ij}(\mathbf{r}) = \sum_{p=1}^{\nu} \sigma^{\circ}_{ij}(p)\,\tilde{\theta}_p(\mathbf{r}) \qquad ..2.23$$

where

$$\sigma^{\circ}_{ij}(p) = \lambda_{ijkl}\,\varepsilon^{\circ}_{ij}(p) \qquad ..2.24$$

Substituting equation 23 into equation 16 gives

$$\Delta E_{relax} = \int_V \left[\sum_{p=1}^{\nu} \sigma^{\circ}_{ij}(p)\,\tilde{\theta}_p(\mathbf{r})\,\varepsilon_{ij} + \frac{1}{2}\,\lambda_{ijkl}\varepsilon_{ij}\,\varepsilon_{kl}\right] dV \qquad ..2.25$$

Solving these expressions, the elastic energy can be evaluated.

On the lines of the Eshelby model, expression for the elastic strain energy of coherent ellipsoidal precipitates in

anisotropic crystalline solids have been derived by Lee *et al.* [8]. The model has been used to evaluate strain energies of isotropic precipitates in an anisotropic matrix, and anisotropic precipitates in an isotropic matrix. One of the assumptions of the theory of Eshelby have been used, namely, when an ellipsoidal precipitate with a constant stress-free transformation strain ε^{o}_{ij} is embedded in an isotropic matrix, the constrained strain, ε^{c}_{ij} is also constant inside the precipitate. The suitability of the model to the anisotropic case has been illustrated in the literature, through examples. The expression for the elastic strain energy per unit volume of the precipitate in a homogeneous system, has been derived as

$$W = \frac{1}{2} \left(\varepsilon^{o}_{kl} - \varepsilon^{c}_{kl}\right) \lambda_{ijkl} \varepsilon^{o}_{ij} \qquad ..2.26$$

In the case of an inhomogeneous system, in which the elastic constants of the precipitate and the matrix are not the same, an 'equivalent' stress-free transformation strain ε^{o}_{kl} is first obtained by solving

$$\lambda^{*}_{ijkl} \left(\varepsilon^{o^{*}}_{kl} - \varepsilon^{c}_{kl}\right) = \lambda_{ijkl} \left(\varepsilon^{o}_{kl} - \varepsilon^{c}_{kl}\right) \qquad ..2.27$$

where λ^{*}_{ijkl} is the elastic constant of the precipitate and $\varepsilon^{o^{*}}_{kl}$ is the actual stress-free transformation strain of the precipitate. Hence, the strain energy per unit volume of such a precipitate is given by

$$W = \frac{1}{2} \left(\varepsilon^{o^{*}}_{kl} - \varepsilon^{c}_{kl}\right) \lambda^{*}_{ijkl} \varepsilon^{o^{*}}_{ij} \qquad ..2.28$$

The model has been validated with data for various inhomogeneous (different properties of matrix and precipitate), isotropic systems. The results have been reported in a normalized form W/W_o, where W_o is the elastic strain energy per unit volume of precipitate in the isotropic homogeneous case, given by

$$W_o = 2\ \mu\ \frac{1+\nu}{1-\nu}\ \varepsilon^2 \qquad ..2.29$$

where μ and ν are the shear modulus $(=C_{44})$ and Poisson's ratio $(=C_{12}/2(C_{12} + C_{44}))$ of the matrix phase. The model has been used to analyze the elastic strain energy variation for various combination of matrix and precipitate properties like shear strength ratios between the precipitate and the matrix, aspect ratio of the precipitate, and anisotropy of the precipitate and the matrix properties. The analysis indicates that in systems having high degree of anisotropy, markedly different results are obtained from those obtained from isotropic elasticity.

2.1.2.2 Elasto-plastic models

Recently, Lee *et al.* [23,24], have proposed models to represent solid-solid phase transformation, even though they still employed the basic Eshelby approach. The novelty of their models is that the concept of plastic deformation has been included in these models. This was lacking in all the earlier models. The models have been developed for three specific cases: the linear elastic case, for a matrix undergoing ideal plastic deformation, and for a strain hardening system with linear hardening and power

law hardening. These models are discussed below.

In the pure elastic case [23], a misfitting spherical precipitate, whose radius is $a(1+\varepsilon)$ in the absence of constraints, is introduced into a spherical hole of radius a in an infinite matrix with shear modulus μ and Poisson's ratio ν. The precipitate centre is taken at the centre of the system. The precipitate is assumed to change to $a(1+\beta\varepsilon)$ under the constraint of the matrix. Assuming spherical symmetry and the equilibrium equations of elasticity, the strain energy per unit volume of precipitate *(note that as per the convention of the model, the volume of the precipitate, that has been used to calculate the energy per unit volume of system, is equal to the volume of the matrix from which it forms)* is given by

$$E_{el} = \frac{6 \mu \alpha \gamma \varepsilon^2}{\alpha (\gamma - 1) + 1} \qquad ..2.30$$

where γ is the ratio of the bulk moduli of the precipitate and the matrix, μ is the shear modulus of the matrix, ε is the stress-free misfit strain and $\alpha = (1+\nu)/(3(1-\nu))$.

Plastically deforming systems have been modelled with the assumption that the precipitate is incapable of plastic deformation under the hydrostatic stresses acting on it [23]. The plastic deformation takes place in the surrounding matrix (Figure 3). In the model, a and r_p are taken to be the precipitate radius and the plastic zone radius, respectively. The Von mises yield criterion has been utilized. The total elasto-plastic strain

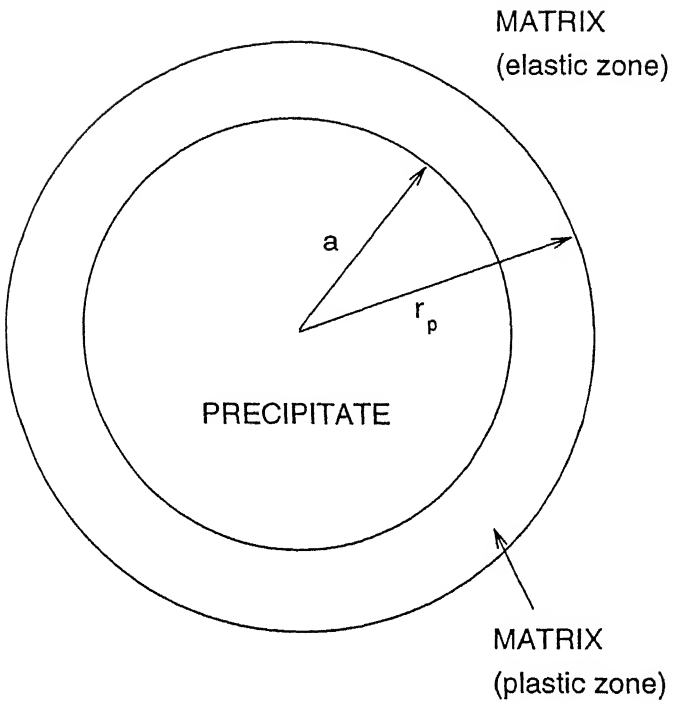

Figure.3 Schematic of plastic zone surrounding a misfitting spherical precipitate [23]

energy for a system exhibiting ideal plastic behavior is given by [23]

$$W = \frac{p^2}{2\gamma K}(1-\gamma) + \frac{\sigma_y}{\alpha\mu}\left\{\frac{1}{6} + \left(\frac{r_p}{a}\right)^3 \ln\left(\frac{r_p}{a}\right)\right\} \quad ..2.31$$

where p is the internal pressure arising from the misfit straining of the precipitate and σ_y is the yield stress of the matrix. The model is applicable for both positive and negative stress-free misfit strain (ε) values. These results indicate that the degree of plastic relaxation is strongly dependent on the precipitate size. The plastic relaxation is seen to increase with decrease in the relative stiffness of the precipitate and decrease with increase in the stress-free misfit strain. The plastic energy contribution of the elasto-plastic deformation is shown to increase with increase in the relative stiffness of the precipitate.

In the case of plastically deforming system following the linear strain hardening law, the total strain energy per unit volume of precipitate is given by [24]

$$W = \frac{\sigma_y^2}{6\alpha f\mu}\left\{1 + \left(\frac{r_p}{a}\right)^3\left[3\ln\left(\frac{r_p}{a}\right) - 1\right]\right\} - \frac{9}{2}K\gamma(\beta-1)\varepsilon^2 \quad ..2.32$$

where, m is the linear strain hardening parameter $(\delta\sigma/\delta\varepsilon_{plastic})$ and $\phi = m/(1-m)$, and $f = 1 + 2\phi(1-\nu)$. Other symbols have the same meanings as above.

In the case of systems exhibiting power law strain hardening, an iterative scheme has been presented to determine the stress and strain relations and hence the strain energy. The strain hardening law $\Delta\sigma = k E \varepsilon^{n}_{plastic}$ has been used, where n is the strain hardening exponent ($0 \leq n \leq 1$) and k is a material constant.

2.1.3 Finite Element models

Brian et al [15] applied the finite element method to evaluate the elastic and plastic strain energies developed in a system due the presence of an ellipsoidal precipitate. The pioneering work in the application of finite element method to the evaluation of stress and strain energies during solid state phase transformation is done by Sen et al [13,14]. They developed a model to calculate the elastic [13] and elasto-plastic [14] strain energies of the matrix and the precipitate as a function of progress of transformation, where the shape of the precipitate was spherical. Precipitation from both the centre outwards and from the surface inwards were considered by them.

2.2 STRAIN ENERGY AND HYSTERESIS IN METAL-HYDROGEN SYSTEMS

Phase transformations in metal-hydrogen systems are manifested by charging hydride forming metals like niobium (Nb), vanadium (V) with hydrogen, with accompanying formation of a hydride once the solubility limit of hydrogen in the metal is

exceeded. Reversal of the conditions result in dehydriding of the system. This process of hydriding and dehydriding shows a loss of efficiency in the form of hysteresis [15].

There three common modes of hysteresis in the metal-hydrogen systems [25]. They are:

(i) Pressure hysteresis : Here the pressure needed for hydride formation, P_f, is greater than that of hydride decomposition, P_d.

(ii) Solvus hysteresis : The terminal solid solubility of hydrogen in the host alloy is greater for hydride formation than for hydride decomposition.

(iii) Thermal hysteresis : At a given solvus composition, the hydride-formation temperature is lower than the hydride-decomposition temperature.

Extensive review of the subject has been done by Balasubramaniam [1] and is presented here.

The origin of hysteresis in metal - hydrogen systems has been the topic of many studies starting as early as 1925 when Lambert and Gates [26] observed the phenomenon in the Pd-H system. Since then, several theories have been proposed to explain hysteresis in metal-hydrogen systems. Theses theories have been critically reviewed by Qian and Northwood [25] and the salient features of these theories would be explained here, briefly. Most of the theories emphasize the contribution of transformation strain as the possible origin of hysteresis. Ubbelhode [22]

proposed an additional strain factor in the phase rule to account for hysteresis. Scholtus and Hall [28] argued that the volume change on hydride formation would lead to a constraining stress on the matrix and they evaluated this stress to be approximately equal the yield stress of the matrix from which the hydride precipitates. Kuijpers and van Mal [29] proposed an explanation similar to that of Scholtus and Hall. The notion that plastic accommodation during hydride formation could be the possible source of hysteresis was proposed by Birnbaum *et al* [30] and extended by Flanagan and co-workers [31]. They proposed that the energy lost during the hysteresis cycle was accommodated by irreversible plastic deformation of the parent phase. Flanagan *et al.* have assumed that the plastic accommodation energy in the parent phase during hydride formation and that in the hydride phase during the hydride decomposition were the same. This is not a valid assumption because the elastic properties (and hence the dislocation formation energies) are significantly different for the metallic and hydride phases. Moreover, Birnbaum *et al.* also assumed that the elastic, chemical and surface accommodation energies were the same for hydride formation and decomposition and hence considered these energies to be reversible. While this may be true for chemical energy, it is not necessarily true correct for surface and elastic energies. Therefore, several simplifying arguments have been used by these workers while attributing the hysteresis effect to irreversible plastic

deformation. The other theories that were proposed to explain hysteresis are based upon saturation properties, chemical properties of the phases, crystallite size, metastable hydride formation, atomistic strain effect, elastic strain effects, and energy dissipation effects during hydrogen transformation.

CHAPTER 3
FINITE ELEMENT MODEL

3.1 INTRODUCTION

The finite element method is a versatile tool for analyzing complicated engineering problems. In recent years it has been applied to the field of phase transformation in materials [11-15]. Using finite element method stress, strain and elastic and plastic accommodation energies developed during phase transformation can be predicted more accurately.

This chapter briefly outlines the theory of Finite Element displacement formulation as applied to solution of problem of statics and the modeling of solid state phase transformation using finite element method. The two dimensional Finite Element displacement formulation of an elastic continuum is explained. Method of solution of plasticity problem using elasto-plastic analysis is stated in short. At the end Finite Element formulation of solid state phase transformation is explained.

3.2 FINITE ELEMENT METHOD

The analysis of an engineering system requires the idealization of the system into a form that can be analyzed, the formulation of governing equilibrium equations of this idealized

system, the solution of the equilibrium equations and the interpretation of the result. In many situations an adequate engineering model of the system is obtained by replacing the system by a finite number of well defined components. In contrast to this are the continuous systems, in which formulation leads to differential equations or equivalent statements, which imply an infinite number of elements. The exact solution of differential equations satisfying all boundary conditions is only possible for relatively simple systems, and numerical procedures must in general be employed to predict system response. In essence these procedures reduces the continuous system to a discrete idealization that can be analyzed in the same manner as discrete physical system. FEM is the most versatile numerical procedure for the approximation of continuum problem.

The Finite Element Method [32]essentially involves, dividing the domain into discrete or finite number of elements. The governing equations are reduced into simpler but approximate forms by discretisation. The resulting equations are replaced by suitable matrices to carry out the solution procedure.

3.2.1 discretisation procedure

The solution of stress and strain distribution in elastic continuum is the major field of application of Finite Element Method. In the Finite Element approximation the continuum is separated by imaginary lines or surfaces into a number of 'finite elements'. The elements are assumed to be interconnected

at discrete number of nodal points situated on their boundaries. The displacement of these nodal points will be the basic unknown parameters of the problem. A set of functions is chosen to define uniquely the state of displacement within each 'finite element' in terms of its nodal displacements.The displacement functions define uniquely the state of strain within an element in terms of nodal displacements. These strains together with any initial strain and the constitutive properties of the material will define the state of stress throughout the element.

For an elastic continuum, the governing differential equations can be obtained by minimizing the total potential energy of the system. The total potential energy , π, can be expressed as [33]

$$\pi = \frac{1}{2} \int_V [\sigma]^T [\varepsilon] \, dv - \int_V [U]^T [P] \, dv - \int_S [U]^T [q] \, ds \qquad ..3.1$$

Where

σ -stress vector .

ε -strain vector.

U -displacement at any point.

p -body forces per unit volume.

q -applied surface tractions.

Integrations are taken over the volume V of the system and loaded surface area S.

The displacement U at any point inside an element is described as a function of nodal values

$$U = [N][U^e] \qquad ..3.2$$

Where [N] is a set of interpolation function termed as shape functions and $[U^e]$ is the vector of nodal displacement.

The strain within the element is expressed in terms of nodal displacement as

$$[\varepsilon] = [B]\ [U^e] \qquad ..3.3$$

where [B] is the strain-displacement matrix, generally composed of derivatives of the shape functions. Stress is related to strains by use of an elastic matrix (property matrix) [D], as

$$[\sigma] = [D]\ [\varepsilon] \qquad ..3.4$$

When the shape function is such that no singularity exist in integrands of functional, the total potential energy of continuum will be the sum of the energy contributions of the individual elements.

$$\pi = \sum_e \pi_e \qquad ..3.5$$

where π_e is the total potential energy of element e.

Using eq(3.1)

$$\pi_e = \frac{1}{2} \int_V [U^e]^T [B]^T [D] [B] [U^e] \, dv - \int_V [U^e]^T [N]^T [p] \, dv - \int_S [U^e]^T [N]^T [q] \, dS \quad ..3.6$$

where V_e is the element volume and S_e is the load surface area.

Performance of the minimization of potential energy for element **e** with respect to nodal displacement U^e results in

$$\frac{\partial \pi}{\partial U^e} = [K^e] [U^e] - [F^e] \quad ..3.7$$

where $[F^e]$ is the equivalent nodal forces for the element,

$$[F^e] = \int_v [N]^T [p] \, dv + \int_v [N]^T [q] \, dS \quad ..3.8$$

and [K] is the element stiffness matrix,

$$[K^e] = \int_v [B]^T [D] [B] \, dv \quad ..3.9$$

The summation of the above terms in eq(3.7) over all the elements, when equated to zero results in a system of equilibrium equations for the complete continuum. These equations are then solved by any of standard technique to yield the nodal displacement.

For an n noded element the shape functions is

$$\{N\} = \{ N_1, N_2, \ldots\ldots\ldots N_n \} \quad ..3.10$$

The strain displacement relationships for an element in plane stress formulation are given by

$$\varepsilon_x = \frac{\partial u}{\partial x} \quad ; \quad \varepsilon_y = \frac{\partial v}{\partial y} \quad ; \quad \gamma_{xy} = \frac{\partial u}{\partial y} + \frac{\partial v}{\partial x} \qquad ..3.11$$

which when expressed in matrix form gives equation 3.3, where strain displacement matrix is

$$[B] = \begin{bmatrix} N_{1,x} & 0 & N_{2,x} & 0 & .... & N_{n,x} & 0 \\ 0 & N_{1,y} & 0 & N_{2,y} & .... & 0 & N_{n,y} \\ N_{1,y} & N_{1,x} & N_{2,y} & N_{2,x} & .... & N_{n,y} & N_{n,x} \end{bmatrix} \qquad ..3.12$$

where u_i, v_i are the displacements in the global coordinates of the i^{th} node of the element and

$$N_{1,x} = \frac{\partial N1}{\partial x} \quad ; \quad N_{1,y} = \frac{\partial N1}{\partial y} \quad ..... \qquad ..3.13$$

In the axisymmetric formulation, the strain matrix is

$$\{\varepsilon\}^e = \begin{Bmatrix} \varepsilon_r \\ \varepsilon_z \\ \varepsilon_\theta \\ \gamma_{rz} \end{Bmatrix} \qquad ..3.14$$

where $\varepsilon_r = (\delta u/\delta r), \varepsilon_z = (\delta v/\delta z), \varepsilon_\theta = (u/r)$ and $\gamma_{rz} = [(\delta u/\delta z) + (\delta v/\delta r)]$, with u and v the displacements in the polar coordinates and r the positional vector of the volume element of cross sectional area dA.

The strain displacement matrix in axisymmetric formulation is

$$[B] = \begin{bmatrix} N_{1,r} & 0 & N_{2,r} & 0 & \cdots\cdots & N_{n,r} & 0 \\ 0 & N_{1,z} & 0 & N_{2,z} & \cdots\cdots & 0 & N_{n,z} \\ N_1/r & 0 & N_2/r & 0 & \cdots\cdots & N_n/r & 0 \\ N_{1,z} & N_{1,r} & N_{2,z} & N_{2,r} & \cdots\cdots & N_{n,z} & N_{n,r} \end{bmatrix} \quad ..3.15$$

The property matrix for the plane stress formulation is

$$[D] = \frac{E}{(1-\nu^2)} \begin{bmatrix} 1 & \nu & 0 \\ \nu & 1 & 0 \\ 0 & 0 & (1-\nu)/2 \end{bmatrix} \quad ..3.16$$

In the case of axisymmetric formulation, the property matrix is

$$[D] = \frac{E(1-\nu)}{(1+\nu)(1-2\nu)} \begin{bmatrix} 1 & (\nu/(1-\nu)) & (\nu/(1-\nu)) & 0 \\ (\nu/(1-\nu)) & 1 & (\nu/(1-\nu)) & 0 \\ (\nu/(1-\nu)) & (\nu/(1-\nu)) & 1 & 0 \\ 0 & 0 & 0 & (1-2\nu)/(2(1-\nu)) \end{bmatrix}$$

..3.17

where, E is the Young's Modulus and ν is the Poisson's ratio of the element material.

3.2.2 plasticity formulation

The difference in elastic and plastic behavior under uniaxial stress is closely brought out in Figure 4. In linear and nonlinear elastic behavior stress can be expressed as a function of strain. The main difference of plasticity formulation from nonlinear elastic formulation is that a unique stress-strain relationship is not available. Plastic deformation is essentially irreversible on unloading and incompressible in nature.

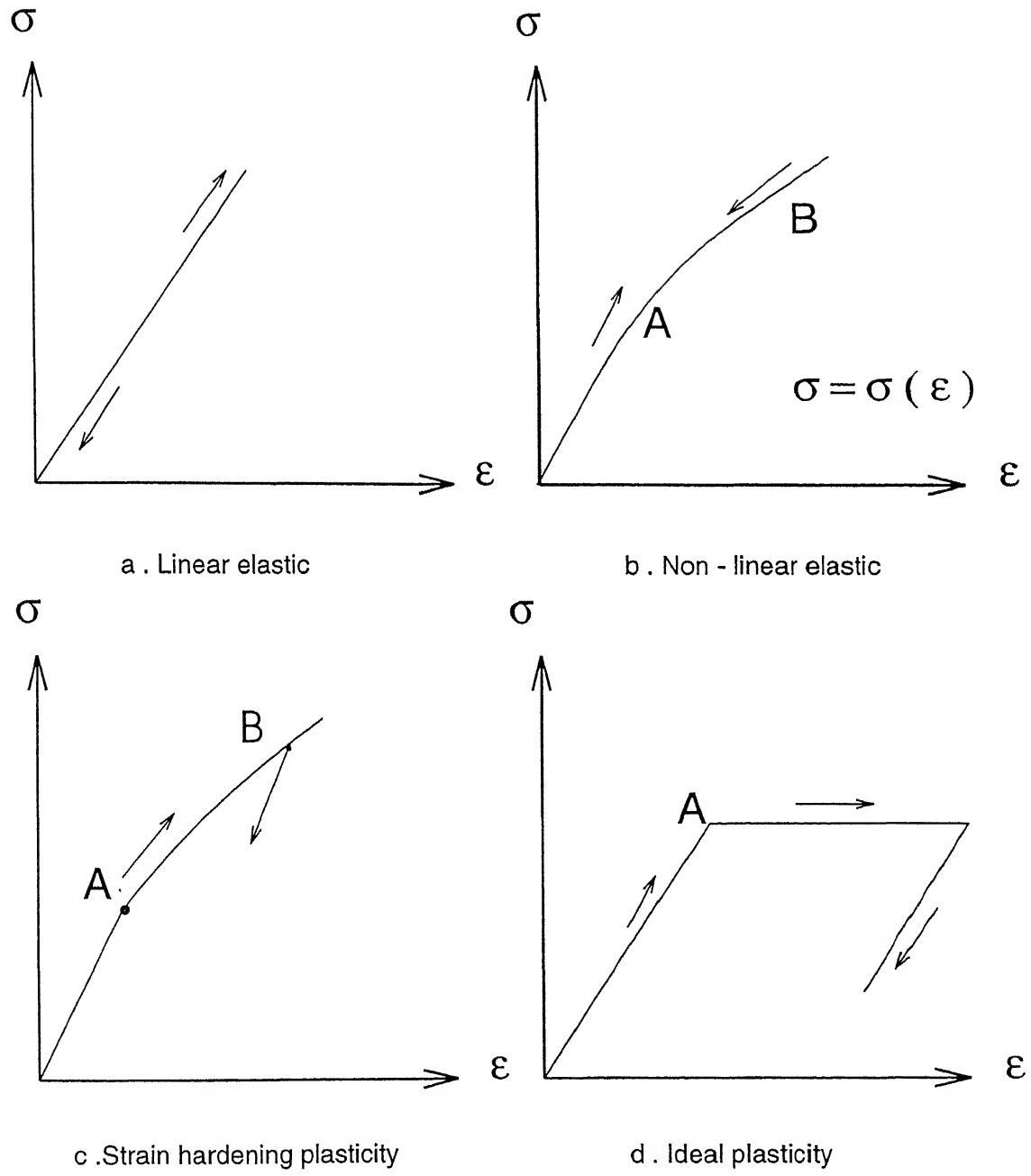

Figure 4. Idealized elastic and plastic behaviour of a material under uniaxial stress. The up and down arrows indicate loading and unloading behaviours, respectively.

The theory for plasticity formulation has been dealt with extensively by Owen and Hinton [33]. The theory has been presented below.

In order to formulate a theory which models elasto-plastic material deformation, three requirements have to be met:

1. An explicit relationship between stress and strain must be formulated to describe material behavior under elastic conditions, i.e. before the onset of plastic yielding.

2. A yield criterion indicating the stress level at which plastic flow commences must be postulated.

3. A relationship between stress and strain must be developed for post-yield behavior, i.e. when the deformation is made up of both elastic and plastic components.

Before the onset of plastic yielding the relationship between stress and strain is given by the standard linear elastic expression:

$$\sigma_{ij} = \lambda_{ijkl}\, \varepsilon_{kl} \qquad ..3.18$$

where σ_{ij} and ε_{kl} are the stress and strain components respectively and λ_{ijkl} is the tensor of elastic constants which for an isotropic material has the explicit form

$$\lambda_{ijkl} = \lambda\, \delta_{ij}\, \delta_{kl} + \mu\, \delta_{ik}\, \delta_{jl} + \mu\, \delta_{il}\, \delta_{jk} \qquad ..3.19$$

where λ and μ are Lamé constants and δ_{ij} is the Kronecker delta defined by

$$\delta_{ij} = \begin{cases} 1 & \text{if } i = j \\ 0 & \text{if } i \neq j \end{cases} \qquad ..3.20$$

The Von Mises yield criterion which has been used in the modeling, can be stated as, yielding occurs when J_2', the second deviatoric stress invariant reaches a critical value,

$$J_2 = k(k) \qquad ..3.21$$

where k is a material parameter.

J_2' can be defined as

$$J_2' = \frac{1}{2}[\sigma_x'^2 + \sigma_y'^2 + \sigma_z'^2] + \tau^2_{xy} + \tau^2_{yz} + \tau^2_{xz} \qquad ..3.22$$

where σ_x', σ_y' and σ_z' are the principal deviatoric stresses in the x, y and z directions respectively in the cartesian coordinates, while τ_{xy}, τ_{yz} and τ_{xz} are the shear components.

The yield criteria may be expressed as

$$\bar{\sigma} = \sqrt{3}\, k \qquad ..3.23$$

where $\bar{\sigma}$ is the effective stress, given by

$$\bar{\sigma} = \sqrt{3}\, (J_2')^{1/2} \qquad ..3.24$$

If a material deforms plastically, in general, the deformation would be composed of an elastic component and a plastic component. If the deformation load is applied incrementally and $(d\varepsilon_{ij})_p$ represents the plastic component of the

strain increment in the n^{th} increment, then the increment in effective plastic strain is given by

$$d\bar{\varepsilon}_p = \sqrt{(2/3)}\,\{(d\varepsilon_{ij})_p\ (d\varepsilon_{ij})_p\}^{1/2} \qquad ..3.25$$

where the effective plastic strain increment is related to the effective stress by the relationship for uniaxial tension

$$\bar{\sigma}_n = \bar{\sigma}_{n-1} + H'\ d\bar{\varepsilon}_p \qquad ..3.26$$

where H' denotes the strain hardening parameter (slope of the plastic portion of the stress-strain curve at the level of the effective stress at the $n\text{-}1^{th}$ load increment).

After initial yielding, the material behavior will be partly elastic and partly plastic. During any increment of stress, the changes of strain can be divided into elastic and plastic components, so that

$$d\varepsilon_{ij} = (d\varepsilon_{ij})_e + (d\varepsilon_{ij})_p \qquad ..3.27$$

The elastic strain increment is related to the stress increment by

$$(d\varepsilon_{ij})_e = \frac{d\sigma'_{ij}}{2\mu} + \frac{(1-2\nu)}{E}\,\delta_{ij}\,d\sigma_{kk} \qquad ..3.29$$

where E and ν are the elastic modulus and Poisson's ratio of the material, respectively, while $d\sigma'_{ij}$ and $d\sigma_{kk}$ are the deviatoric and the hydrostatic stress components respectively.

The plastic component of the strain is formulated as follows. Taking f as the yield function,

$$(d\varepsilon_{ij})_p = d\lambda\ \frac{\delta f}{\delta \sigma_{ij}} \qquad ..3.30$$

termed as the flow rule or normality condition since $\delta f/\delta\sigma_{ij}$ is a vector directed normal to the yield surface at the stress point under consideration. $d\lambda$ is the plastic multiplier (a proportionality constant). Combining equations 3.28, 3.29 and 3.30, we get

$$(d\varepsilon_{ij}) = \frac{d\sigma'_{ij}}{2\mu} + \frac{(1-2\nu)}{E}\delta_{ij}\, d\sigma_{kk} + d\lambda \frac{\delta f}{\delta\sigma_{ij}} \quad ..3.31$$

3.3 MODEL FOR TRANSFORMATION THROUGH PREDESTINED PATH

In this section, modeling of the solid state transformation using finite element method is explained. The plane stress case has been taken to explain the principles. In the plane stress case, the non-zero stress and strain components are the two principal x and y components and one xy shear component on the x-y plane.

3.3.1 Linear elastic analysis

Stresses develop in the system during transformations due to the forces at matrix-precipitate interface. As the precipitate tries to occupy a space that is smaller (or larger) than the matrix from which it forms, the surrounding matrix (i.e. the untransformed region) resists this. Consider a metal-hydrogen system of finite size which is stress free at the external surfaces.

Assume that a region of matrix (radius r) is cut out and allowed to transform freely to the hydride (Figure 5). This free expansion leads to straining of the hydride. The developed strain is assumed to be constant in all directions and in the finite element analysis treated as a misfit or initial strain (ε_o). In the present case of the Nb→NbH transformation, the value of the misfit strain can be determined from the relation

$$\varepsilon_o = \frac{1}{3}\left[\frac{\bar{V}_{ppt} - \bar{V}_{matrix}}{\bar{V}_{matrix}}\right] \qquad ..3.32$$

where $\bar{V}_{ppt}$ is the molar volume of the precipitate and $\bar{V}_{matrix}$ is the molar volume of the matrix. The size of the precipitate would, in that case, increases in proportion to ε_o. The resulting size of the precipitate would hence be equal to $[r(1+\varepsilon_o)]$. If this transformed phase (of a larger size) is to be put back into the initial empty space of radius r in the matrix, a force proportional to ε_o would have to be applied to the precipitate. When the transformed phase is inserted back into the space from where it had been originally removed, the precipitates would apply a force on the surrounding matrix creating a strain field. The matrix and the precipitate tend to restrict their own elastic deformations, since both the matrix and the precipitate have non-zero elastic modulii. Therefore, at equilibrium, the precipitate would attain a size between r and $[r(1+\varepsilon_o)]$. The

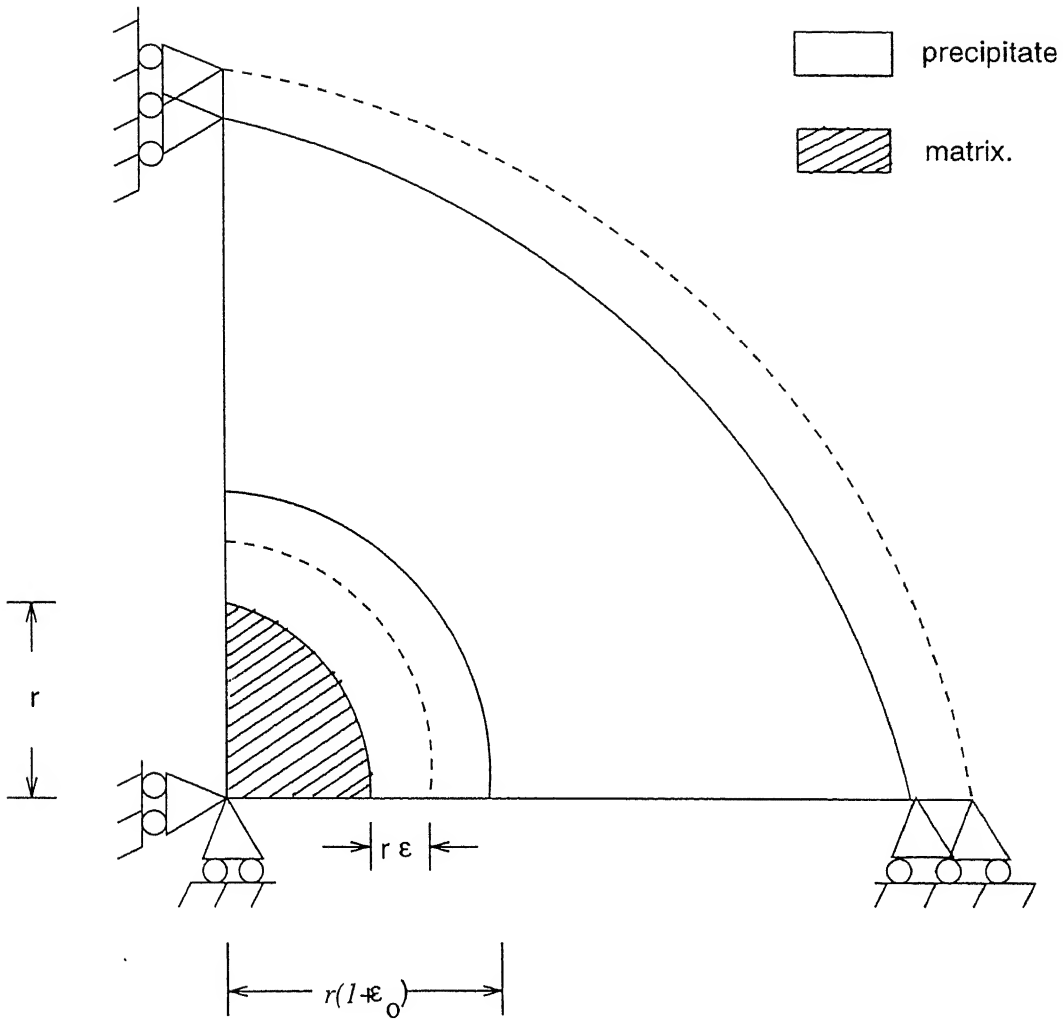

Figure 5. Definition of strain parameters used in the initial strain approach during forward hydrogen transformation for centre to surface path.

equilibrium position of the boundaries of each phase is indicated by dashed lines in Figure 5. It is interesting to note that the initial strain approach resembles the classic Eshelby approach [2,3] in determining the elastic strain energies of a misfitting precipitate. The forces due to the misfit strain act internally at the precipitate-matrix interface. Their nature are opposite during the forward and reverse transformations, due to the reverse nature of the misfit strains. Figure 6 shows the nature of the misfit-strain forces at the precipitate-matrix interface during forward and reverse hydrogen transformations. The system is divided into small elements for the purpose of finite element analysis. The equivalent mechanical force of each element, $\{F_o\}$, required to create ε_o is given by[32]

$$\left\{ F_o \right\} = \int \left[B \right]^T \left[D \right] \left\{ \varepsilon_o \right\} \, dV \qquad ..3.33$$

where [B] is the strain-displacement matrix, [D] the material property matrix, $\{\varepsilon_o\}$ the initial-strain vector and V the volume of the element. The superscript, T, refers to the transpose. The integration is performed over each element and the resulting force matrices are assembled to obtain the global load vector for the entire system. The strain-displacement matrix relates the nodal displacement vector {U} of each element to its total strain vector $\{\varepsilon\}$. The total strain vector for each element, $\{\varepsilon\}$, is obtained from the relation

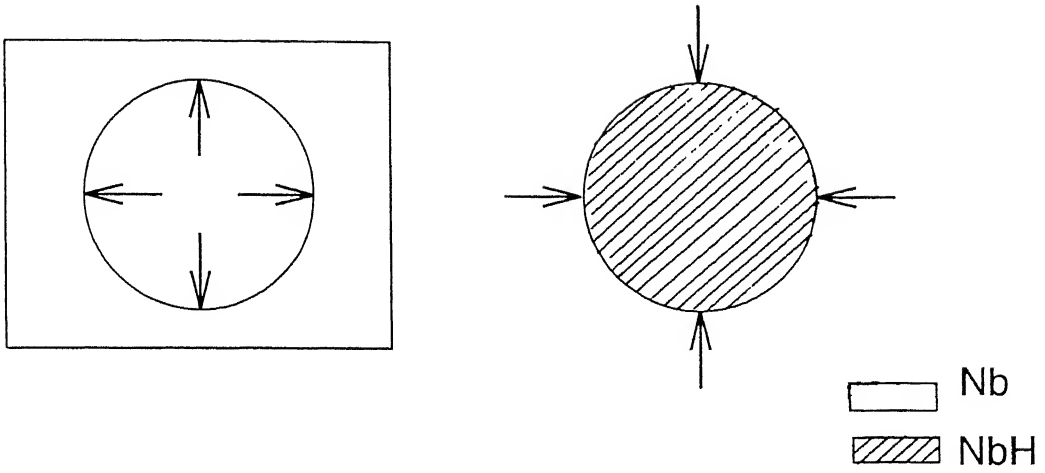

(a) forward transformation

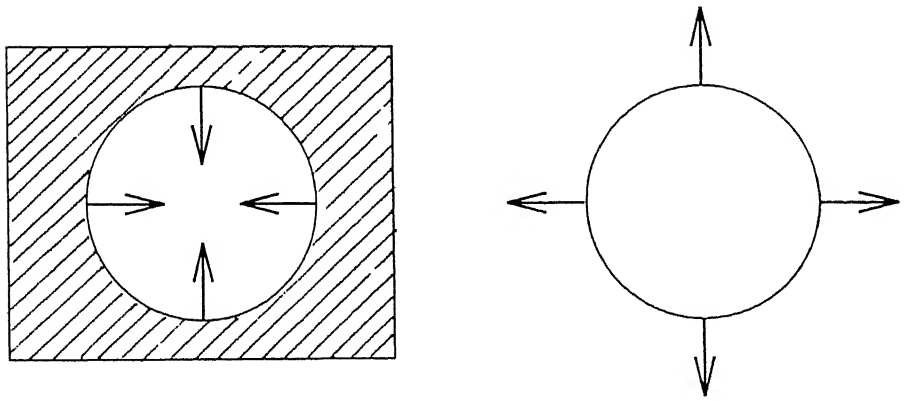

(b) reverse transformation

Figure 6. Nature of misfit-strain forces at the precipitate-matrix interface during (a) forward and (b) reverse hydrogen transformations.

$$\{\varepsilon\} = [B]\{U\} \qquad ..3.34$$

The nodal displacements and the initial-strain loads are related by

$$[K]\{U\} = \{F_o\} \qquad ..3.35$$

where [K] is the assembled stiffness matrix of the system. The elemental stiffness matrix $[K]_{element}$ is given in the matrix formed by the equation

$$[K]_{element} = \int [B]^T [D] [B] \, dV \qquad ..3.36$$

The unknown nodal displacement vector {U} is obtained by solving equation (3.35). The actual strain of each element is equal to the difference of the derived strain vector {ε}, obtained from equation (3.34), and the initial-strain vector $\{\varepsilon_o\}$. The initial-strain vectors are zero for the untransformed elements, while they are non-zero for the elements representing the transformed region. Therefore, in general, the elemental stress vectors are obtained from the expression

$$\{\sigma\}_{element} = [D]_{element} \left[\{\varepsilon\} - \{\varepsilon_o\}\right]_{element} \qquad ..3.37$$

where {σ} is the transformation stress vector.

The elastic strain energy of the system ($E_{elastic}$) is then given by the relationship

$$E_{elastic} = \frac{1}{2} \int \left[\sigma \right]^T \left[\left\{ \varepsilon \right\} - \left\{ \varepsilon_o \right\} \right] dV \qquad ..3.38$$

The total energy of the system is obtained by summing up the energies of individual elements.

$$E_{elastic} = \frac{1}{2} \sum_{i=1}^{\text{no. of elements}} \left\{ \sigma \right\}_i \left[\left\{ \varepsilon \right\} - \left\{ \varepsilon_o \right\} \right]_i V_i \qquad ..3.39$$

where the matrices have the same meanings as explained above but are now referenced to the elements.

3.3.2 Elasto-plastic analysis

The FEM formulation of elasto-plastic analysis using the incremental deformation theory is discussed below. The main advantage of adopting the incremental deformation theory is that no iterative procedure is required in this case. The disadvantage is that very small load increments should be used. The matrix formulations used for the elasto-plastic analysis are similar to those used for the elastic axisymmetric formulation in the previous section, except that elasto-plastic stiffness have been used instead of the purely elastic stiffness used earlier. The initial-strain load is applied incrementally within each step of transformation.

Incremental application of loading is essential for calculation

of stresses and strains during plastic deformation. In the incremental loading procedure, the load matrix for the n^{th} step of transformation is calculated only for the elements in the n^{th} layer of the mesh. This load is applied in p increments. The initial strain used in calculating the strain energies in every increment of loading (in each step of transformation) is $1/p^{th}$ of the initial strain calculated for the entire transformation step. The stresses and strains developed incrementally during a particular step of transformation are added to the previous ones, and the procedure continued.

In incremental loading, the problem of material change need special attention, when the initial-strain approach has to be applied to a new layer of elements which earlier had the properties of the matrix but are now assigned the properties of the precipitate. The effective stresses, effective strains and total plastic strains for the the elements to undergo transformation are initialized before applying the loads because a new layer of elements undergoing transformation is assumed to be elastic at the beginning of the transformation step. In case the plastic deformation has occurred in the previous loading step, the accumulated plastic strain (up to the previous step of transformation) is added to the specified misfit strains to calculate the initial-strain load for the current step of transformation. The problem of material change during transformation is illustrated in Figure 7 which illustrates the

stress-strain curves used for Nb and NbH in the present analysis. NbH has been assumed to have a considerably high strain hardening coefficient such that it does not undergo yielding at any stage of phase transformation. Taking the strains to be instantaneously the same at the time the properties of the transforming elements change from that of the matrix to that of the precipitate, the stresses vary locally. During the forward transformation, a stress level at **b'** in the matrix would momentarily change to **a** in the precipitate, at the existing strain level, assuming elastic properties of the two phases (Figure 7). Similarly, a stress level at **a** in the matrix would instantaneously change to **b** in the precipitate during the reverse transformation. The difference between the two stresses are converted into load vectors for the transforming elements using the following relation [14]

$$\left\{ \Delta\sigma \right\} = \left[\Delta D \right] \left\{ \varepsilon_{elastic} + \varepsilon_{plastic} \right\} \qquad ..3.40$$

and

$$\left\{ \Delta F_{\circ} \right\}_{T} = \int \left[B \right]^{T} \left\{ \Delta\sigma \right\} \, dV \qquad ..3.41$$

where

$$\left[\Delta D \right] = \left[D \right]_{precipitate} - \left[D \right]_{matrix} \qquad ..3.42$$

In situation where the initial-strain-load has to be applied in an element that was earlier defined as belonging to the matrix and had undergone plastic deformation, the plastic strain

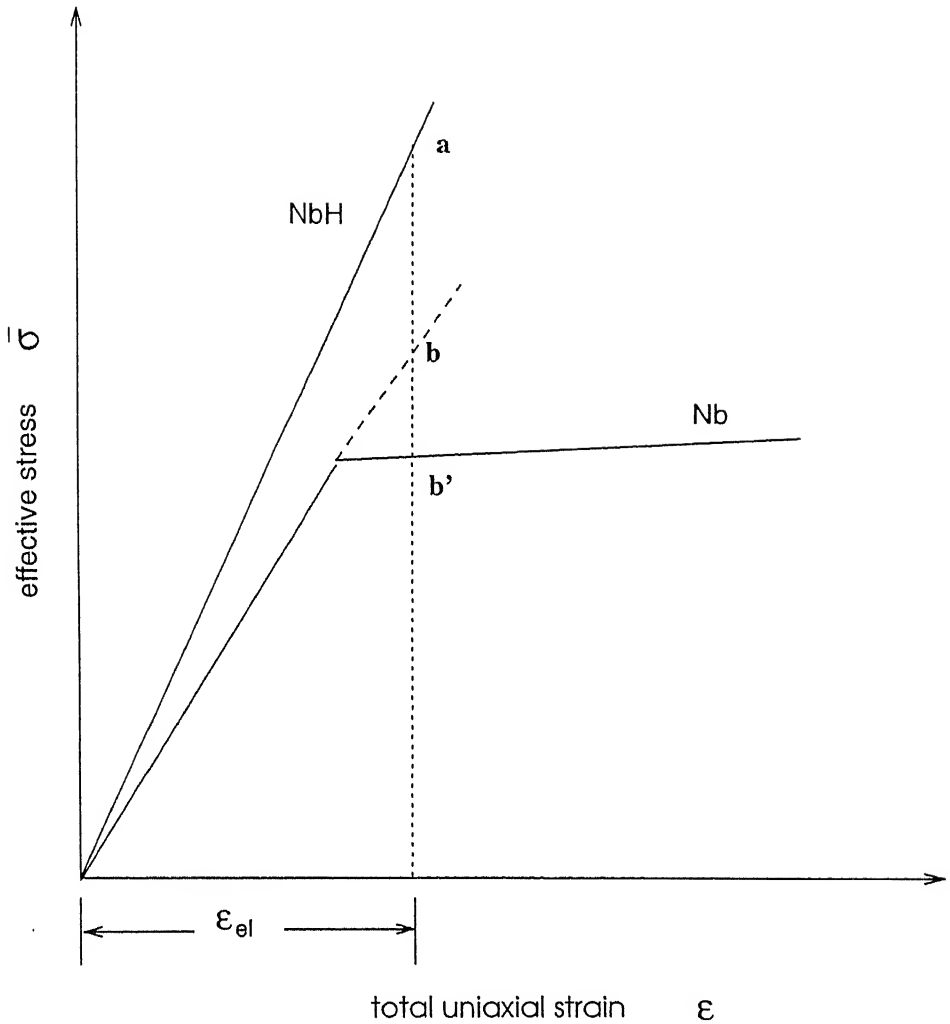

Figure 7. Schematic stress-strain curves of Nb and NbH showing the effect ot materal change.

must be subtracted, since this is the amount of strain already undergone by the element and it can only expand through balance of the total initial strain when the transformation occurs. The initial strain matrix $\{\varepsilon_o\}$ is modified to account for the plastic deformation undergone by the element to transform. For axisymmetric formulation

$$\left\{ \varepsilon_o \right\}' = \begin{Bmatrix} e_o - \varepsilon_{r(p)} \\ e_o - \varepsilon_{\theta(p)} \\ 0^o - \varepsilon_{rz(p)} \\ e_o - \varepsilon_{z(p)} \end{Bmatrix} \qquad ..3.43$$

and for plane stress formulation

$$\left\{ \varepsilon_o \right\}' = \begin{Bmatrix} e_o - \varepsilon_{x(p)} \\ e_o - \varepsilon_{y(p)} \\ e_o - \varepsilon_{xy(p)} \end{Bmatrix} \qquad ..3.44$$

where e_o is the initial strain calculated as (1/3) of the volumetric strain for free transformation of the matrix to precipitate and $\varepsilon_{r(p)}$, $\varepsilon_{\theta(p)}$, $\varepsilon_{rz(p)}$, $\varepsilon_{z(p)}$, $\varepsilon_{x(p)}$, $\varepsilon_{y(p)}$ and $\varepsilon_{xy(p)}$ are the components of the total plastic strain undergone by the elements to undergo transformation in the $n\text{-}1^{th}$ step. The initial load vector $\{F_o\}$ given by equation (3.33) for purely elastic behavior of the element is modified using equations 3.41 and 3.43 to account for the plastic deformation and change of the element material from the matrix to the precipitate to give

$$\left\{F_o\right\} = \int \left[B\right]^T \left[D_{elastic}\right] \left\{\varepsilon_o\right\}' \, dV + \left\{\Delta F_o\right\}_T \qquad ..3.45$$

The stresses for the transforming elements currently stored are updated to

$$\left\{ \sigma \right\} = \left[D_{precipitate} \right] \left\{\varepsilon_{elastic}\right\} \qquad ..3.46$$

The complete FEM solution procedure for the elasto-plastic case is given below. (The matrices have the same meanings as defined earlier. All symbols with Δ preceding it represent increment of property) :

Step 1 : Calculation of total initial strain matrix $\{\varepsilon_o\}$ and initial load matrix $\{F_o\}$ for the transforming step using equation (3.45).

Step 2 : Application of part($[\Delta F_o]$) of the load $[F_o]$ in each increment. Calculation of elemental stiffness with [D] replaced by $[D_{elasto-plastic}]$ for the elements using

$$\left[K \right]_{element} = \int \left[B \right]^T \left[D \right] \left[B \right] dV \qquad ..3.47$$

Step 3 : Evaluation of displacements with the current load increment using

$$\left[K \right] \left\{ \Delta U \right\} = \left\{ \Delta F_o \right\} \qquad ..3.48$$

where $\{\Delta U\}$ is the incremental displacement matrix for the current loading step.

Step 4 : Calculation of incremental (elemental) stresses assuming elastic behavior by using

$$\left\{ \Delta\sigma \right\} = \left[D_{elastic} \right] \left[\left\{ \Delta\varepsilon \right\} - \left\{ \Delta\varepsilon_o \right\} \right] \quad ..3.49$$

where

$$\left\{ \Delta\varepsilon \right\} = \left[B \right] \left\{ \Delta U \right\} \quad ..3.50$$

and $\{\Delta\sigma\}$ is the incremental stress matrix.

Step 5 : In the case of elements that have neither yielded earlier nor in this increment, incremental stresses calculated in step 4 are retained. For elements that have yielded in earlier increments but unloaded in the present one, the change in stresses in the present increment are taken as calculated in step 4. For elements that have yielded or further plastically deformed during the current load increment, the stresses calculated in step 4 are reduced to the yield surface iteratively[33].

Step 6 : The incremental stresses are added to previously stored ones (from earlier steps).

Step 7 : The cumulative elastic strains are obtained by the matrix relation

$$\left\{ \varepsilon_{elastic} \right\}_{element} = \left[D_{elastic} \right]^{-1}_{element} \left\{ \sigma \right\}_{element} \quad ..3.51$$

Step 8 : The incremental and total effective plastic strains $\bar{\varepsilon}_p$ and stresses $\bar{\sigma}$ are calculated from the stress and strain matrices obtained by step 7 from Von Mises criterion using [35]

$$\bar{\sigma} = [\sqrt{(3/2)}] \{\sigma'_{ij}\ \sigma'_{ij}\}^{1/2} \quad ..3.52$$

and

$$\bar{\varepsilon}_p = [\sqrt{(2/3)}] \{(\varepsilon'_{ij})_p\ (\varepsilon'_{ij})_p\}^{1/2} \quad ..3.53$$

where $(\varepsilon'_{ij})_p$ is the total plastic strain component and σ'_{ij} is the deviatoric stress component.

Step 9 : The cumulative elastic energy is obtained using

$$E_{elastic} = \frac{1}{2} \int \left\{ \sigma \right\}^T_{element} \left\{ \varepsilon_{elastic} \right\}_{element} dV \quad ..3.54$$

while the incremental plastic strain energy is calculated from the following relation and added to the previously stored cumulative plastic strain energy

$$\Delta E_{plastic} = \sum_{i=1}^{no.\ of\ elements} \sigma_{effective_{[i]}} \Delta\varepsilon_{plastic_{[i]}} \quad ..3.55$$

where $\sigma_{effective}$ is the effective stress of the element and $\Delta\varepsilon_{plastic}$ is the change in effective plastic strain of the element due to the load increment.

$$\Delta\varepsilon_{plastic_{[i]}} = \left\{ \bar{\varepsilon}_{p_{[i]}} \right\}_{p^{th}\ increment} - \left\{ \bar{\varepsilon}_{p_{[i]}} \right\}_{(p-1)^{th}\ increment} \quad ..3.56$$

Yielding occurs if the effective stresses at a point exceeds the yield strength of the material at that point, where yield strength is given by

$$\sigma_y = \sigma_y^o + H' \bar{\varepsilon}_p \qquad ..3.57$$

where σ_y^o is the uniaxial yield strength of the material and H' is the strain hardening parameter.

Step 10: Steps 2 to 9 are repeated till all the increments in each step have been applied. This is repeated for all the steps till completion of the transformation.

CHAPTER 4
RESULTS AND DISCUSSION

This chapter presents the accommodation energies obtained by the finite element model of hydrogen transformations presented in chapter 3. The results are presented in two sections. In the first section, the results obtained by linear elastic analysis are presented. The accommodation energies of the system obtained by plane stress formulation where the precipitate is in the shape of a thin disk and the accommodation energies obtained by axisymmetric formulation where the precipitate is a prolate spheroid are presented in that section. In the second section, the results of elasto-plastic analysis are presented. In this case also, energies of the system were calculated for disk shaped and prolate spheroid precipitates. Figure 8 shows the shape of the precipitate along with the element used to model the system in plane stress and axisymmetric analyses. The term aspect ratio refers to the ratio of semimajor axis to the semiminor axis in the case of disk shaped precipitate and in the context of axisymmetric analysis, the aspect ratio refers to the ratio a_1 to a_2 where a_1, a_2, a_3 are the principle axes of prolate spheroid ($a_2 = a_3$). A comparison of the accommodation energies for different aspect ratios (1, 2, 3 and 4) of the precipitate have been presented and discussed.

The present model evaluates the accommodation energies during α-β hydrogen transformations in the Nb-H and Pd-H (Appendix

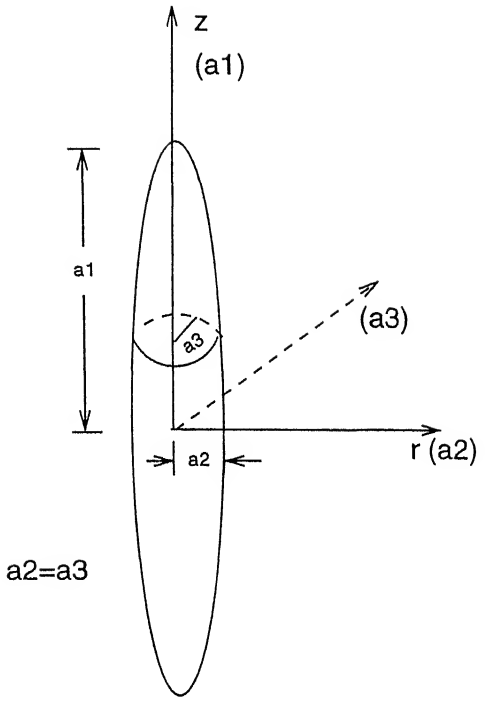

prolate spheroid

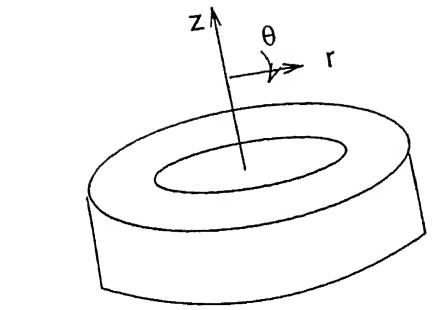

isometric view

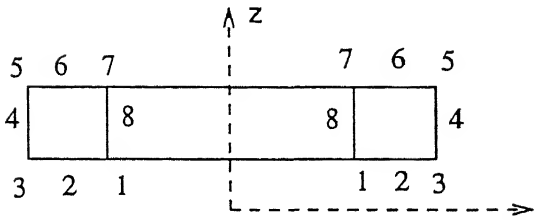

cross section containing z-axis.

axisymmetric finite element.

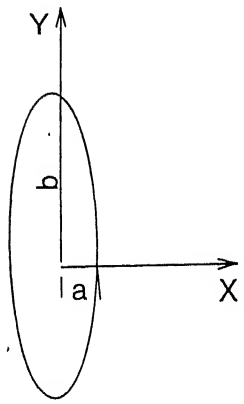

thin disk

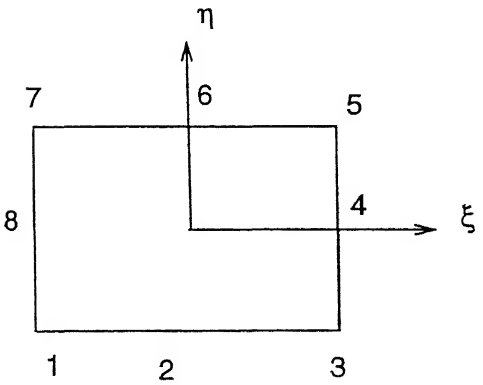

eight noded plane element.

Figure 8. Shape of precipitate and the element used to model the system in axisymmetric and plane stress analyses. The axes used are also indicated.

A) systems by considering transformation progressing by two paths, viz precipitation starts at the centre and grows outwards towards the free surface (centre to surface path) and the precipitation starts at the surface of the system and grows inwards towards the centre (surface to centre path). The α-β transformation in niobium-hydrogen system has been specifically addressed because the properties of the Nb and NbH and the experimental accommodation energies at 313 K are known [1]. (The results obtained for the hydrogen transformation in the palladium hydrogen system are given in Appendix A). Niobium has a bcc structure (lattice parameter 3.3 Å). The physical and mechanical properties of Nb and NbH used in the calculations are listed in Table 1 along with the reference source of data. The misfit volume strain was obtained from the molar volumes of Nb and NbH, and the linear misfit strain was assumed to be one third of the volumetric strain. The misfit strain during the forward transformation is positive and during the reverse transformation is negative. The misfit strain is found to be equal to 0.0439394 during $\alpha \rightarrow \beta$ transformation and equal to -0.0420899 during $\beta \rightarrow \alpha$ transformation using equation [3.32]. The FEM calculations were performed on a HP-9000/850 computer.

4.1 SELECTION OF FEM MODEL PARAMETERS

While correct modelling of the physical problem into mathematical equations forms the core of the entire analysis, the selection of appropriate element and elemental mesh decides the accuracy of results. The judgment about the selection of various parameter needs a good deal of numerical experiment before a

Table 1. Physical and mechanical properties of Nb and NbH at 31 K. Reference source is also indicated.

Property	Nb	NbH
Young's Modulus(E) (N/m^2)	$1.22*10^{11}$ [1]	$1.269*10^{11}$ [1]
Poisson's ratio(ν)	0.38 [1]	0.38 [1]
Yield stress (σ_y) (N/m^2)	$2.4828*10^{8}$ [1]	$4.3137*10^{8}$ [1]
Crystal structure	BCC [1]	Distorted BCC [1]
Lattice parameter (Å)	3.3002 [1]	3.445 [1]
Shear Modulus (μ) (N/m^2)	$0.3752*10^{11}$ [1]	$0.452*10^{11}$ [1]
Work hardening parameter (H') (N/m^2)	$3.48*10^{8}$ [35]	$3.48*10^{100}$#
Molar volume ($\overline{V}$) (m^3mol^{-1})	$10.8224*10^{-6}$ [1]	$12.3126*10^{-6}$ [1]

Value assumed to prevent yielding in NbH

particular set of values is used for final analysis. In the present analysis, eight-noded isoparametric elements are used to model the system. A study of the sensitivity of the results with the type of element have been carried out using four-noded and eight-noded isoparametric elements and it was observed that both the type of elements yielded the same results. A similar observation was also noted by Sen et al [36]. The results obtained using different number of eight-noded isoparametric elements to model the system in the elastic axisymmetric analysis of forward transformation by the centre to surface path for aspect ratio 1 are presented in Figure 9. The calculated accommodation energies marginally depends upon the number of elements in to which the system is divided or, alternatively stated, the number of steps chosen to accomplish transformation. Calculations showed that using 10 steps of transformation or more, with the quadrant divided in to 4 radial sectors, gave converging results using either the eight-noded or the four-noded isoparametric elements.

It has was earlier noted in Section 3.3.2 that in the elasto-plastic analysis, the load corresponding to the misfit transformation strain is applied in each stage of transformation in steps. The main advantage of adopting the incremental deformation theory is computer time-intensive iterative procedure is not necessary. In the incremental deformation theory used in the elasto-plastic analysis, the load should be applied in small increments so that in each load increment the amount of plastic deformation occurred is relatively small. The effect of varying the number of increments by which the load is applied during each

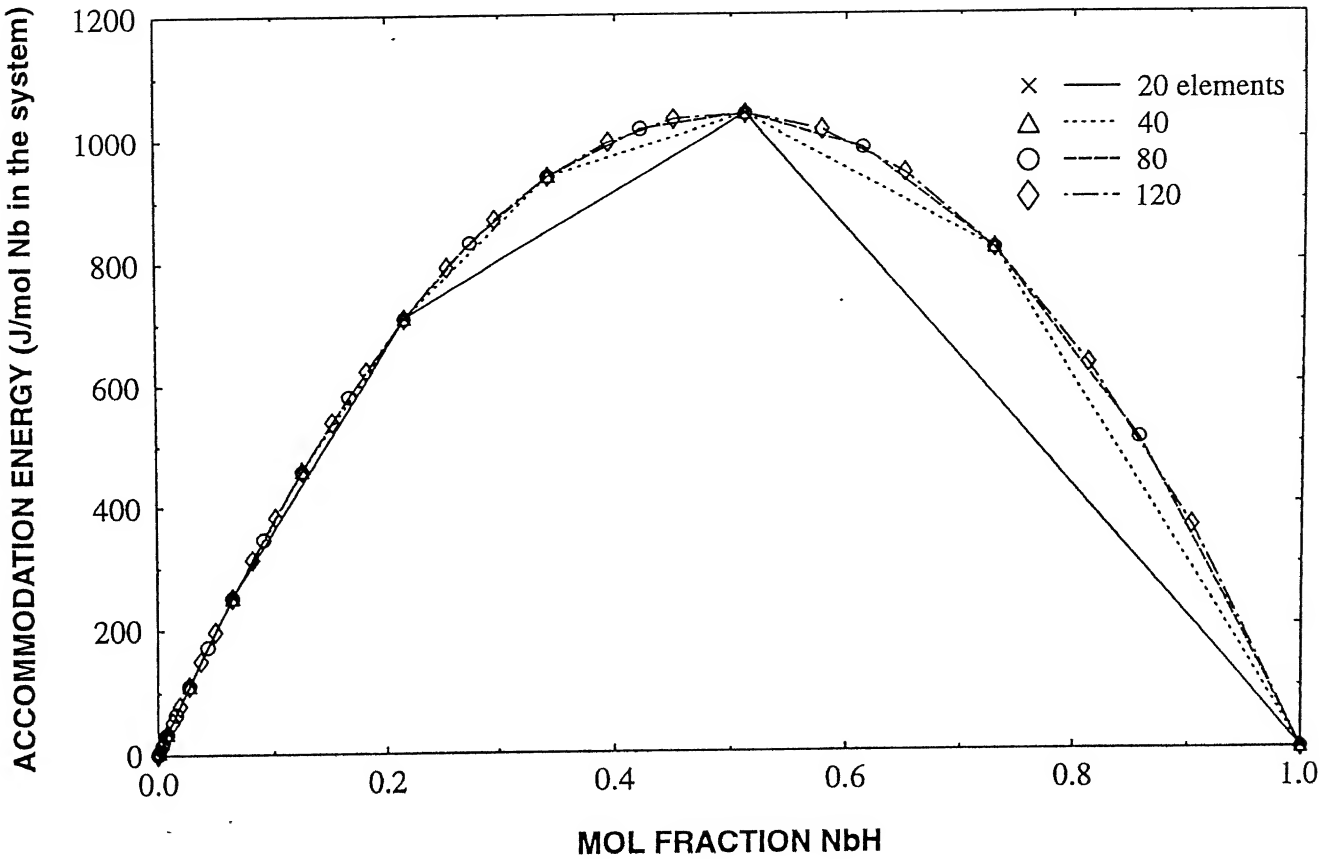

Figure 9. Total accommodation energy for Nb-NbH transformation by centre to surface path for various mesh configurations using elastic axisymmetric analysis.

transformation stage on the system accommodation energy was studied. Figure 10 shows the system elasto-plastic accommodation energy during forward transformation by the center to surface path for different number of load increments (5, 10 and 20) used for the application of load in each stage of transformation. It is to be noted that the stress that is developed in each load increment for the 5 increment case is about 15% of the yield stress, which again is applied in a number of steps in each increment as explained by Owen et al [33], while it is 10% and 3% of the yield stress when the number of increments are 10 and 20, respectively. There is no significant change in the energy of the system by changing the number of load increment steps. Therefore, in all the elasto-plastic analyses to be presented below, the number of load increments used in each transformation stage was 5.

In the present analyses the domain is divided into eighty elements and the transformation is modeled to occur in 20 steps. Two types of domain used to model the system are shown in Figure 11. Figure 11a shows the cross sectional view of one quadrant of the ellipsoidal domain and Figure 11b shows the cross sectional view of one quadrant of the cylindrical domain. In the case of cylindrical system, the shape of the precipitate changes from that of the ellipsoid to cylinder on logarithmic scale with most of the shape change occurring in last few steps. Figure 12 shows the results of elasto-plastic analysis of the forward transformation through the centre to surface path for the two different shapes of the system. The results obtained are similar. Therefore, the finite element mesh shown in Figure 11a is used to

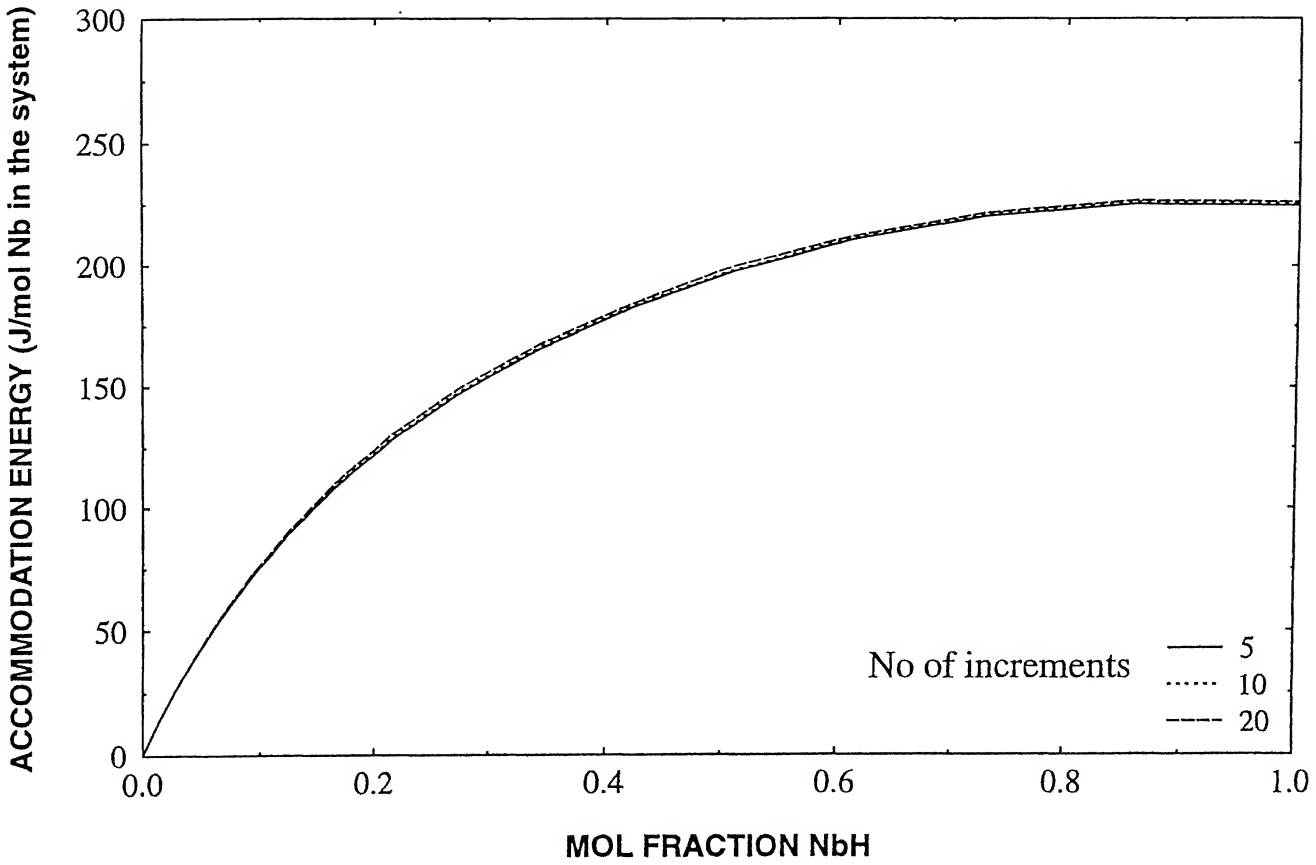

Figure 10. Comparison of the system elasto-plastic accommodation energies during forward transformation through centre to surface path obtained by applying the load corresponding to the volume mismatch in different no of increments in each stage of transformation.

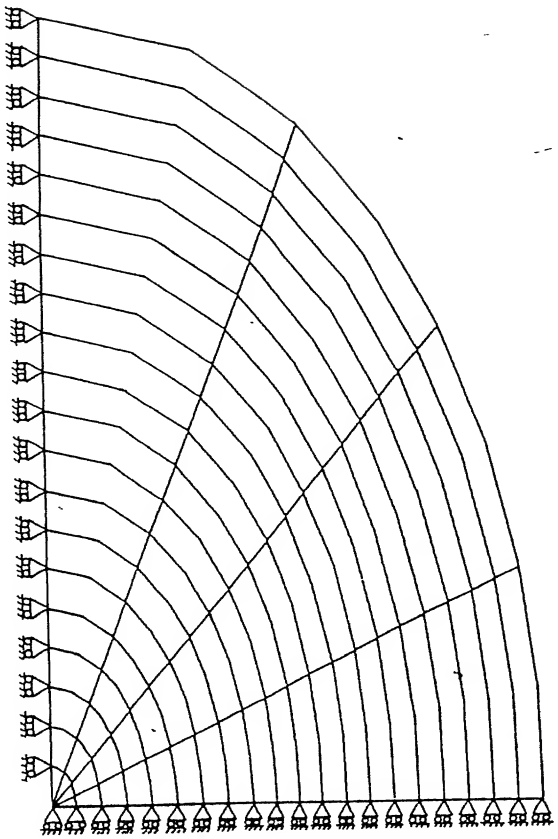

(a) ellipsoidal domain

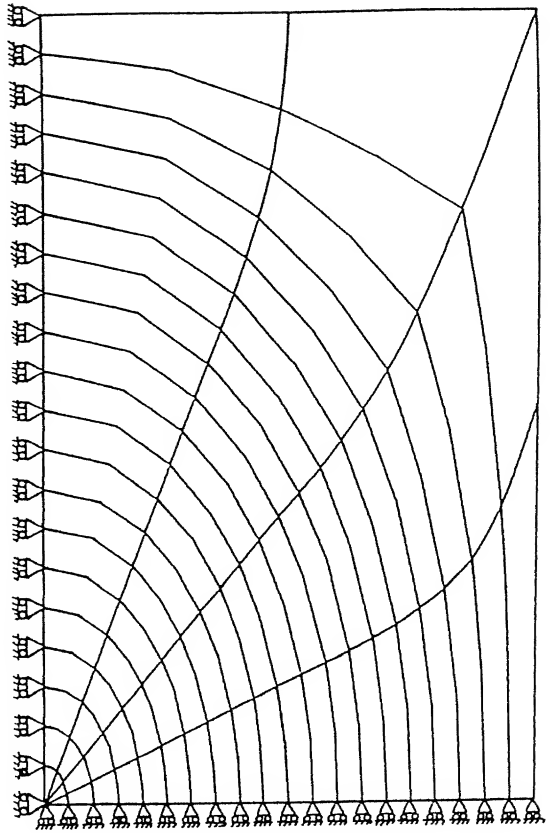

(b) cylindrical domain.

Figure 11. The finite element meshes along with the boundary conditions used for the calculation of accommodation energy in (a) an ellipsoidal domain and (b) cylindrical domain.

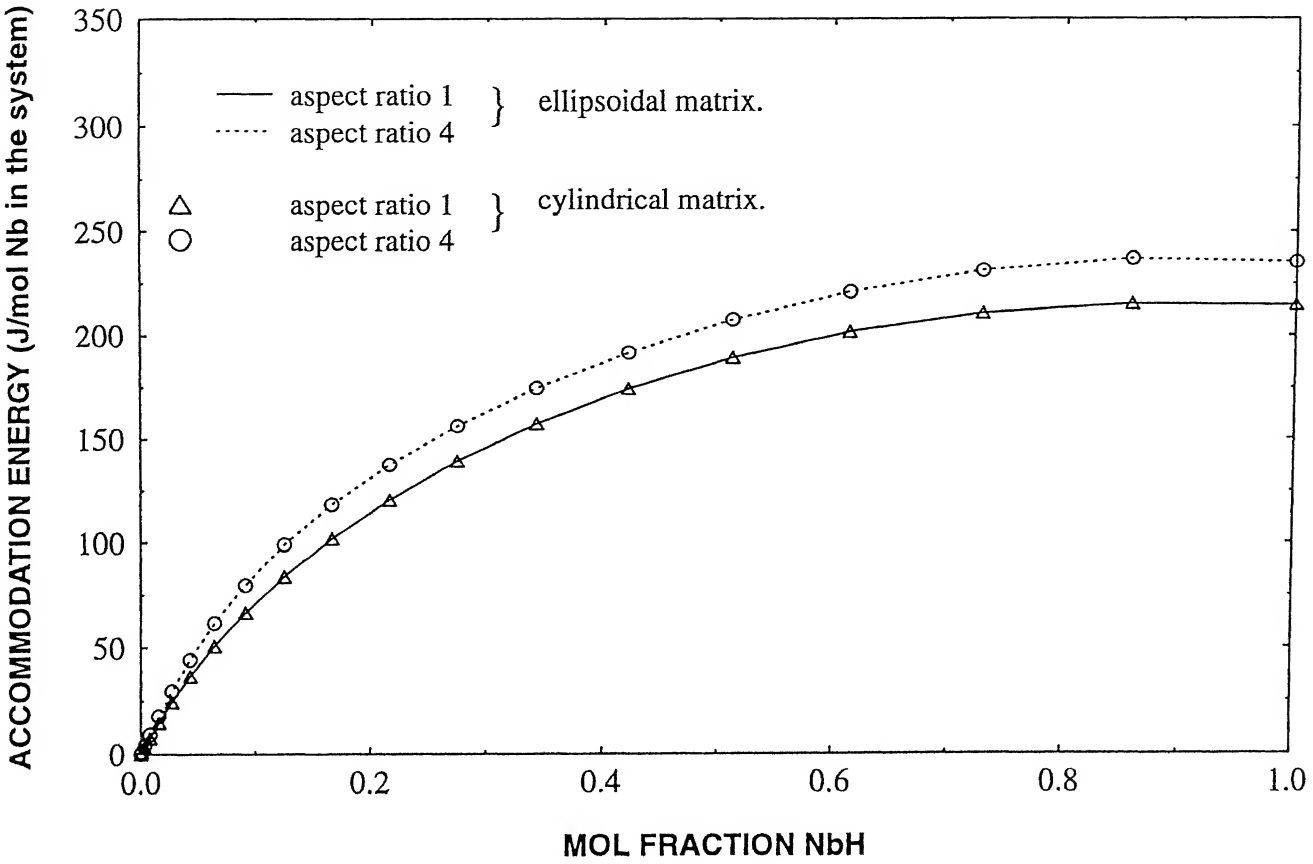

Figure 12. Comparison of system elasto-plastic accommodation energies during forward transformation through the centre to surface path for different aspect ratios of an ellipsoidal precipitate in a cylindrical and an ellipsoidal matrix.

model the system in the analysis to be presented henceforth.

4.2 VALIDATION

The results obtained by the linear elastic analysis of α-β transformation in Nb-H system using finite the element model have been compared with the accommodation energies obtained by applying other mathematical models of elastic accommodation. The models proposed by Eshelby [2] and Lee et al [23] are used for the comparison. In the model of Eshelby and Lee et al., the matrix is an infinite continuum. Table 2 compares the elastic accommodation energies during during α-β hydrogen transformation in Nb-H system, wherein the precipitate is a spheroid. The reported FEM values are the elastic strain energies when the precipitate size tend to zero for the centre to surface path, the condition closely representing precipitation in an infinite continuum matrix. The magnitude of elastic accommodation energy in the Nb-H system depends upon the elastic strain energy model used. It was found that the results obtained by finite element method [14] is comparable with the results based on the models of Eshelby and Lee et al.

4.3 LINEAR ELASTIC ANALYSIS

4.3.1 Axisymmetric formulation

The axisymmetric modeling of the ellipsoidal system was performed using eight-noded isoparametric elements (Figure 8). Only one quadrant of the system has been considered because of symmetry. The domain is divided in to 20 concentric layers each consisting of four elements (Figure 11a). The 20 concentric layer were transformed successively to depict 20 stages of the

Table 2. Comparison of elastic accommodation energies during α-β phase transformation in Nb - H system at 313 K.

Model used for calculation. [ref]	Formula	Elastic accommodation energy (joules per mole metal in precipitate)	
		forward	reverse
Finite Element Method	$\frac{1}{2} \int [\sigma] \; [\{\varepsilon\} - \{\varepsilon_o\}] \, dv$	4216	4349
Eshelby [2]	$\frac{2\mu \; (\nabla\bar{V})}{3\alpha' \bar{V}_{max}}$	3966	4068
Lee et al. [23]	$\frac{6\mu\alpha\gamma\varepsilon \; \bar{V}_{max}}{\alpha(\gamma-1)+1}$	3537	4327

*Definition of symbols used:

μ = shear modulas of matrix.

$\bar{V}$ = molar valume.

$\nabla\bar{V} = |\bar{V}_{NbH} - V_{Nb}|$

$\gamma = \frac{K_{ppt}}{K_{matrix}}$

K = Bulk Modulas.

ν = poisson's ratio

$\alpha = 1+4\mu_{matrix} / 3K_{matrix}$

$\alpha = \frac{(1+\nu_{matrix})}{3(1-\nu_{matrix})}$

transformation. All the elements in the transformed region were assigned the elastic properties (elastic modulii and poisson's ratio) of the precipitate. The untransformed elements were assigned the elastic properties of the matrix. Calculation of the stresses, strains and strain energies were made at each stages of the transformation. The load matrix at each stage of the transformation was modified according to equation [3.33]. At every stage, transformation was assumed to begin from the unstrained condition. Therefore, the energy calculated at every stage of transformation is the cumulative energy until that stage of the transformation. The transformation progressing from centre of the matrix outwards (centre to surface path) and from surface of the matrix inwards (surface to centre path) are addressed in the present analysis. The accommodation energies are calculated for different aspect ratios of the precipitate.

As the matrix is stress free at the beginning and at the end of the transformation, the strain energies will be zero at beginning and end of the transformation irrespective of the aspect ratio. This is true for all transformation paths. At any intermediate stage of transformation, there will be two phases each constraining the expansion/contraction of other phase. Therefore, there will be a net strain energy at any intermediate stage of transformation.

Figure 13 shows the variation of elastic accommodation energy of the system as a function of progress of transformation by centre to surface transformation path for $\alpha \rightarrow \beta$ transformation. The energy is expressed in joules per mole of Nb in the system.

The advantage of using this energy unit has been discussed elsewhere [12]. Figures 14a and 14b show the elastic strain energies stored in the matrix and the precipitate, respectively, for various aspect ratios for the forward transformation. Since NbH is assumed to be a stochiometric monohydride, one atom of hydrogen atom is associated with an atom of the metal in the hydride. Therefore, the number of moles of Nb in the system is a constant for given domain. The abscissa is the mole fraction of NbH, which increases with progress of transformation in the $\alpha \rightarrow \beta$ transformation and decreases with progress of transformation in $\beta \rightarrow \alpha$ transformation. Figure 14b shows that the precipitate energy increases with aspect ratio whereas the matrix energy (Figure 14a) and total accommodation energy (Figure 13) decrease with an increase in aspect ratio of the precipitate. For the transformation progressing from the centre to surface, the precipitate NbH will be constrained by a surrounding shell of matrix. When the aspect ratio is one, i.e. precipitate is a sphere, the state of stress inside the precipitate is purely hydrostatic. In this case the precipitate constraint on the matrix is high, there by making the elastic deformation of matrix relatively large compared to the elastic deformation of precipitate. Hence, the matrix energy is dominant in this case. For aspect ratios other than one, the precipitate is no longer in a state of pure hydrostatic stress. There will be shear stresses present inside the precipitate which increase with increase in aspect ratio. Therefore,the constraint offered by the precipitate decrease with increasing aspect ratio, which results in a

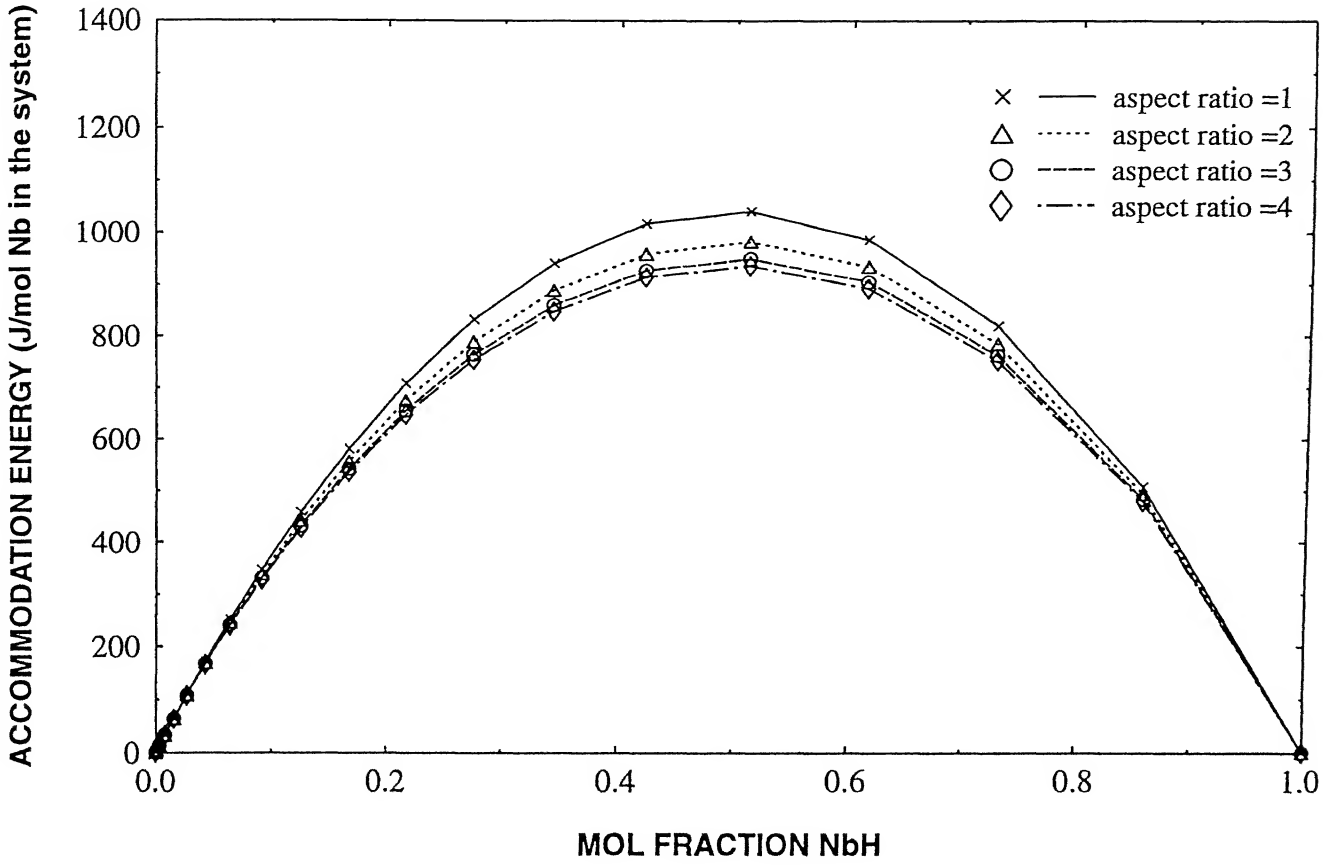

Figure 13. Variation of system accommodation energy as a function of fraction transformed during forward transformation through centre to surface path for different aspect ratios of the precipitate using elastic axisymmetric analysis.

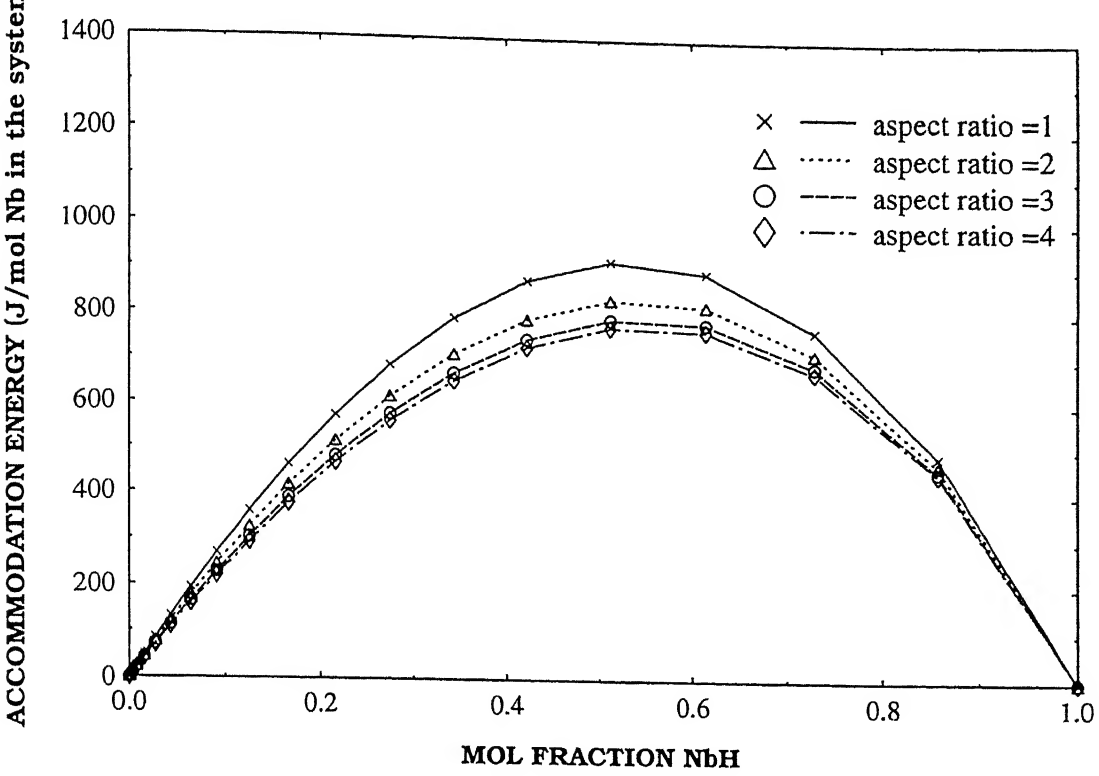

(a) matrix energy

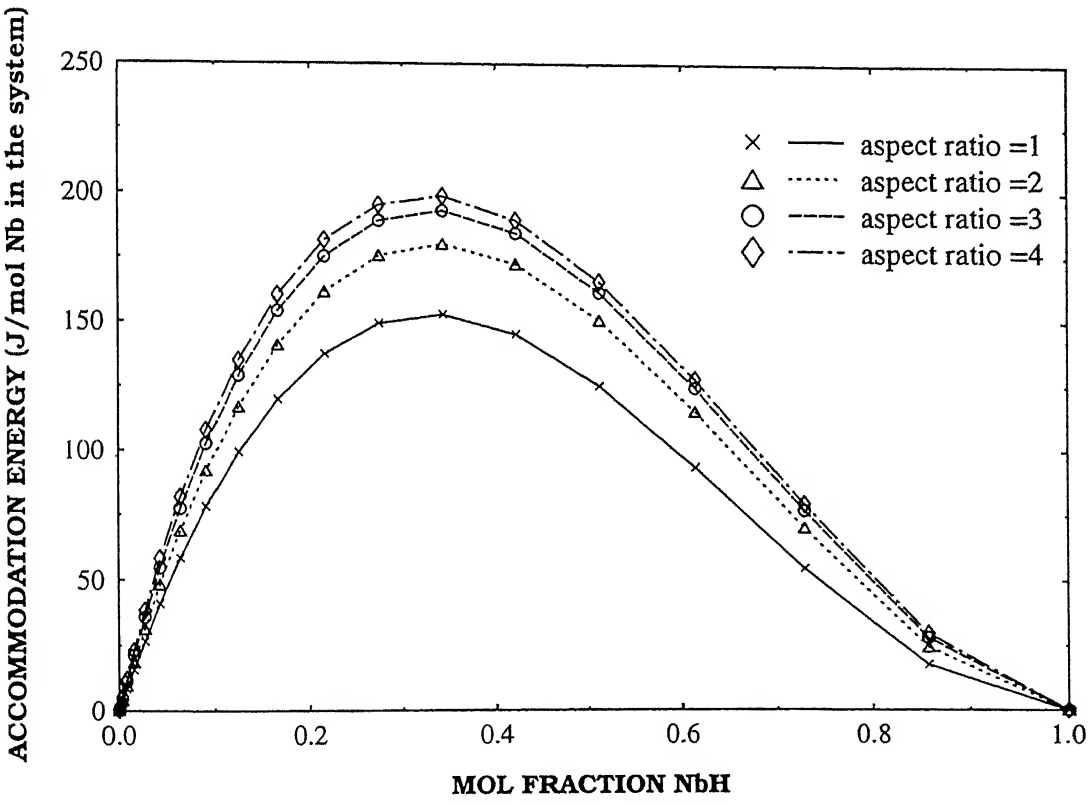

(b) precipitate energy

Figure 14. Variation of accommodation energy stored in the (a) matrix and (b) precipitate during forward transformation through centre to surface

decrease in the energy of matrix with increasing aspect ratio (Figure 14a). The strain energy in the precipitate increases with an increase in aspect ratio since elastic deformation inside the precipitate will be more in this case (Figure 14b). In order to understand the effect of shear components on the accommodation energies, the average effective stress in the precipitate and the matrix at 50% transformations for the forward and reverse transformations are tabulated in Table 3. The effective stress $\bar{\sigma}$ is defined as

$$\bar{\sigma} = \sqrt{3}\ (J_2')^{1/2} \qquad ..4.1$$

where J_2' is the second deviatoric stress invariant.

$$J_2' = \frac{1}{2}\ [\sigma_x'^2 + \sigma_y'^2 + \sigma_z'^2] + \tau_{xy}^2 + \tau_{yz}^2 + \tau_{xz}^2 \qquad ..4.2$$

Effective stress provides information about the existence of shear components of stress. It can be seen from Table 3, that the effective stresses in the precipitate is negligible when the aspect ratio of the precipitate is one and increases as the aspect ratio increase, whereas the effective stresses inside the matrix decreases as the aspect ratio increases. For the centre to surface transformation path, the major contribution to the total accommodation energy is from the matrix, so the total accommodation energy of the system decreases with increase in aspect ratio. As the precipitate approaches the external boundary stresses get relaxed. Therefore, the strain energy decreases during the last stages of transformation for all the aspect ratios (figures 13 through 16). Eventually, the strain energy decreases

Table 3. Average effective stress (GPa) inside the precipitate and the matrix at 50% transformation for different aspect ratios of the precipitate.

		Average Effetctive stress (GPa)							
		precipitate				matrix			
		aspect ratio				aspect ratio			
		1	2	3	4	1	2	3	4
centre to surface	forward	~ 0	1.50	1.68	1.71	6.31	5.54	5.34	5.29
	reverse	~ 0	1.46	1.62	1.70	6.29	5.50	5.29	5.20
surface to centre	forward	5.98	5.14	4.93	4.88	~ 0	1.75	1.98	2.04
	reverse	5.51	4.77	4.57	4.52	~ 0	1.67	1.90	1.96

to zero as all of the specimen is transformed and there are no more misfit constraints present in the system.

For the reverse transformation starting from centre of the system, the variation of the accommodation energies stored in the system, the matrix and the precipitate, which are depicted in figures 15, 16a and 16b, respectively, show the same pattern as in the forward transformation. The above results shows that for centre to surface transformation path, whether it is forward or reverse transformation, most of the elastic strain energy is accommodated in the outer phase surrounding the inner phase.

The parabolic relationship of the strain energy for the case of spheroid precipitate (figure 13 through 20) is not surprising and it is expected regardless of the relaxation. If ω is the elastic strain energy (per unit volume of precipitate) and ϕ is the volume fraction of the precipitate phase, then the total strain energy is given by $\omega\phi(1-\phi)$, which is the well known parabolic relationship [37]. Strictly speaking ω is a function of ϕ, but it is relatively insignificant as the transformation strain/stress field is of short range.

Figure 17 shows the variation of system accommodation energy with progress of transformation during forward transformation through the surface to centre path, while Figures 18a and 18b provide the matrix and the precipitate energies, respectively. In the case of transformation starting from surface growing inwards, a shell of precipitate material grows into the

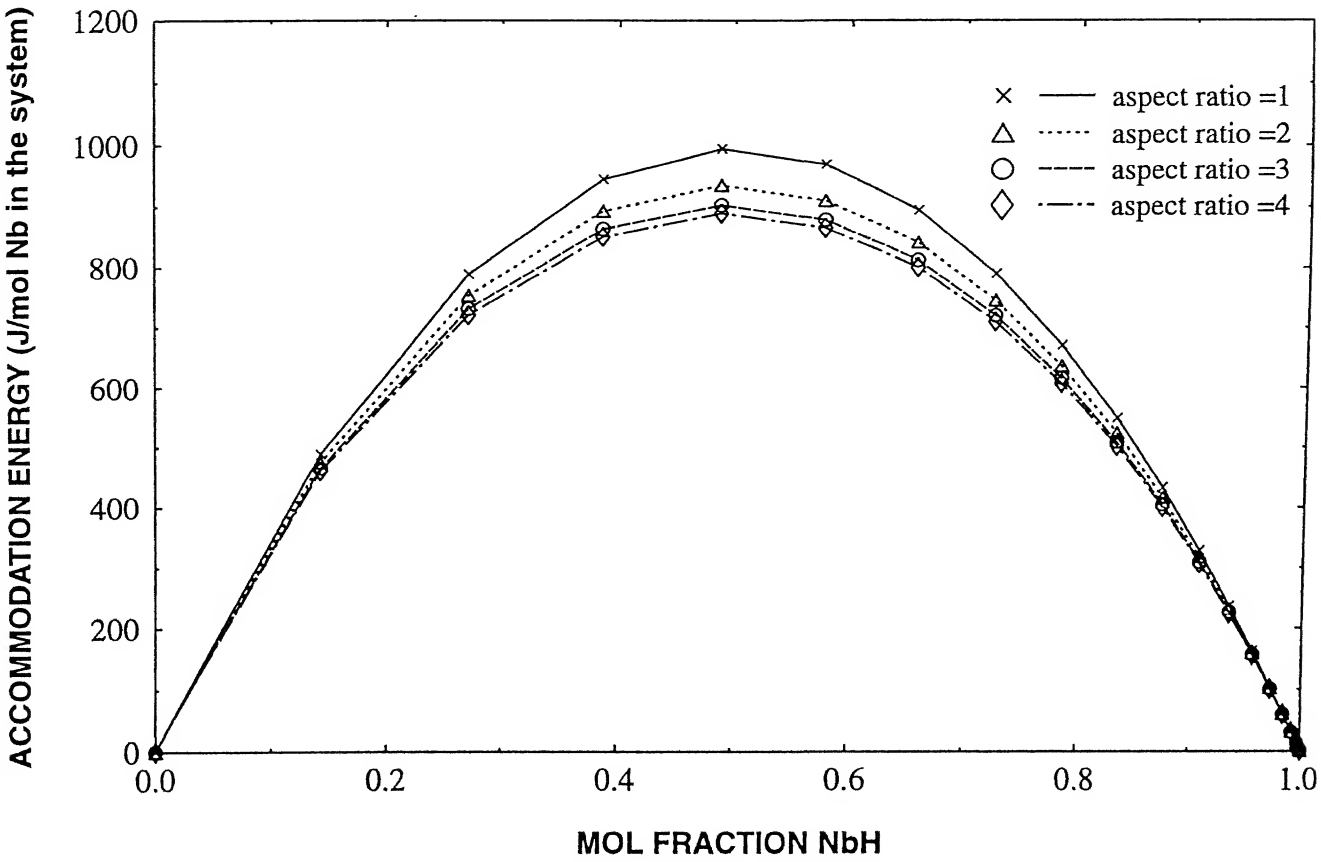

Figure 15. Variation of system accommodation energy during reverse transformation through the centre to surface path for different aspect ratios of the precipitate using elastic axisymmetric analysis.

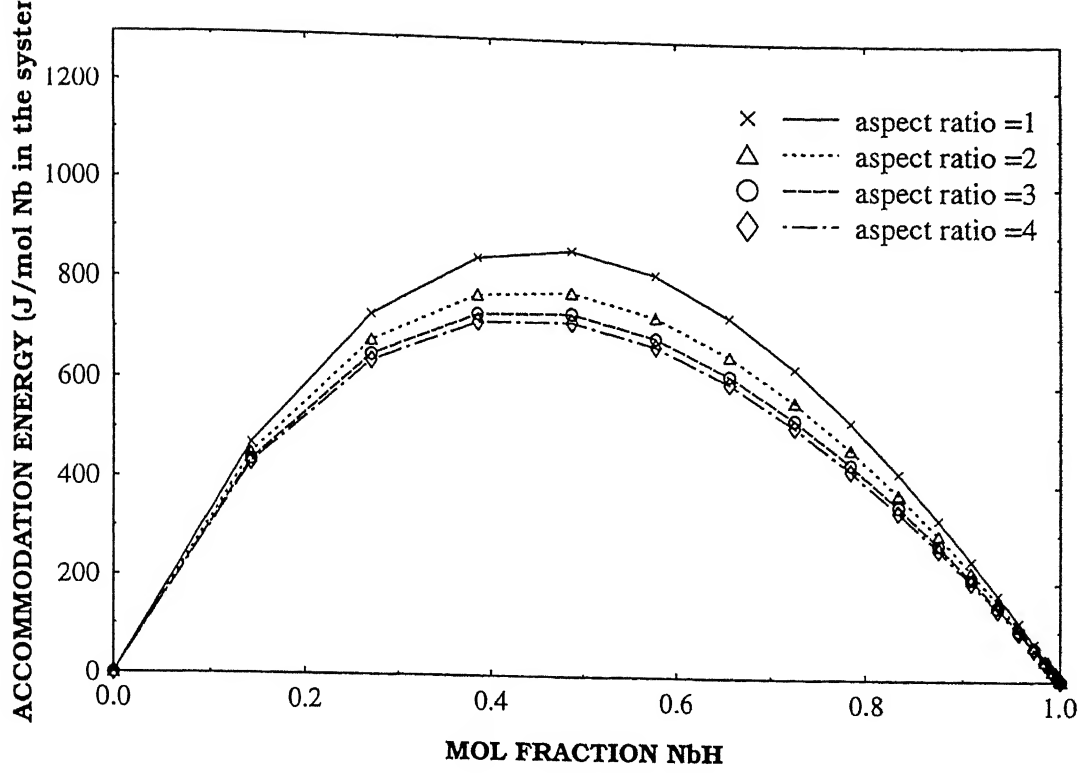

(a) matrix energy

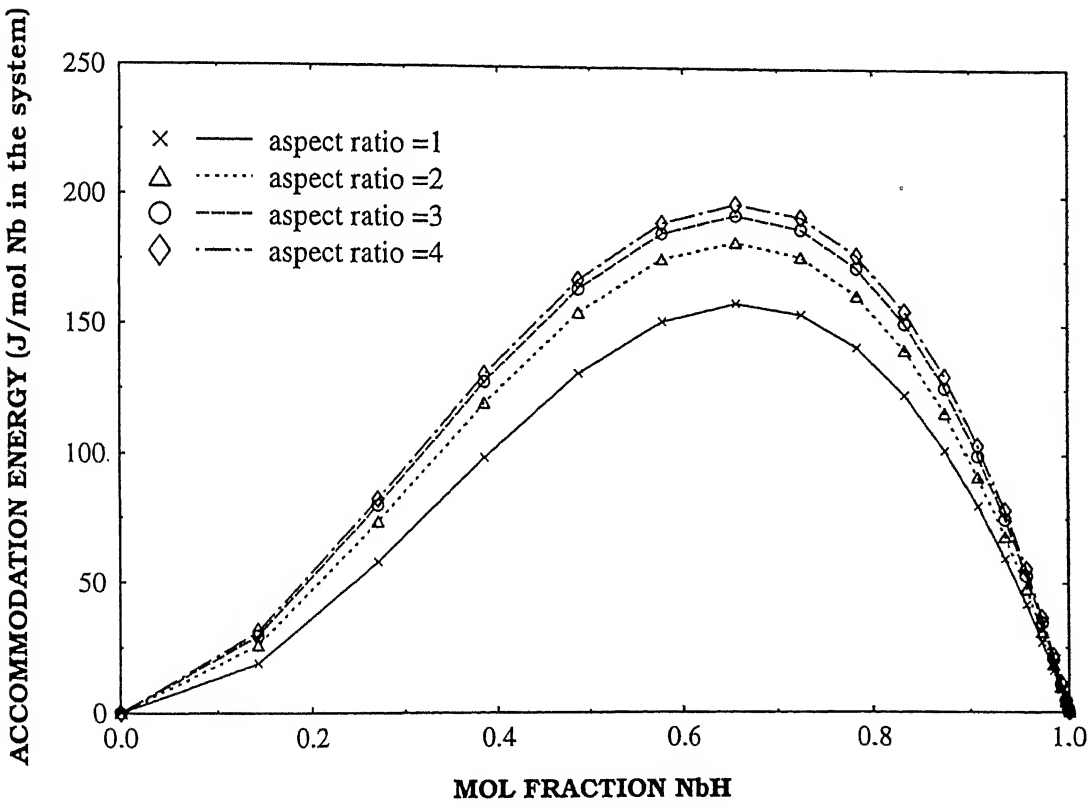

(b) precipitate energy

Figure 16. Variation of accommodation energy stored in the (a) matrix and (b) precipitate during reverse transformation through centre to surface

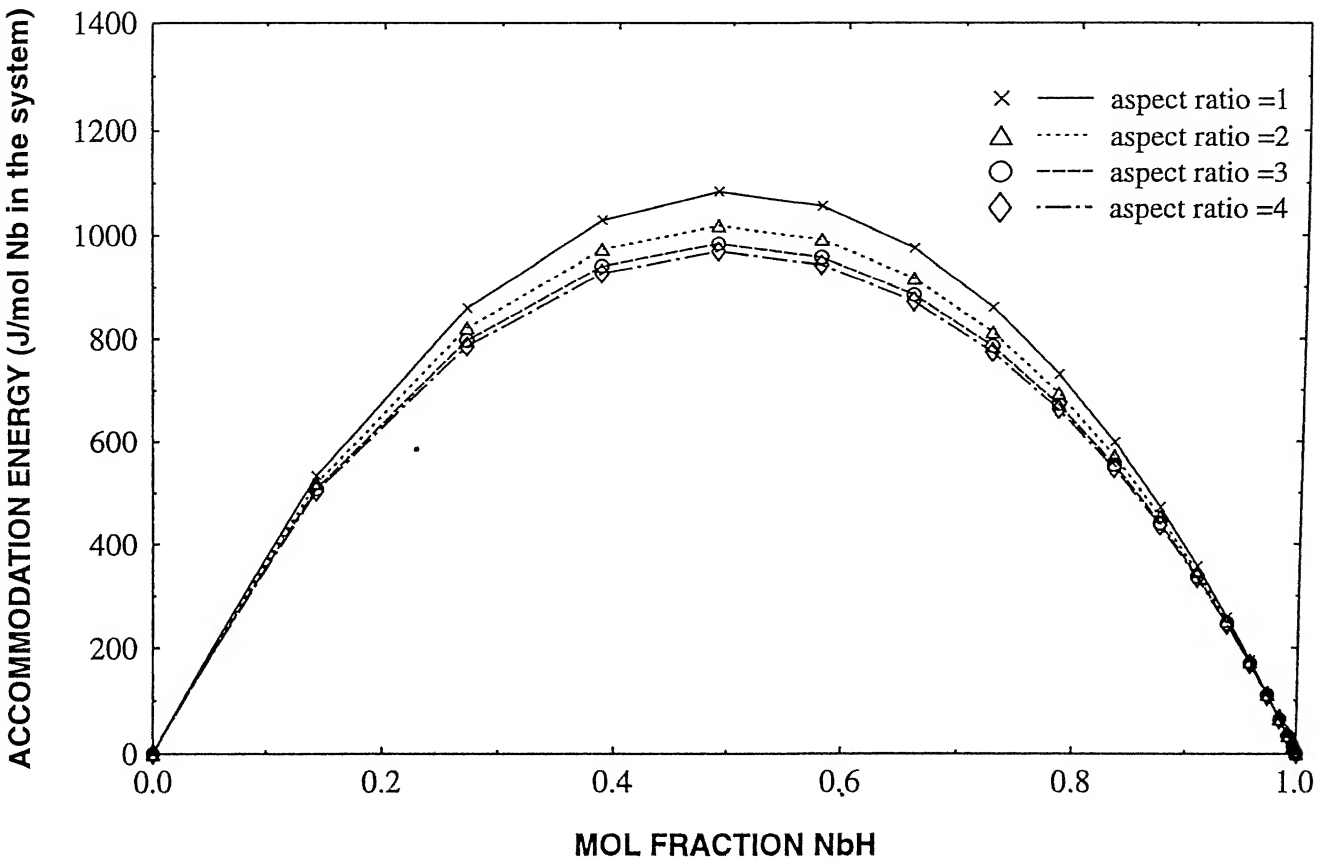

Figure 17. Variation of system accommodation energy during forward transformation through the surface to centre path for different aspect ratios of the precipitate using elastic axisymmetric analysis.

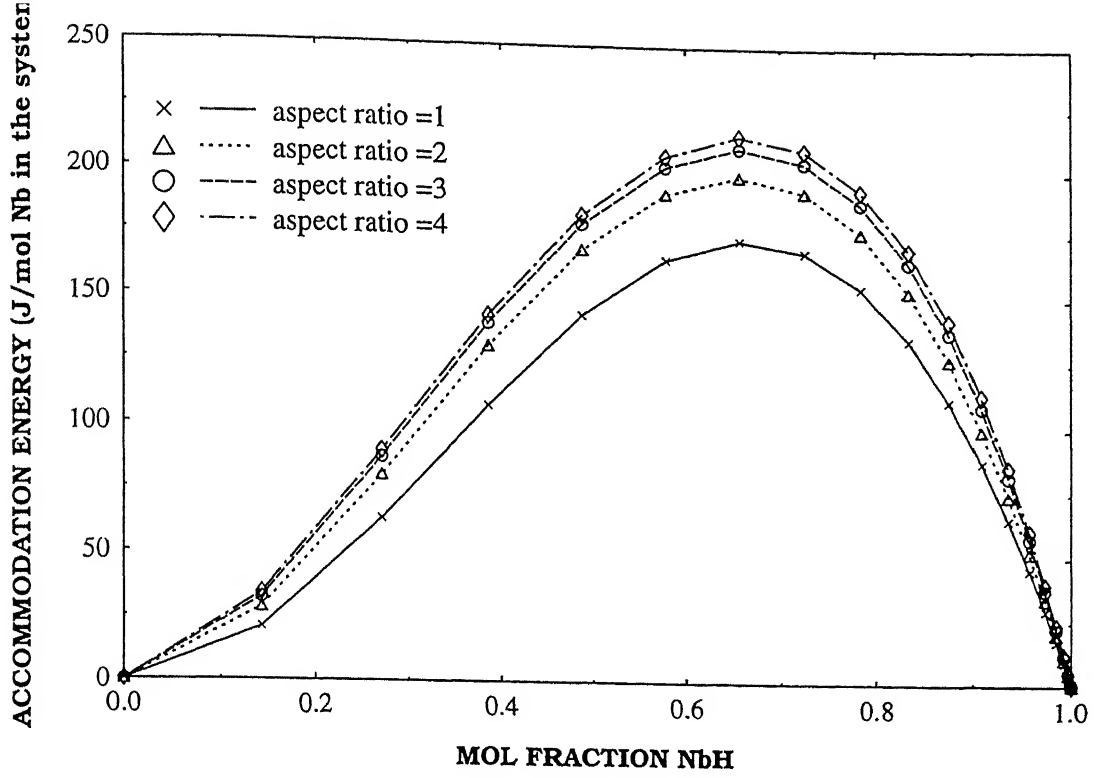

(a) matrix energy

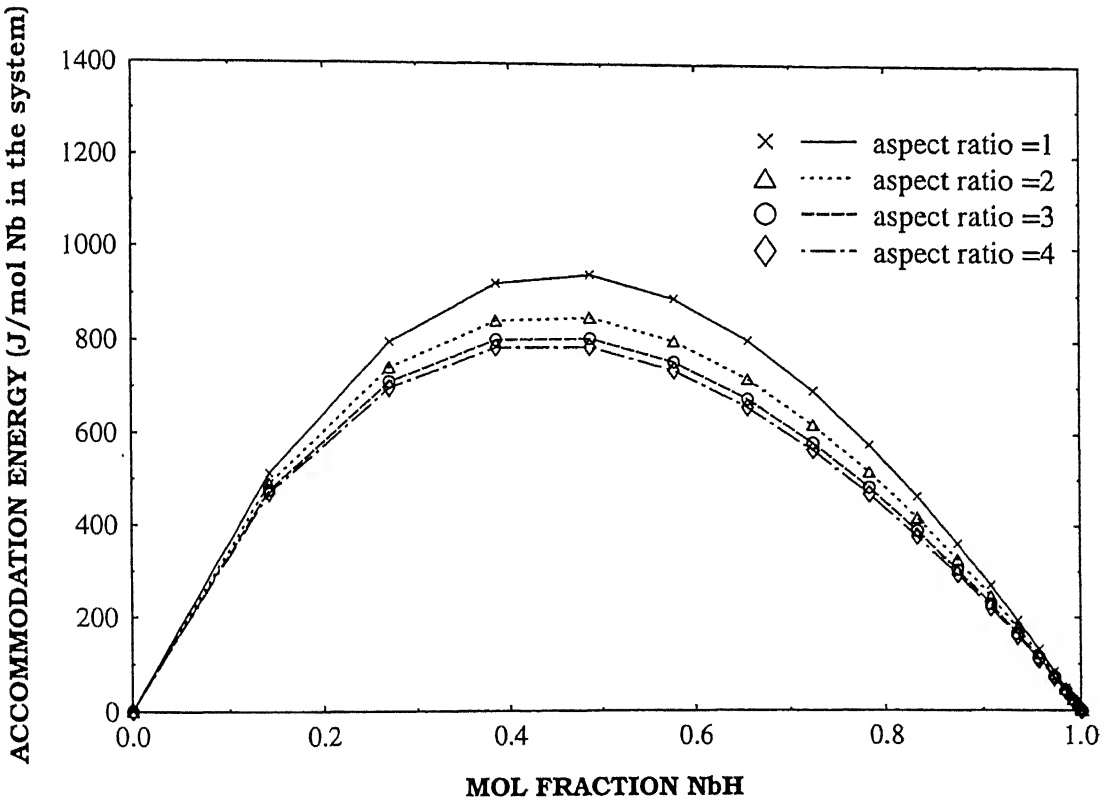

(b) precipitate energy

Figure 18. Variation of accommodation energy stored in the (a) matrix and (b) precipitate during forward transformation through surface to centre path

matrix. The results show that the energy of the matrix (Figure 18a) increases with increase in the aspect ratio of the precipitate, whereas the precipitate energy (Figure 18b) and the total energy of the system (Figure 17) decreases as the aspect ratio of the precipitate increase. When the aspect ratio is one, the matrix will be under pure hydrostatic state of stress. In this case the contribution from the matrix to the total energy of the system is small. As the aspect ratio increases, shear stresses develop inside the matrix thereby increasing its elastic deformation (Table 3) and, therefore, The matrix energy increases with aspect ratio (Figure 18a). The constraint on the precipitate by matrix decreases with an increase in the aspect ratio since it is no longer in the hydrostatic state of stress. This reduces the strain energy inside the precipitate shell (Figure 18b), which is the major contributor to the total energy. The total energy decreases with an increase in the aspect ratio of the precipitate (Figure 17).

The accommodation energy of the system during reverse transformation through surface to centre path is shown in Figure 19 and the accommodation energies stored in the matrix and the precipitate are shown in Figure 20a and Figure 20b, respectively. The energies show the same variation as in the forward transformation through surface to centre path. As in the case of centre to surface transformation, most of the strain energy in the surface to centre case is accommodated in outer phase surrounding the inner phase (i.e. NbH in the forward transformation and Nb in the reverse transformation).

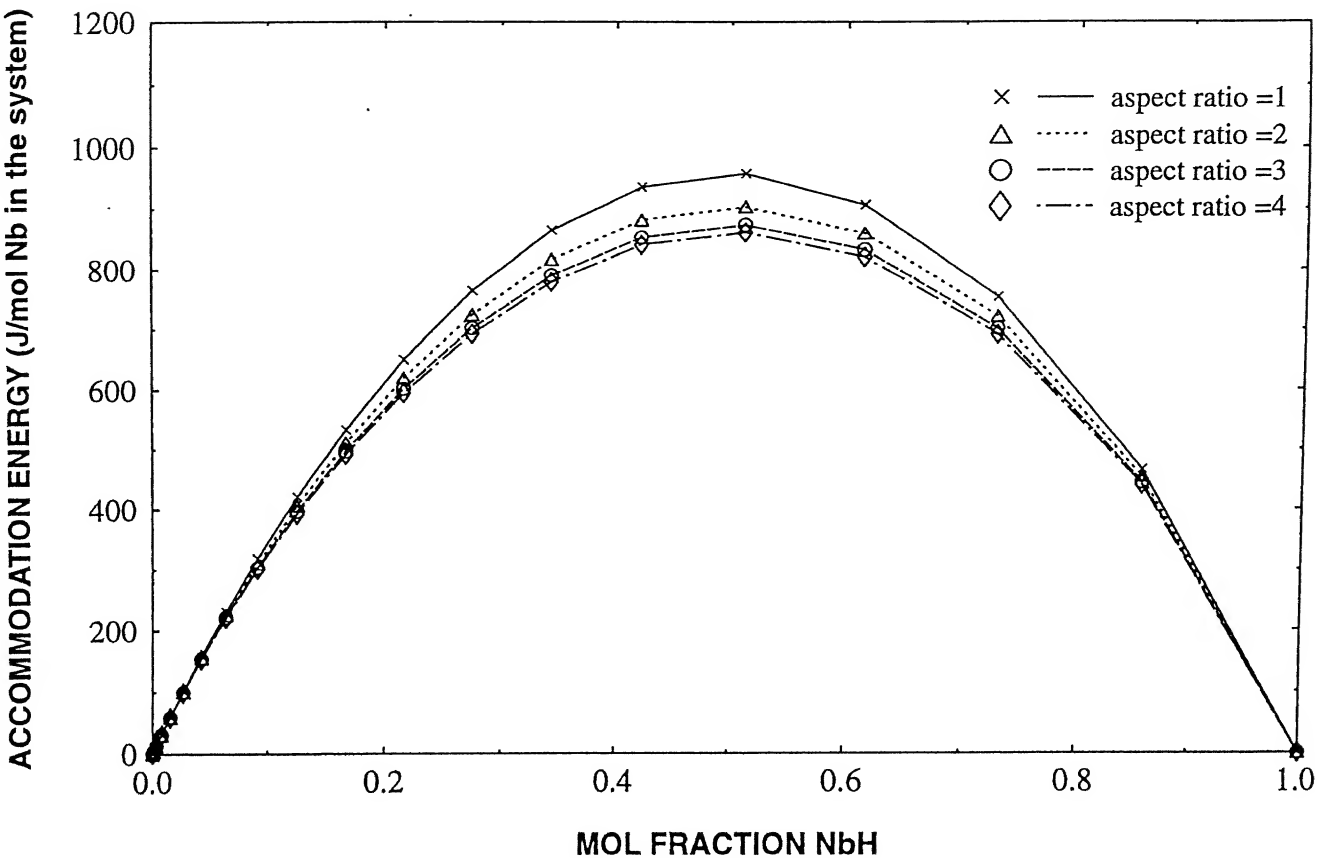

Figure 19. Variation of system accommodation energy during reverse transformation through the surface to centre path for different aspect ratios of the precipitate using elastic axisymmetric analysis.

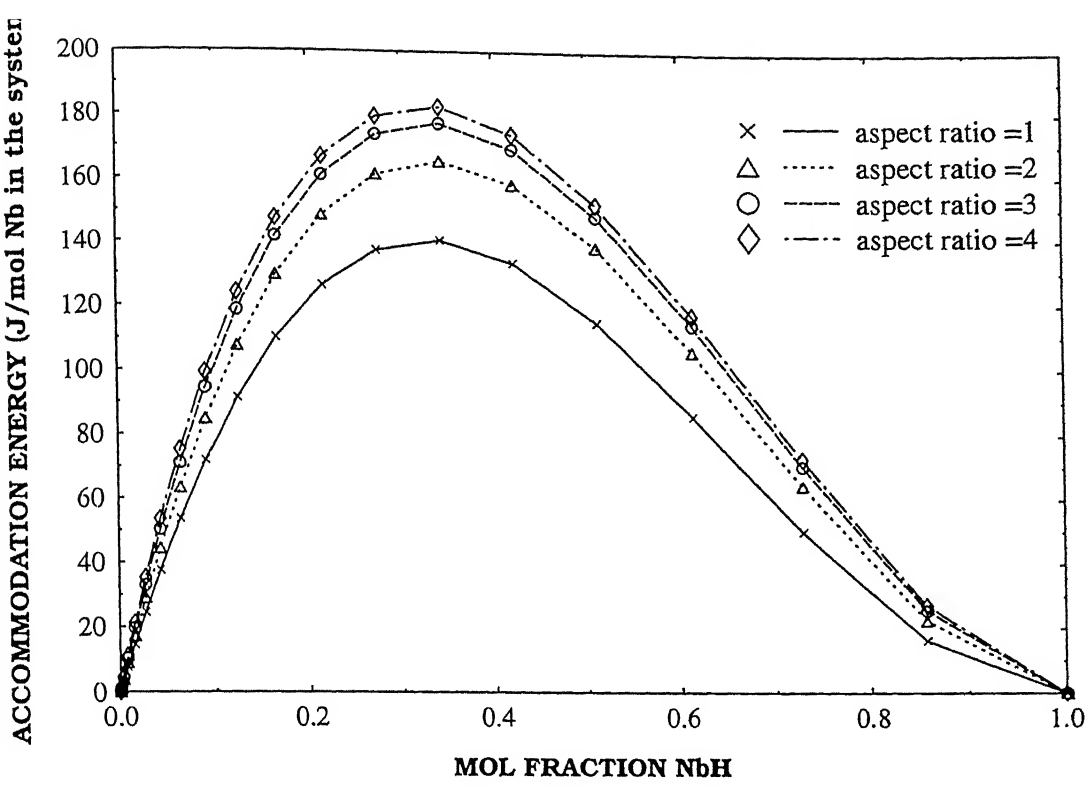

(a) matrix energy

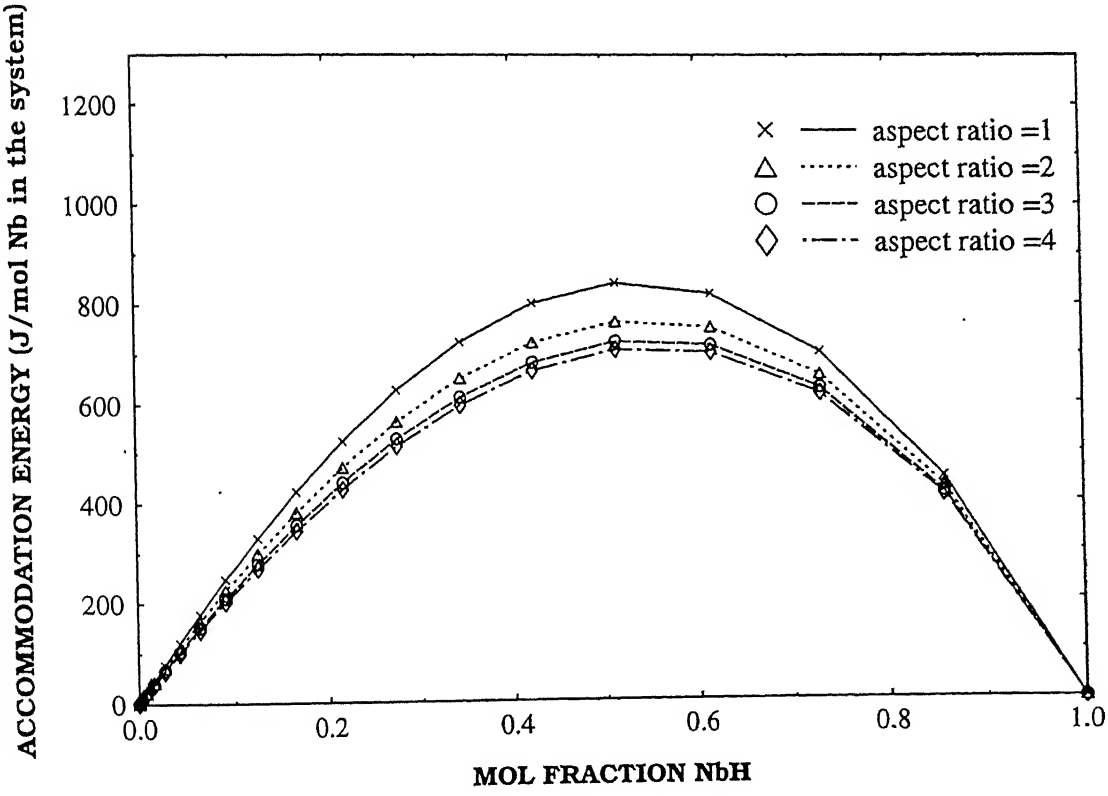

(b) precipitate energy

Figure 20. Variation of accommodation energy stored in the (a) matrix and (b) precipitate during reverse transformation through surface to centre path

4.3.2. Plane stress formulation

Eight-noded isoparametric elements have been utilized to model the system in the case of plane stress formulation. The system is specified with a thickness of 1μm and a cross sectional area of 7.8539×10^{-3} m^2 (which corresponds to the area of a circular system of radius 0.05m). The precipitate is disk shaped. Only one quadrant of the system has been considered due to symmetry. Each quadrant has been divided in to 80 elements with 281 nodal points.

The calculated variation of the elastic strain energy as a function of fraction of matrix that has been transformed to precipitate for the forward ($\alpha \rightarrow \beta$) and reverse ($\beta \rightarrow \alpha$) hydrogen transformations by the centre to surface and surface to center paths are presented in Figures 21 and 22, respectively. The energy is expressed as joules per mole of metal in the system. The abscissa denotes the volume fraction of hydride in the system at each stage of transformation.

The elastic strain energies shows the same variation as that in axisymmetric case. However, as the constraints to the free expansion is lesser in plane stress case compared to the axisymmetric case, the numerical values of the strain energy at any particular stage of transformation is lower in plane stress case when compared to axisymmetric case.

4.4 ELASTO-PLASTIC ANALYSIS

The finite element model described in the earlier section to evaluate the elastic strain energies during room temperature α-β hydrogen transformation yields results comparable

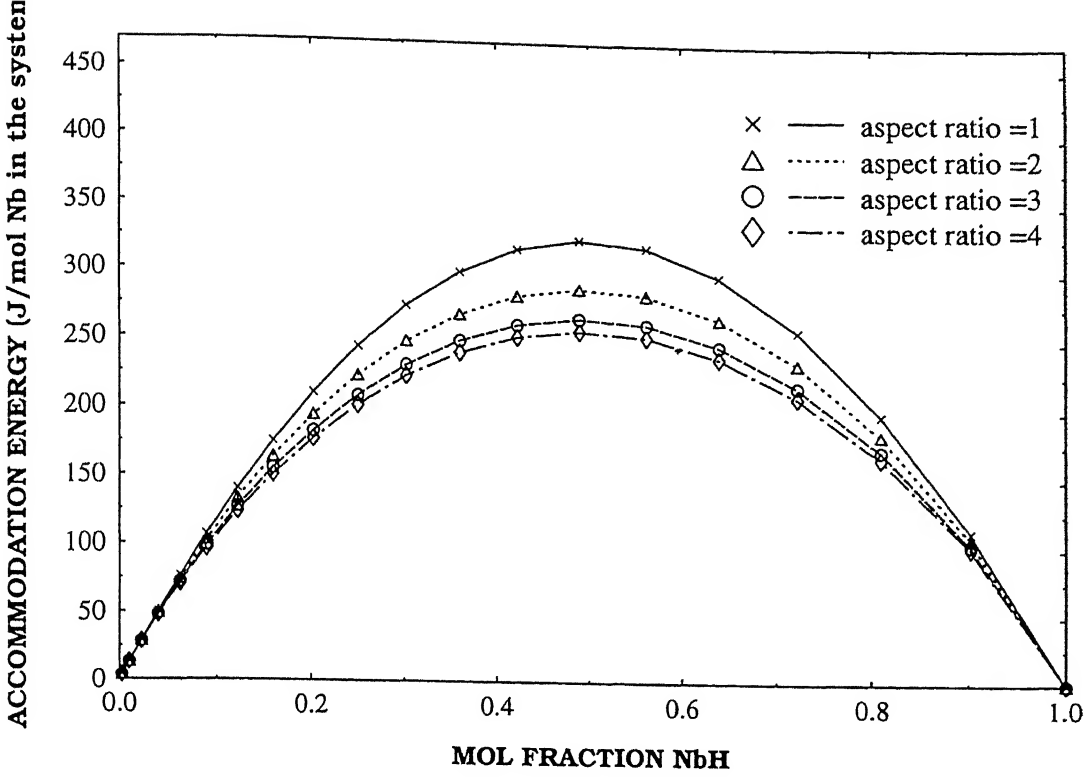

(a) forward transformation

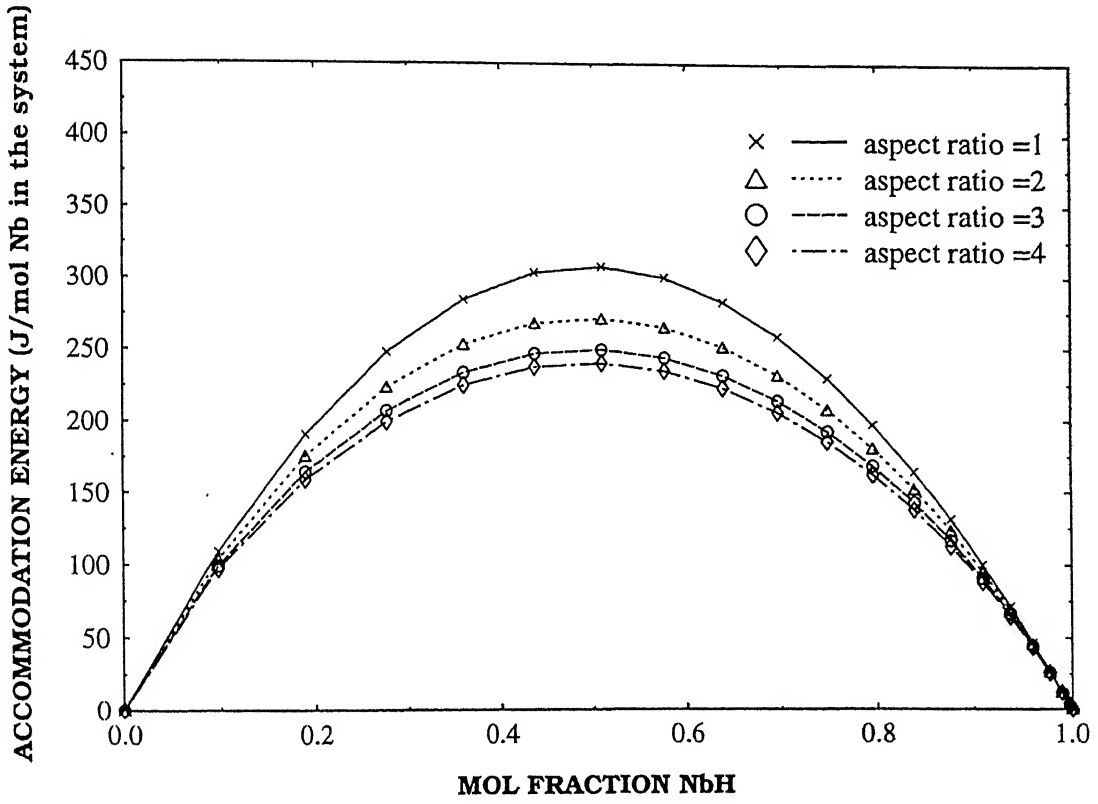

(b) reverse transformation

Figure 21. Variation of system accommodation energy during (a) forward and (b) reverse transformation through centre to surface path for different aspect

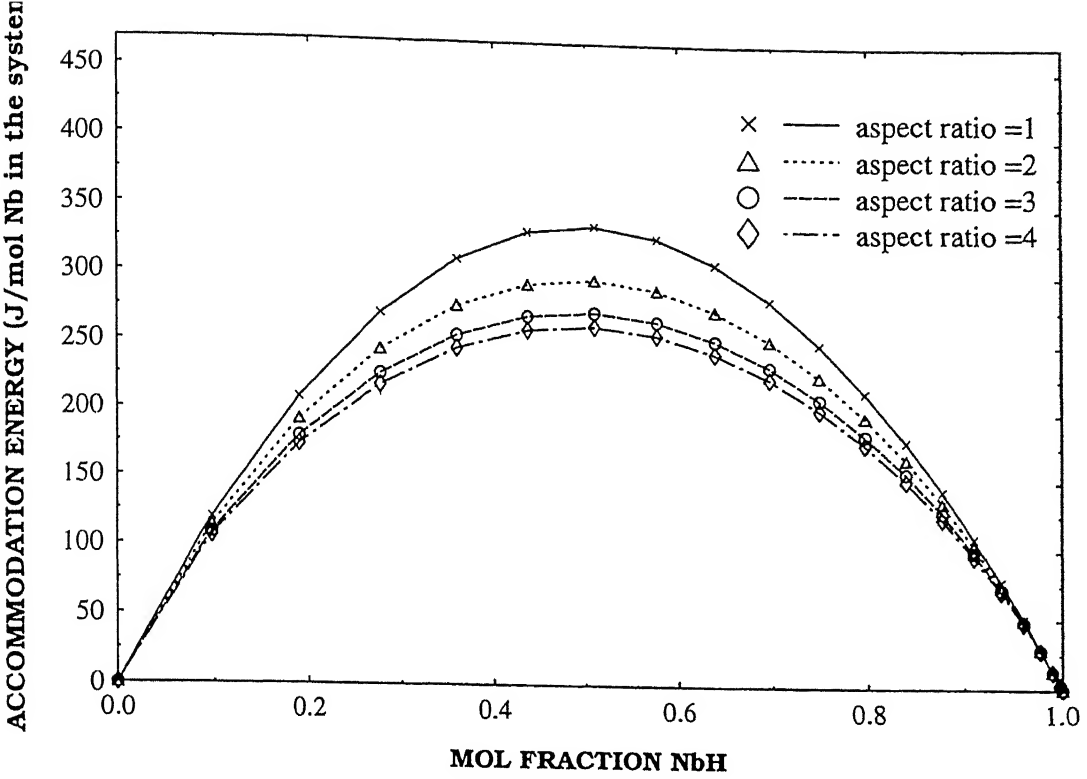

(a) forward transformation

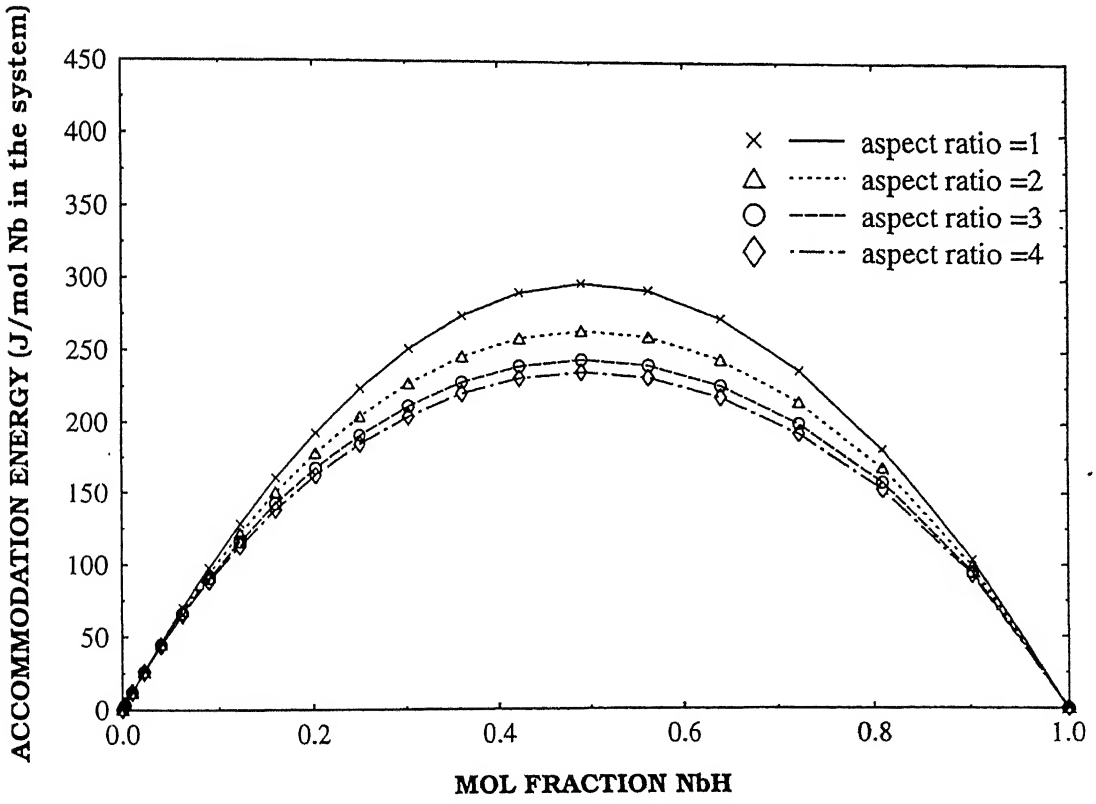

(b) reverse transformation

Figure 22. Variation of system accommodation energy during (a) forward and (b) reverse transformation through surface to centre path for different aspect

to the elastic strain energies obtained with other mathematical models [2,17]. However, the calculated strain energy in the Nb-H system would be largely reduced due to plastic deformation which is expected to occur due to the relatively large misfit strain(~4%) involved during the α-β transformations in the Nb-H system [1]. Transmission microscopic studies of hydride formation in niobium [31,38] have revealed that α phase deforms plastically during both the forward and reverse hydrogen transformation. The effect of plastic deformation in lowering elastic strain energy during solid phase transformation has been earlier studied by Lee et al by considering the matrix to be ideally plastic [23] and to strain harden according to the power law [24]. However, these models cannot be used to estimate the accommodation energy if the precipitate deforms plastically as is the situation during the reverse ($\beta \rightarrow \alpha$) hydrogen transformation through centre to surface path in metal hydrogen systems.

The present FEM model has been utilized to evaluate the elasto-plastic accommodation energies during the α-β transformations in the Nb-H system. The results obtained by both the plane stress analysis (where the precipitate is disk shaped) and the axisymmetric analysis (where the precipitate is an oblate spheroid) are presented below. The effect of changing the aspect ratio on the accommodation energy of the system is specifically addressed. NbH is assumed to be elastic as it has been experimentally observed that β phase does not yield during the hydrogen transformation in Nb-H system [39].

4.4.1. Axisymmetric formulation

The axisymmetric modelling of the ellipsoidal (prolate spheroid) system was performed using eight-noded isoparametric elements. The dimensions of the prolate spheroid were chosen such that the total volume is same for all aspect ratios. The system is specified by a volume of 5.235e-4 m^3 which corresponds to a sphere of radius 0.05m. It has been observed that a small change in volume does not affect the accommodation energies which have been normalized by dividing the energy by the volume of the system. The evaluation of the accommodation energies have been performed for different aspect ratios (1, 2, 3 and 4). Only one quadrant of the system has been considered due to the symmetry. Each quadrant was divided in to 80 elements with 281 nodal points. The transformation was modelled to occur in 20 steps. In each step, the load corresponding to the volume mismatch due to transformation was applied in 5 steps.

In the elasto-plastic analyses, NbH is assumed to be elastic in all the transformations, and hence the plastic deformation, if any, is confined to only Nb. The results of the elasto-plastic finite element analysis are presented in Figures 23 through 32. The strain energies are expressed as a function fraction of matrix transformed. Figure 23 compares the accommodation energies for the forward transformation through centre to surface path obtained by elastic and elasto-plastic analysis in the case of a spherical precipitate. The total accommodation energy in the elasto-plastic case is lower than the elastic strain energies generated in the elastic analysis except

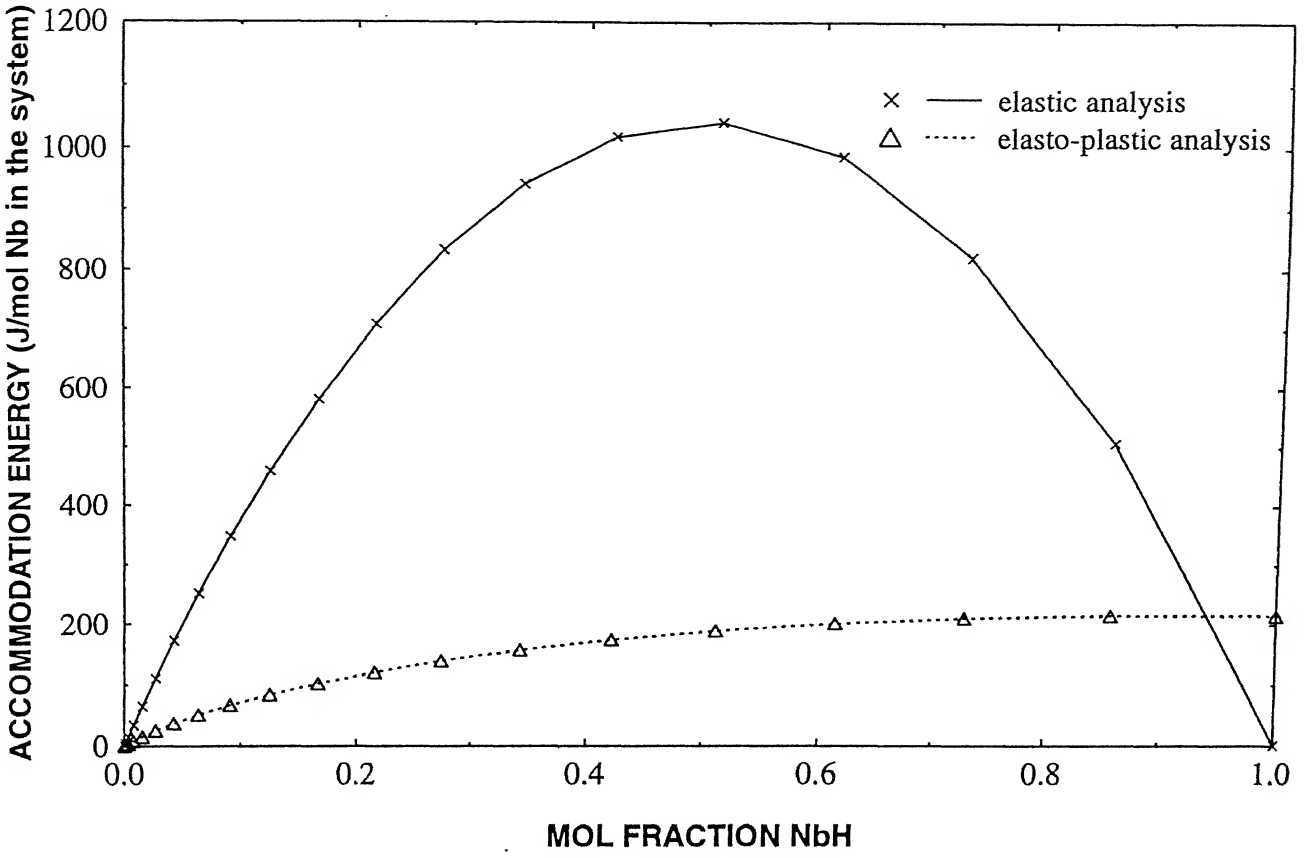

Figure 23. Comparison of system accommodation energy obtained by elastic and elasto-plastic axisymmetric analyses during forward transformation through centre to the centre to surface path.

at the end of transformation. This reduction in the total energy in the elasto-plastic case is due to the plastic deformation in the matrix. The energy in the matrix due to plastic deformation is irreversible which is expended during the transformation. This appears as the residual energy at the end of the transformation in the elasto-plastic case. The present results are in conformity with that of Sen et al [14].

The system energy obtained by the elasto-plastic analysis of the forward transformation assuming centre to surface path is give in Figure 24, while the matrix and precipitate energies are provided in Figures 25a and 25b. Here NbH, which is assumed to be elastic, precipitates inside the matrix (Nb) and grows outwards. The total strain energy of the system for different aspect ratios of the ellipsoidal precipitate is shown in Figure 24 which is the sum of plastic energy of the matrix and elastic energy of both matrix and precipitate. The energy of the matrix and precipitate are shown in Figures 25a and 25b, respectively. The major contribution to the system strain energy, at any stage of transformation, is from the matrix. Figure 25b shows an increase in accommodation energy of the precipitate with an increase in aspect ratio. When the aspect ratio is one the precipitate is under hydrostatic state of stress. As the aspect ratio is increased, shear stresses also develop inside the precipitate and therefore, strain energy of the matrix is composed of elastic and plastic component, of which plastic strain energy is dominant. The computed values of deviatoric components of stress inside matrix, which causes the plastic deformation

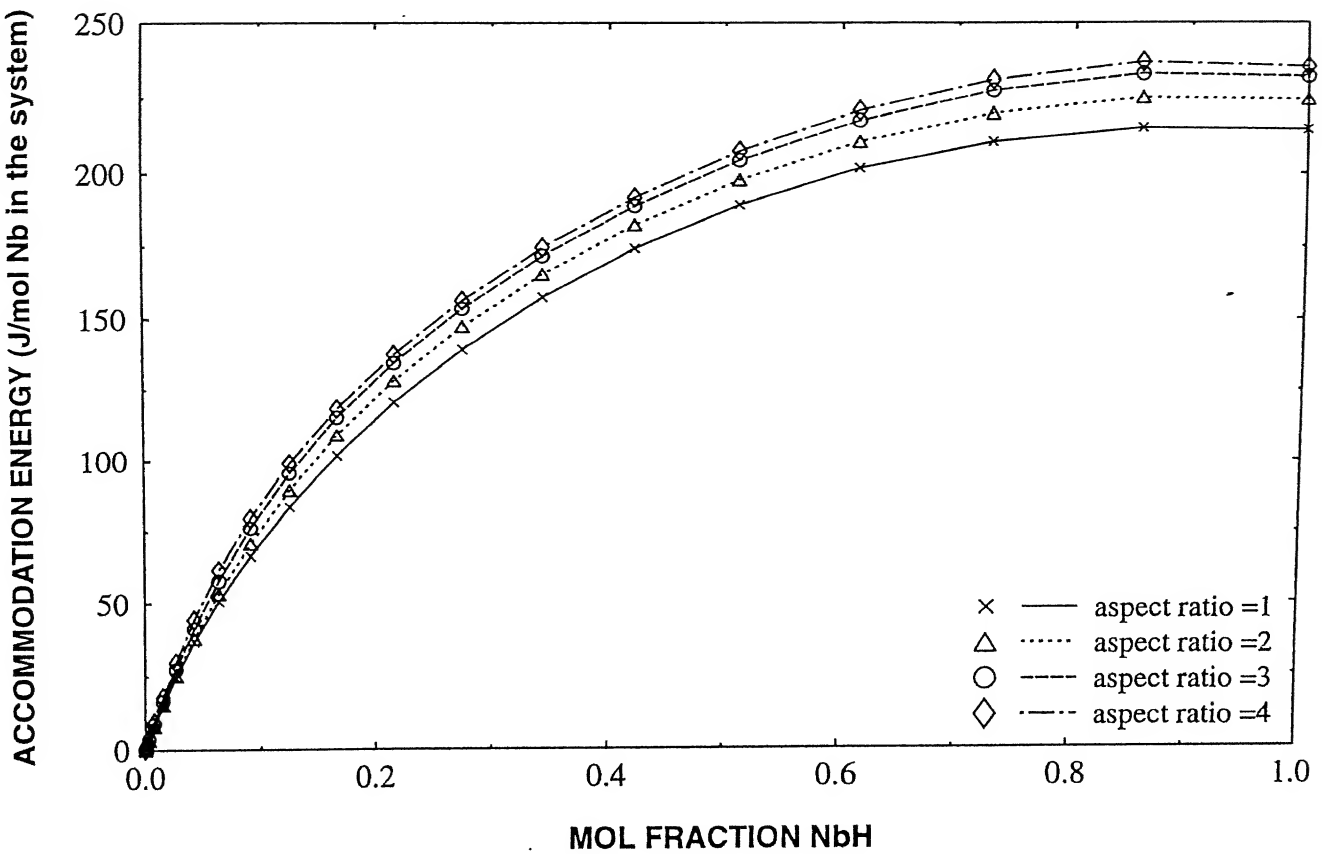

Figure.24 Variation of system elasto-plastic accommodation energy during forward transformation through centre to surface path for different aspect ratios of the precipitate using axisymmetric formulation.

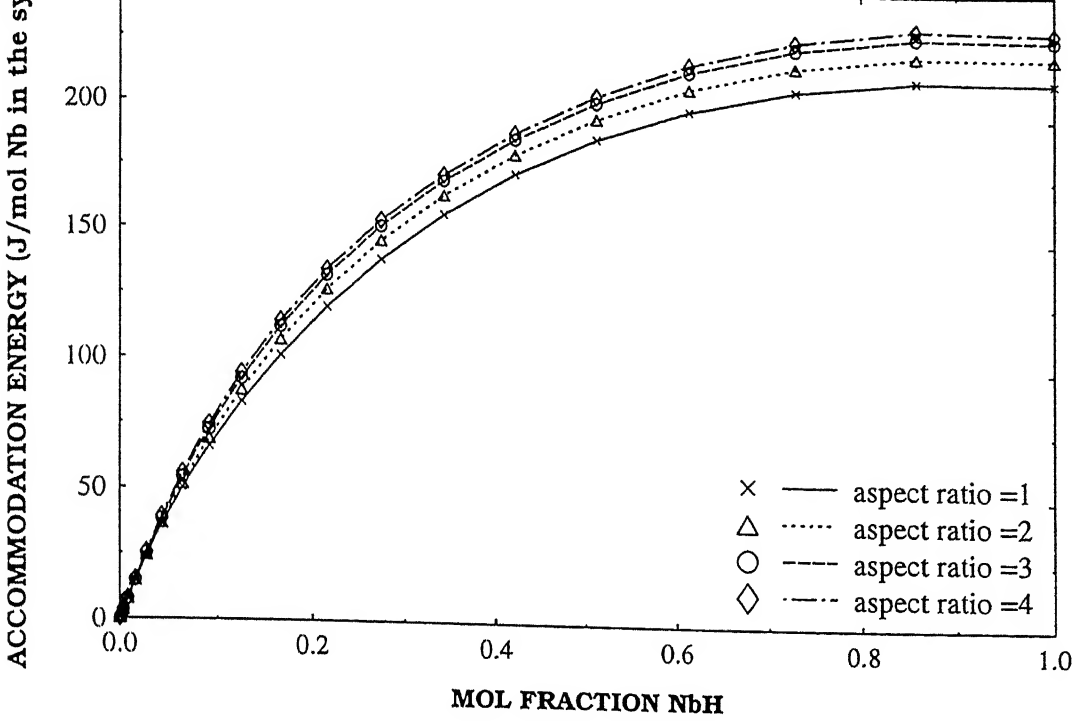

(a) matrix energy

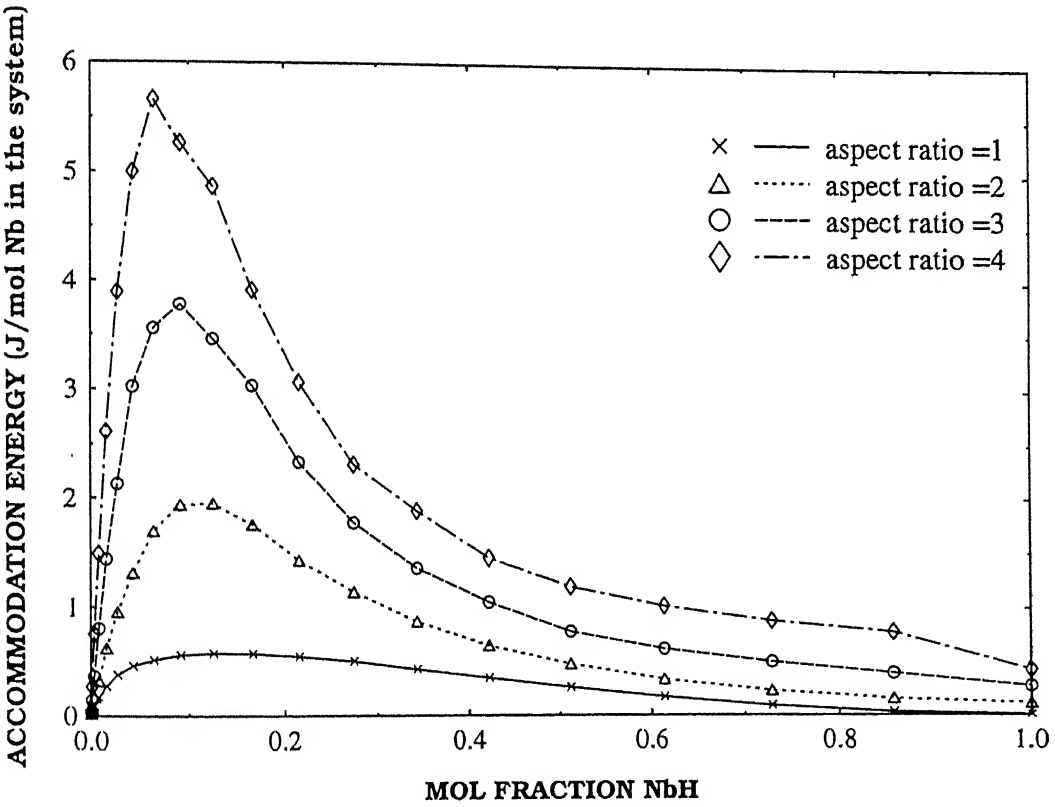

(b) precipitate energy

Figure 25. Variation of elasto-plastic accommodation energy stored in the (a) matrix and (b) precipitate during forward transformation through centre to surface path for different aspect ratios of the precipitate using axisymmetric

increases as the aspect ratio increases. Therefore, the strain energy of the matrix increases with increase in aspect ratio (Figure.25a). The strain energy of the matrix is large relative to that of the precipitate, and hence the total energy of the system increases as aspect ratio increases (Figure 24).

The variation of the strain energy in the case of precipitation of Nb (reverse transformation) from the centre of the system outwards is presented in Figures 26 through 28. Here the matrix phase (NbH) is assumed to be elastic. The energies are given as a function of progress of transformation and it is to be noted that at the beginning of transformation the mole fraction of the NbH (abscissa) is one and it decreases as the transformation progresses and finally reaches zero when the whole matrix is transformed to Nb. The matrix strain energy (Figure 27a) which is purely elastic, decreases with increase in aspect ratio in the first few stages of transformation. This variation is similar to the results obtained by the linear elastic analysis (Figure 16a). The strain energy of the precipitate (Nb) is the sum of elastic and plastic strain energies of which the elastic part is significant. The elastic and plastic part of the strain energy of the precipitate is shown in Figure 28. The state of stress is not uniform about the θ-axis and this nonuniformity becomes more pronounced as the aspect ratio increases. It has been observed that the plastic part of the strain energy stored in the precipitate increases with increase in aspect ratio, whereas the elastic strain energy decreases. This decrease in elastic part of the total energy of the phase in the initial stages of

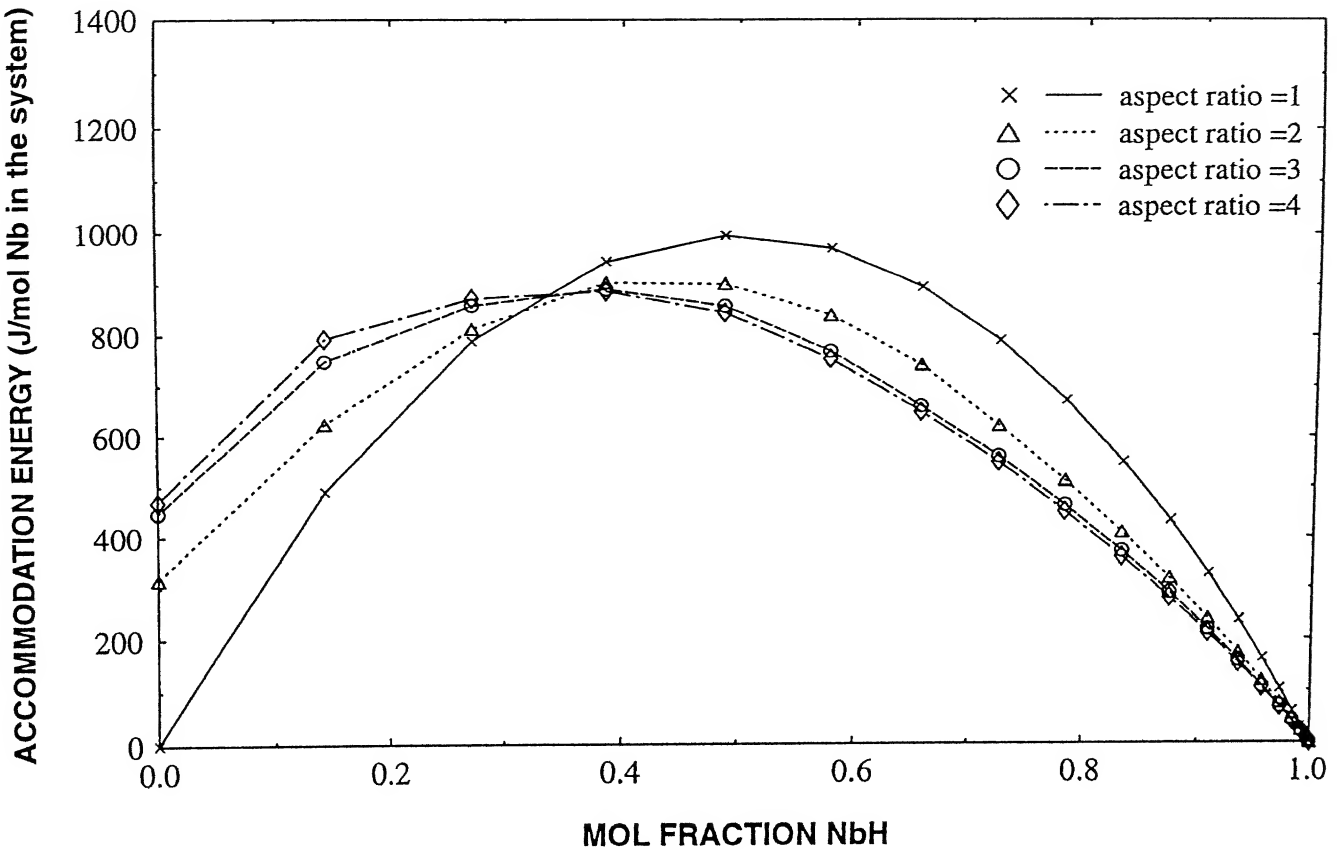

Figure.26 Variation of system elasto-plastic accommodation energy during reverse transformation through the centre to surface path for different aspect ratios of the precipitate using axisymmetric formulation.

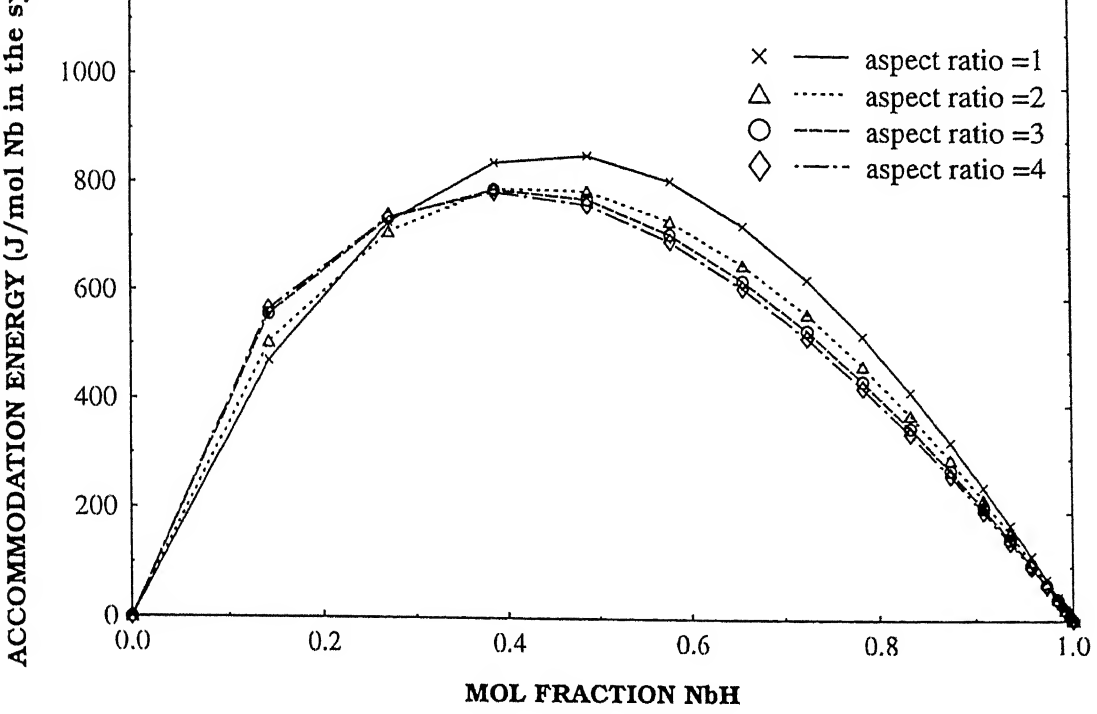

(a) matrix energy

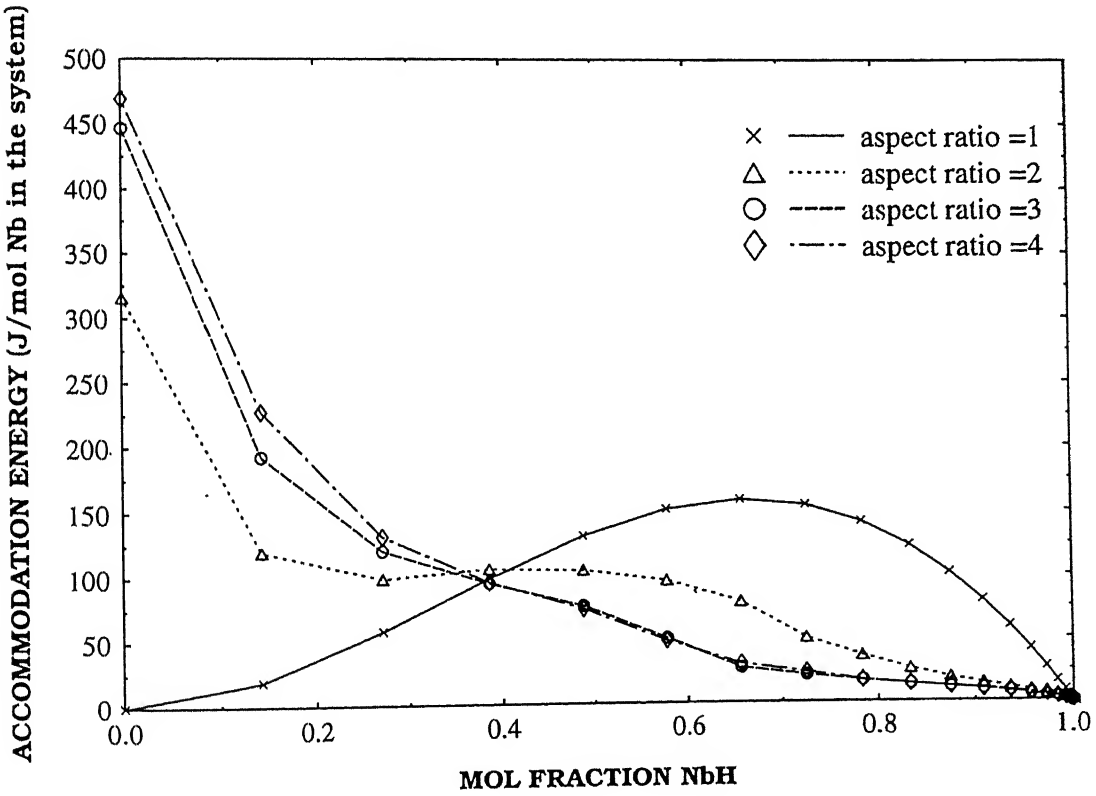

(b) precipitate energy

Figure.27 Variation of elasto-plastic accommodation energy stored in the (a) matrix and (b) precipitate during reverse transformation through the centre to surface path for different aspect ratios of precipitate using axisymmetric formulation

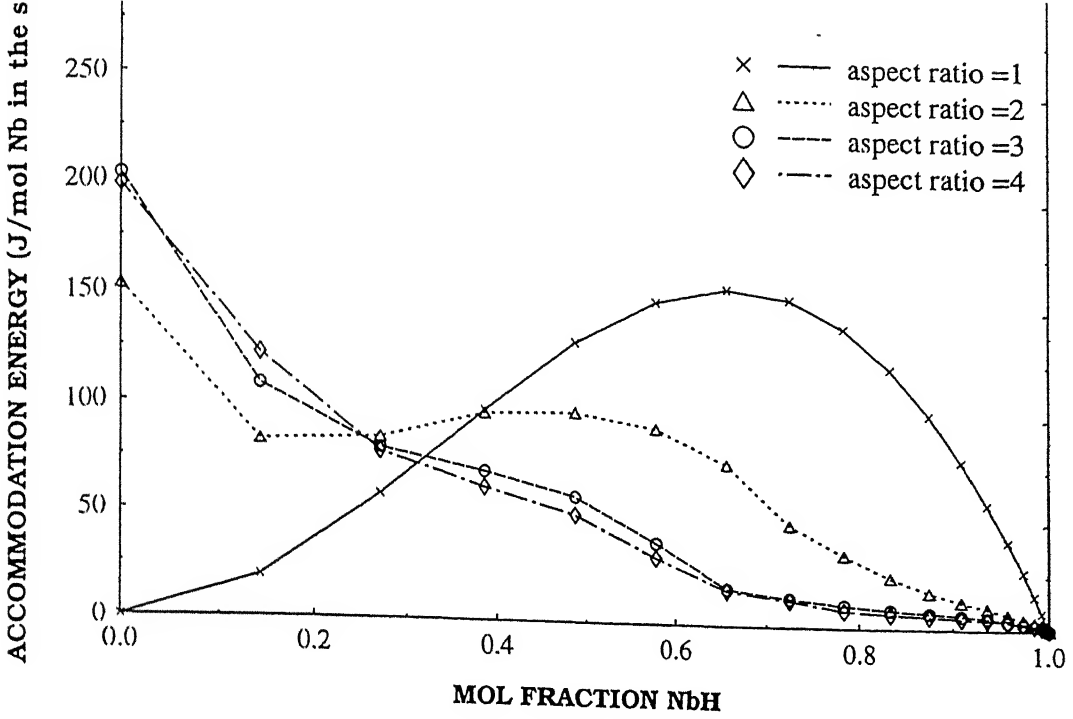

(a) elastic strain energy

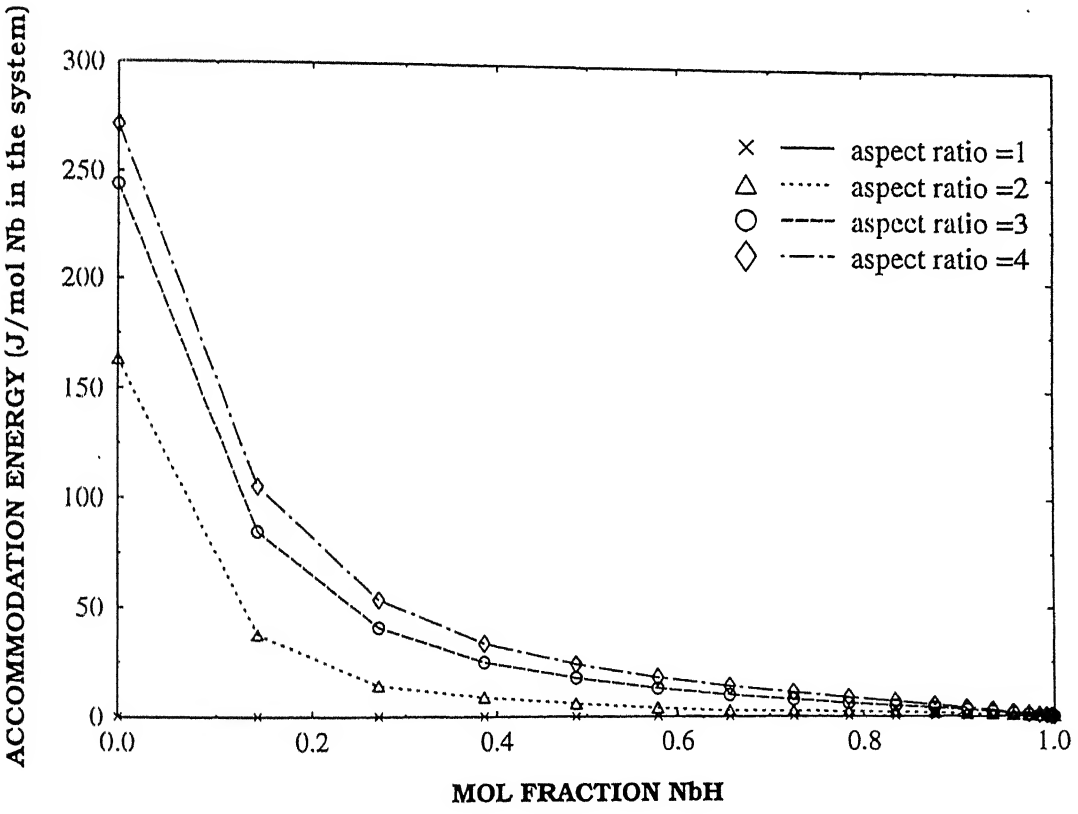

(b) plastic strain energy

Figure 28. Variation of (a) elastic and (b) plastic part of accommodation energy stored in the Nb precipitate during reverse transformation through the centre to surface path for different aspect ratios of the precipitate using

transformation with increasing aspect ratio is found in all the situations where the phase is plastically deforming. The elastic energy is maximum for the precipitate having aspect ratio one and decreases as the aspect ratio increases. The above picture is true only for the initial stages of transformation. The non-uniform plastic deformation of the precipitate leads to the locking up of elastic strains inside the precipitate. The effect of locked up elastic strains is more pronounced in the latter stages of transformation, i.e when considerable plastic deformation has already occurred. Since the stress distribution will be more uniform as aspect ratio is nearly one, the locked up elastic strains will be smaller for these cases. In the latter stages of transformation, the elastic strain energy of the precipitate is small in the case of aspect ratio equal to one and increases as aspect ratio increase (Figure 28a). The plastic part of strain energy of the precipitate increases with an increase in aspect ratio as shown in Figure 28b. The variation of the total energy of the precipitate (Figure 27b) is same as that of elastic part of the strain energy. The locked up elastic strain inside the precipitate which is present in the latter stages of transformation offer constraint to the matrix. The effect of this constraint is to increase the elastic strain energy of the matrix for higher aspect ratios in the latter stages of transformation as shown in Figure 27a. Figure 26 shows that the pattern of variation of total accommodation energy of the system is same as that of the NbH matrix. But at the end of transformation there will be net energy lost due to the

irreversible plastic deformation.

The elasto-plastic analysis of the $\alpha \rightarrow \beta$ transformation has also been performed when the transformation begins from the surface and the precipitate grows inwards (surface to centre path). The results of this analysis for the forward transformation is given in Figures 29 and 30. In this case NbH precipitates as a hollow sphere. The precipitate will not yield at any stage of transformation due to its high work hardening parameter and high yield strength. When the precipitate is a hollow sphere (aspect ratio 1), the matrix is under hydrostatic state of stress. Therefore there will be no plastic deformation of the matrix in this case. As the aspect ratio increases, the strain energy inside the precipitate, which is purely elastic, decreases (Figure 30b) as obtained in the linear elastic analysis (Figure 18b). The strain energy of the matrix (Nb) for aspect ratio other than one has two components, elastic strain energy and plastic strain energy. It has been observed that the plastic part of strain energy of the matrix increases with an increase in aspect ratio whereas the elastic strain energy of the matrix decreases with an increase in aspect ratio. Note that this is pattern of variation is same as the variation of precipitate energy that obtained for initial stages of the reverse hydrogen transformation from centre to surface. The variation of the total energy of the matrix is shown in Figure 30a. The total accommodation energy of the system which is the sum of the energies of matrix and the precipitate is shown in Figure 29. The total energy follows the path of precipitate energy in the initial stages of transformation but at

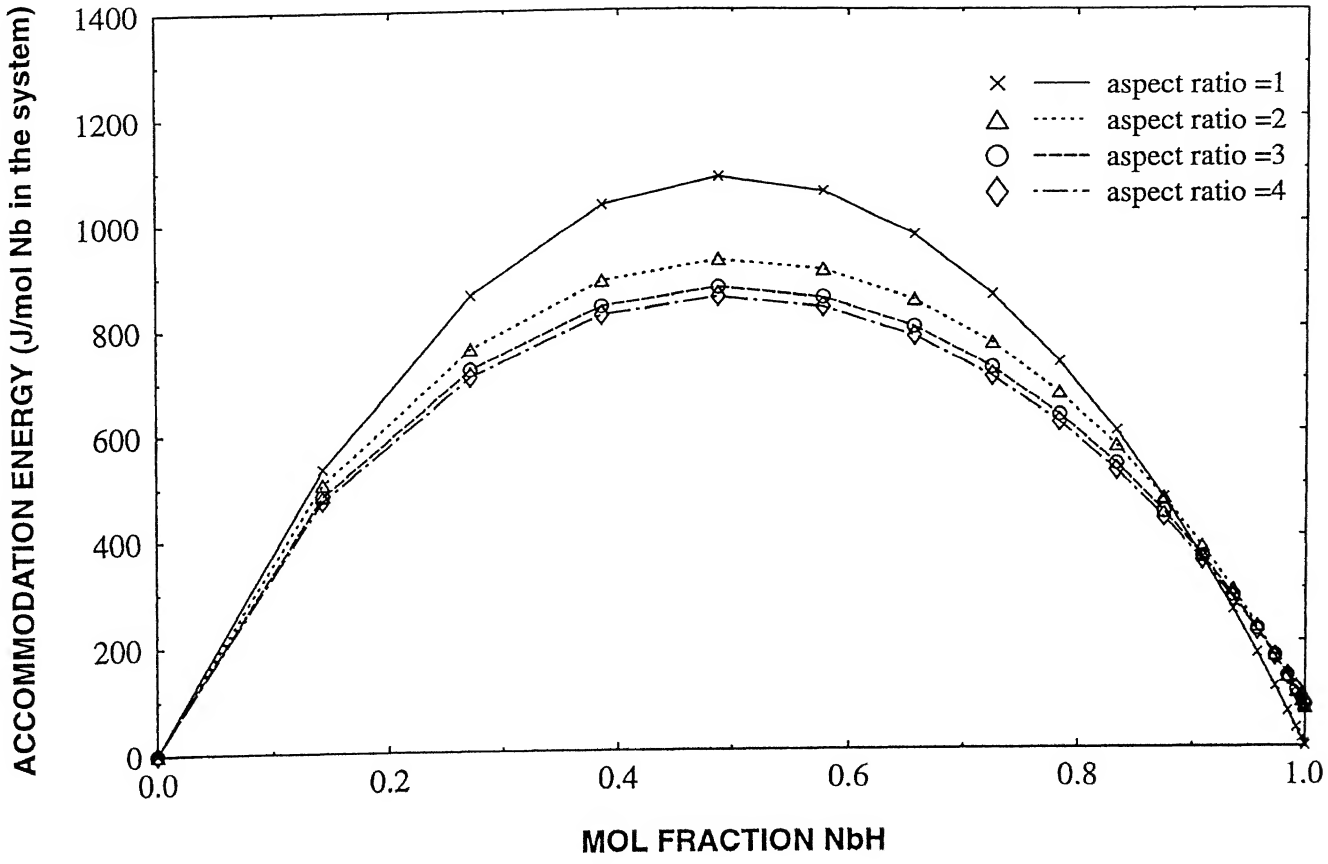

Figure.29 Variation of system elasto-plastic accommodation energy during forward transformation through the surface to centre path for different aspect ratios of the precipitate using axisymmetric formulation.

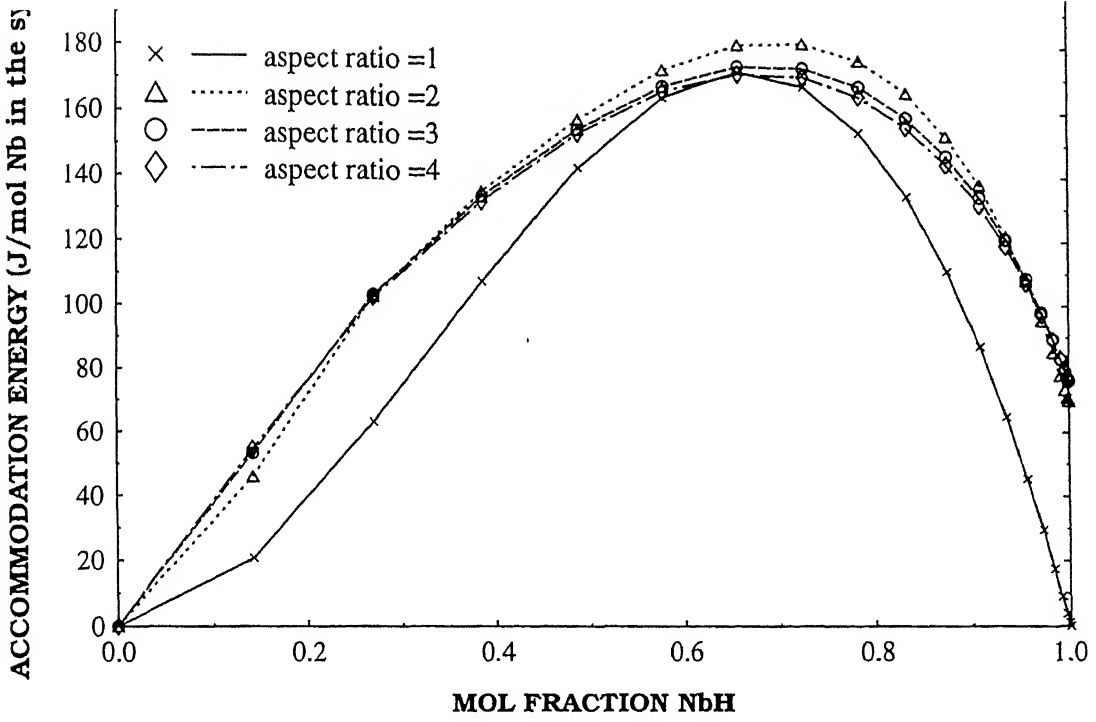

(a) matrix energy

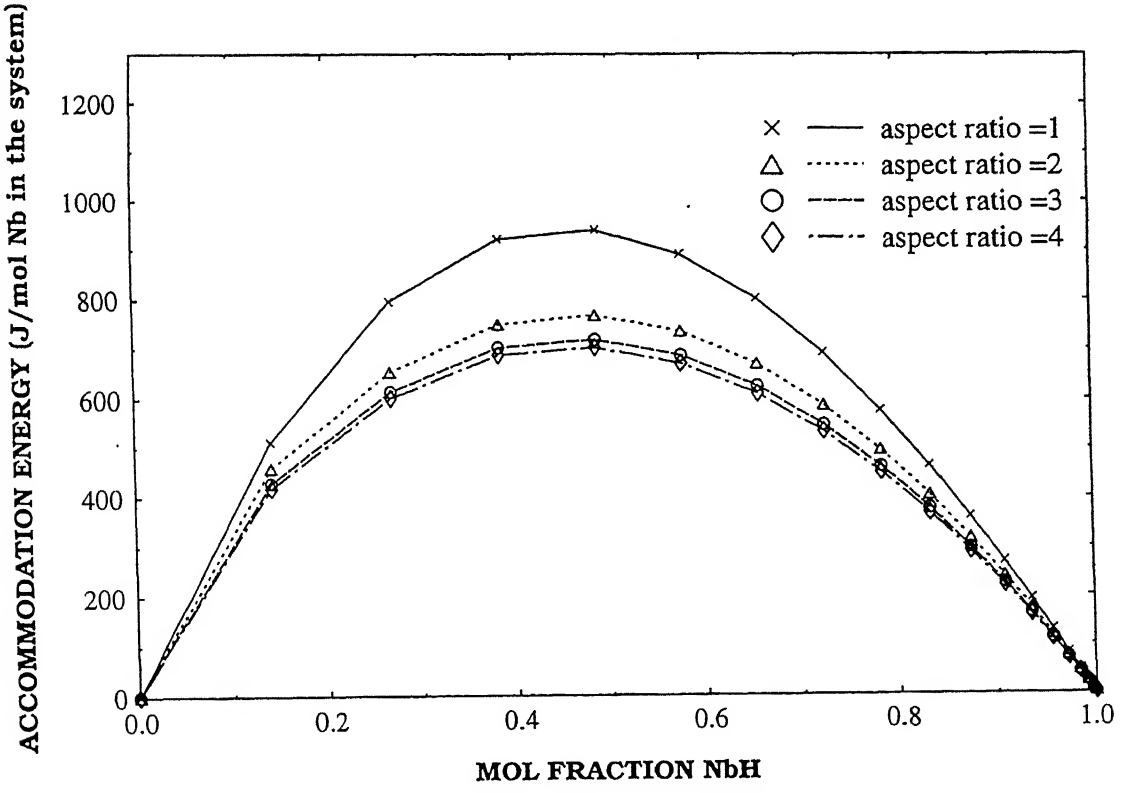

(b) precipitate energy

Figure 30. Variation of elasto-plastic accommodation energy stored in the (a) matrix and (b) precipitate during forward transformation through surface to centre path for different aspect ratios of the precipitate using axisymmetric formulation.

the end of transformation total energy is equal to plastic part of the strain energy. The results shows that for aspect ratio other than one there is not much change in the strain energy at the end of transformation with change in aspect ratio.

Figures 31 and 32 present the accommodation energies during the reverse transformation (NbH→Nb) progressing from the surface towards centre of the system. The precipitate in this case is Nb which yields due to the volume misfit strain as in the case of forward transformation through centre to surface path. Figure 32b shows the variation of the precipitate (Nb) energy during the transformation. The elastic energy of the precipitate is found to be negligibly small in this case. As the aspect ratio increases the plastic part of the strain energy inside the Nb precipitate shell increases and therefore the total strain energy of the precipitate increases. The inner NbH matrix here is assumed to be elastic throughout the transformation. The energy of the matrix (NbH) is shown in the Figure 32a which shows that the energy of the matrix increases with the aspect ratio similar to the results obtained by linear elastic analysis of the reverse transformation through surface to centre path (Figure 20a). The total energy of the system is presented in Figure 31 as a function of fraction transformed and the variation is similar to the variation of energies of the precipitate shell which is prime contributor to the total energy. The strain energy at the end of transformation is found to be more or less same for all the aspect ratios other than one.

Table 4 presents the residual energies present at the

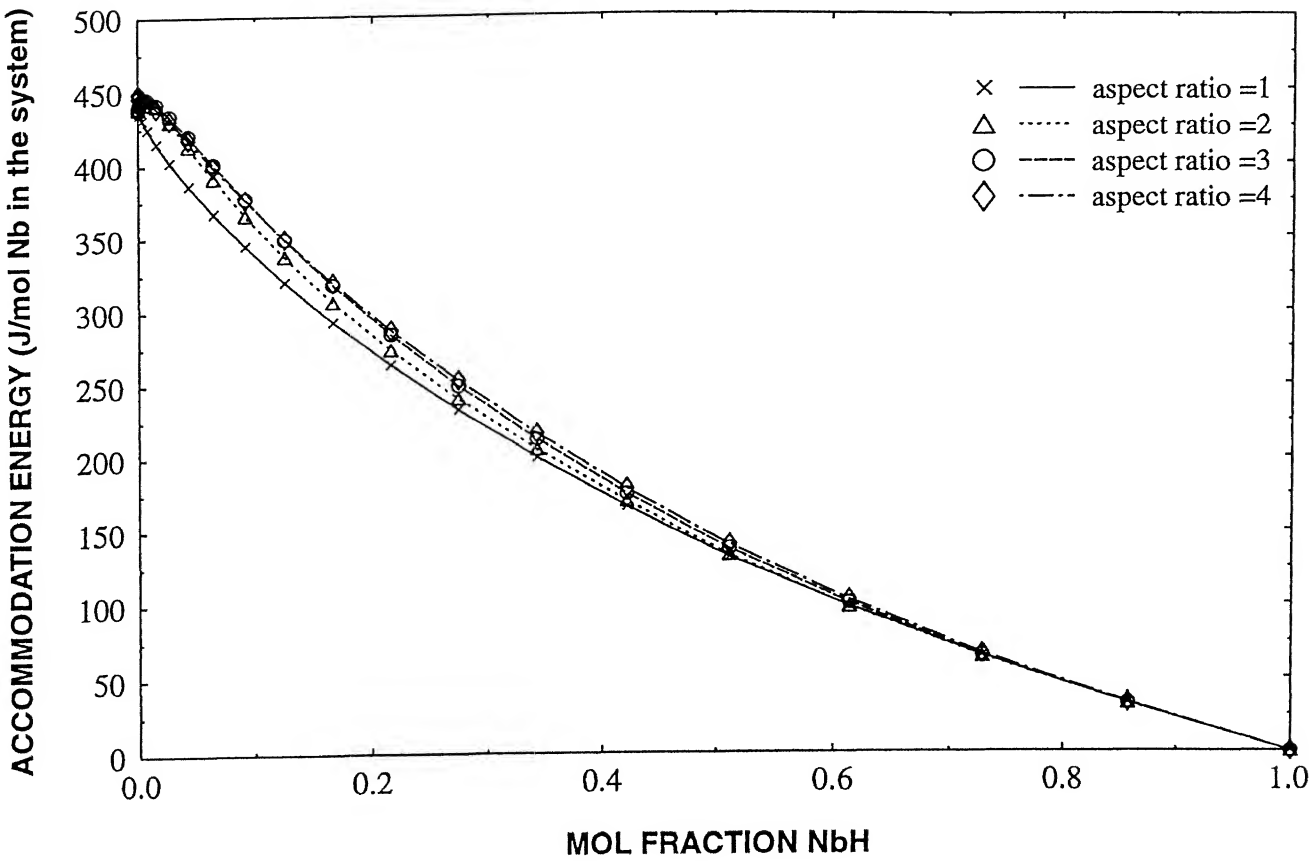

Figure.31 Variation of system elasto-plastic accommodation energy during reverse transformation through the surface to centre path for different aspect ratios of the precipitate using axisymmetric formulation.

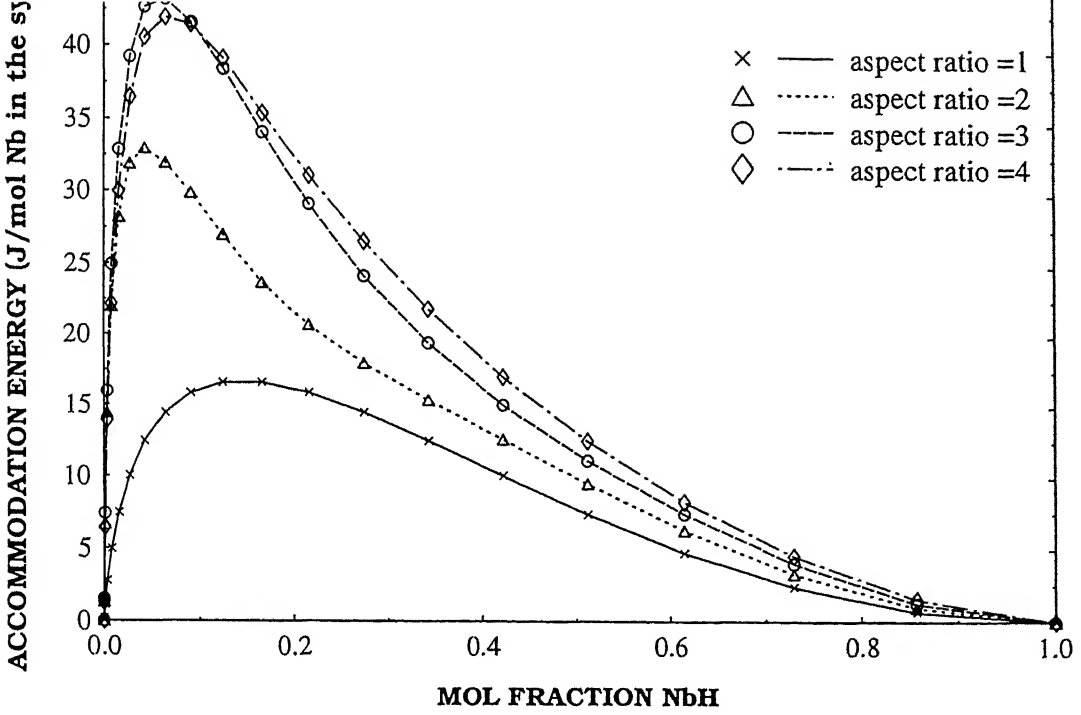

(a) matrix energy

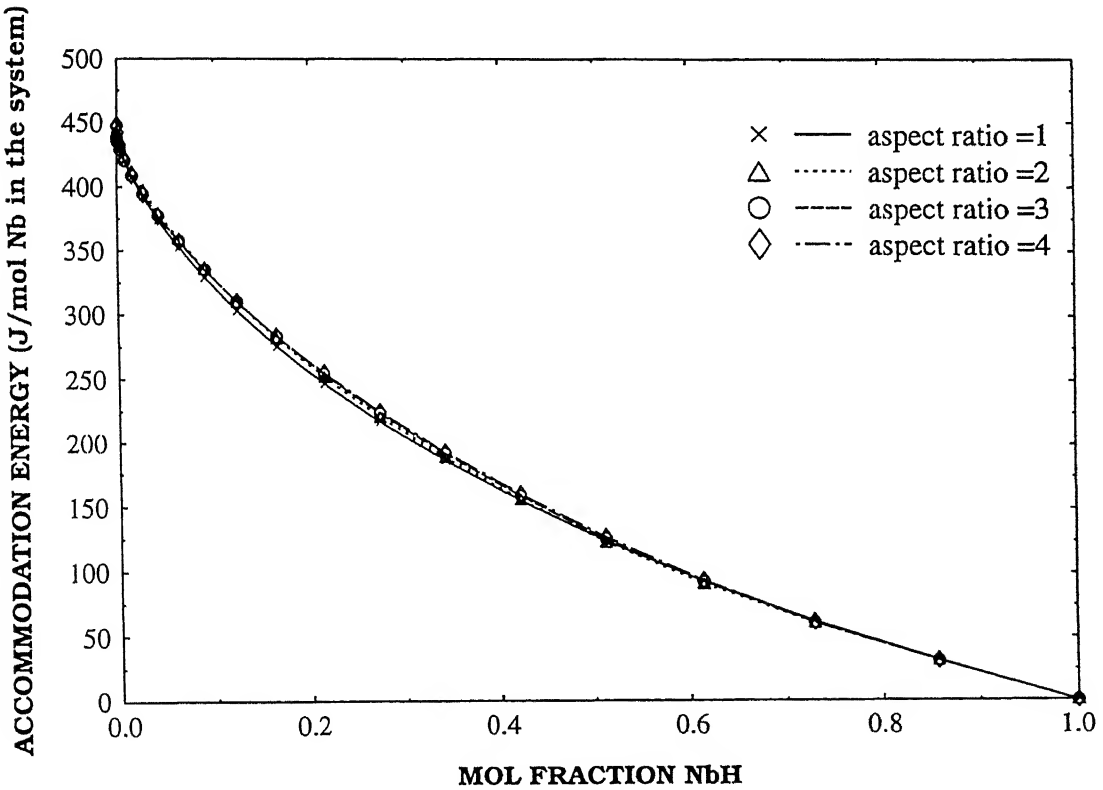

(b) precipitate energy

Figure.32 Variation of elasto-plastic accommodation energy stored in the (a) matrix and (b) precipitate during reverse transformation through surface to centre path for different aspect ratios of the precipitate using axisymmetric formulation

Table 4. Elasto-plastic accommodation energy (joules per mol metal) at the end of hydrogen transformation in Nb-H system obtained by axisymmetric formulation.

Transformation path	aspect ratio of the precipitate			
	1	2	3	4
centre to surface: forward	214.71	224.64	232.22	235.40
reverse	0.00	315.97	446.73	469.07
surface to centre: forward	0.00	73.00	78.04	78.47
reverse	437.25	439.06	437.98	446.56

end of transformation for all the cases described above. In the case of a spherical precipitate (for aspect ratio 1), the strain energy at the end of transformation are zero for reverse transformation through centre to surface path and forward transformation through surface to centre path. In both cases, niobium is under hydrostatic state of stress. The maximum energies are obtained for the reverse transformations wherein the final phase is plastically deformed niobium. It can also be noticed in the table that the accommodation energies increase with increasing aspect ratio except in the case of reverse transformation by the surface to centre to centre path. This could be due to the presence of shear components in increasing magnitude as the aspect ratio is increased which results in a larger amount of plastic deformation energies with increasing aspect ratios. The accommodation energy at any given aspect ratio in the case forward transformation is significantly lower for the surface to centre path when compared to the centre to surface path. As noticed earlier, in the case of elastic analysis, most of the energy is accommodated by the outer phase that surrounds the inner phase due to the greater deformation suffered by it. When the deformable metallic matrix (Nb) surround the inner phase (as in the case of forward transformation through the centre to surface path), it plastically deforms to a greater extent than when the metallic matrix is present as the inner phase (as in the case of forward transformation by the surface to centre path). Therefore, the energies are down for the latter case when compared to the former.

The Table 4 provides the accommodation energies at the

end of transformation. In order to understand the behaviour at midway in the progress of transformation, the individual accommodation energies of the precipitate and matrix phases for the centre to surface forward and surface to centre reverse transformations at 50% transformation are presented in the Table 5. Note that, at 50% transformation, in both these cases, the inner phase NbH is enveloped by the outer phase Nb. The results in Table 5 indicates that, as already noted, the system accommodation energy in the elastic case decreases with increasing aspect ratio and this due to the major contribution of the outer phase (Nb), whose accommodation energy shows a similar trend in the variation with aspect ratio. As already noted, this is reflected in the decrease in average effective stress in the outer (Nb) phase with increasing aspect ratio (Table 3). In the elasto-plastic analysis, it is first observed that the accommodation energies are lowered when compared to the elastic case and this is due to plastic deformation, as has been shown analytically by Lee et al [23]. However, here the total accommodation energy increases with increase in the aspect ratio which is essentially due to a similar variation in the energy of the outer phase (Nb) with aspect ratio. Most of the accommodation energy of the outer phase (Nb) is plastic in nature. The increased plastic accommodation energy in the Nb matrix when it occurs as the outer phase is due to increased yielding of this phase with increase in aspect ratio due to the generation of additional shear stresses in this phase. This leads to the total accommodation energy increasing with increasing aspect ratio as plasticity

Table 5. Accommodation energies (Joules per mol Nb) stored in the matrix and the precipitate at 50% transformation for different aspect ratios of the precipitate, where the inner phase is NbH and outer phase is Nb.

			aspect ratio of the precipitate			
			1	2	3	4
elastic	inner phase	centre to surface forward	125	150	161	165
		surface to centre reverse	115	138	148	152
	outer phase	centre to surface: forward	916	832	789	771
		surface to centre: reverse	840	763	724	707
elasto-plastic	inner phase	centre to surface forward	0.2	0.5	0.8	1.2
		surface to centre reverse	7.4	9.5	11	12.5
	outer phase	centre to surface: forward	189	197	203	206
		surface to centre: reverse	124	123	126	127

determines the accommodation energies in the elasto-plastic case.

4.4.2 plane stress formulation

The thickness of the specimen used for the experimental investigation of reversible hydrogen transformations, for example by the pressure-composition-temperature (PCT) technique, is very small compared to its other dimensions. The transformation in such a system can be modelled as a plane stress problem, which reduces the complexity of the model while maintaining sufficient accuracy. The results obtained by the plane stress analysis of hydrogen transformation in the Nb-H system are presented below. Here the the precipitate is disk shaped. Eight-noded isoparametric elements have been used to model the system. The system is specified by a thickness of 1 μm and a cross sectional area of 7.8539×10^{-3} m^2. Due to symmetry only one quarter of the system has been considered, which is divided in to 20 layers each having 4 elements. The loading procedure is similar to that used in axisymmetric analysis, i.e. five incremental steps for each stage of transformation.

The system accommodation energy during the forward transformation progressing from centre of the system outwards is presented in Figure 33a. Note that the total energy of the system increases with an increase in the aspect ratio. The variation of accommodation energy with progress of transformation and the variation of energy with respect to aspect ratio are similar to the results obtained in elasto-plastic analysis of the axisymmetric ellipsoidal system. The strain energy at the end of

transformation in this case is smaller compared to the residual energy obtained by axisymmetric analysis.

Figure 33b depicts the variation of the accommodation energy during reverse hydrogen transformation through the centre to surface path. In the axisymmetric case, the precipitate was under hydrostatic stress for aspect ratio one, whereas here the precipitate has shear component even for aspect ratio one. Therefore, plastic deformation occurs in the precipitate for all the aspect ratio. The results shows that among the four aspect ratio considered, the maximum residual energy is obtained for aspect ratio 3. Apart from this the variation of the total energy with aspect ratio follows the same pattern as is obtained in axisymmetric analysis.

In the case of forward transformation through surface to centre path, the dependence of the accommodation energy on aspect ratio shows the same trend (Figure 34a) as that was obtained for an ellipsoidal precipitate. However, the matrix energy in this case will have plastic component for aspect ratio one since it is not under pure hydrostatic state of stress as in the case in axisymmetric analysis. For aspect ratio other than one, there is no significant change in the residual energy of the system with a change in aspect ratio. It is to be noted that most of the energy is accommodated in the matrix (Nb) as seen in Figure 35. The plastic and elastic components of the accommodation in the Nb matrix is provided in Figure 36 which shows that most of the energy in the Nb matrix is plastic in nature.

The total strain energy of the system during the reverse

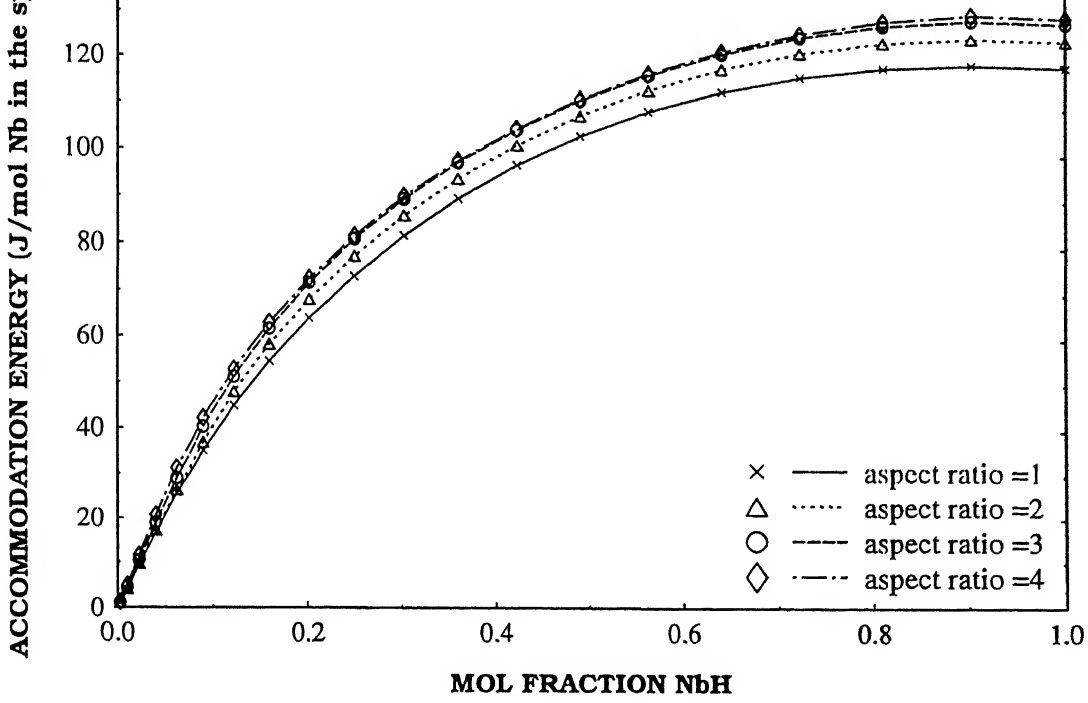

(a) forward

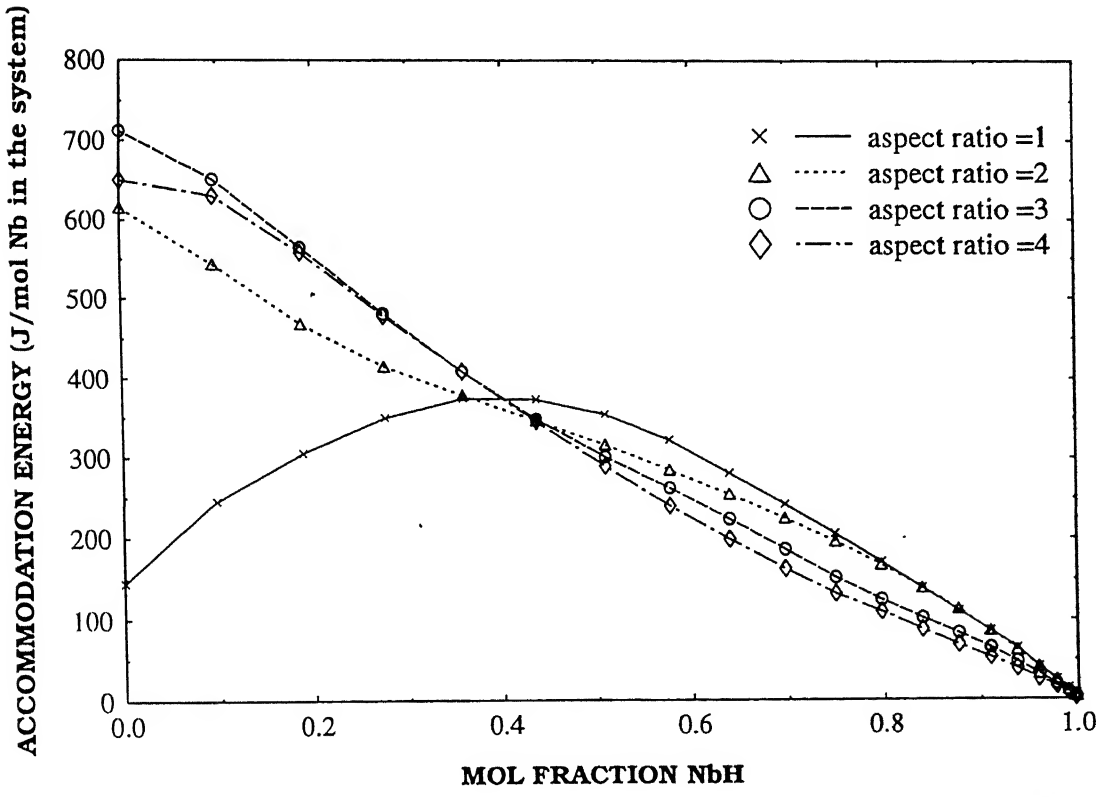

(b) reverse

Figure 33. Variation of system elasto-plastic accommodation energy during (a) forward and (b) reverse transformations through the centre to surface path for different aspect ratios of the precipitate using plane stress formulation.

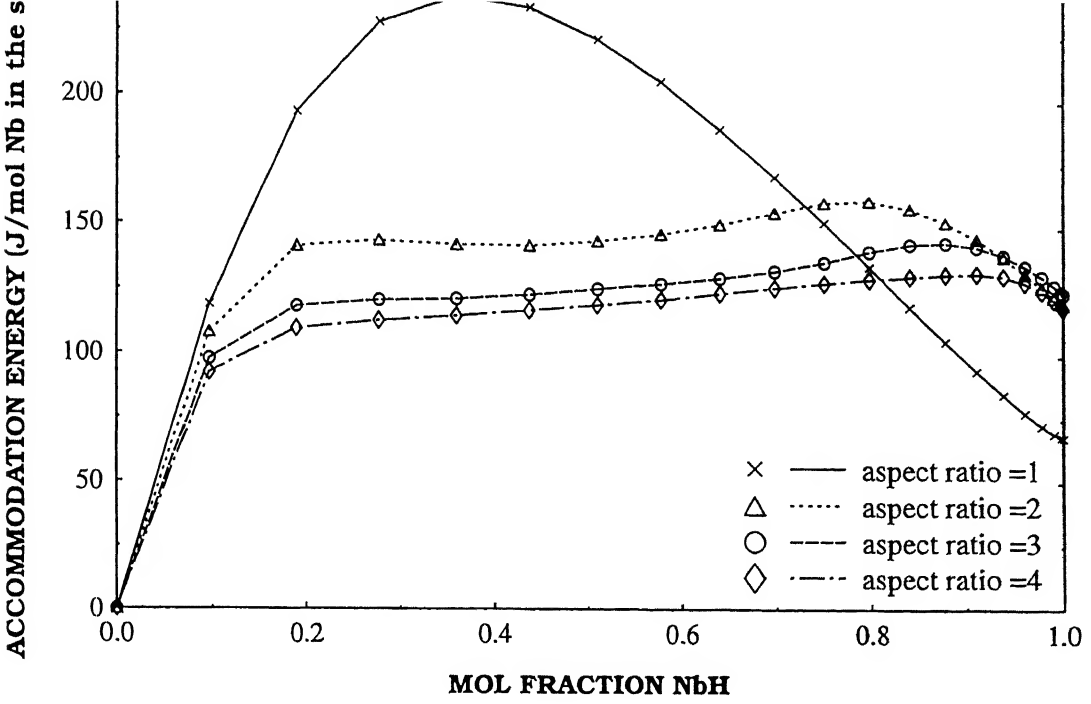

(a) forward

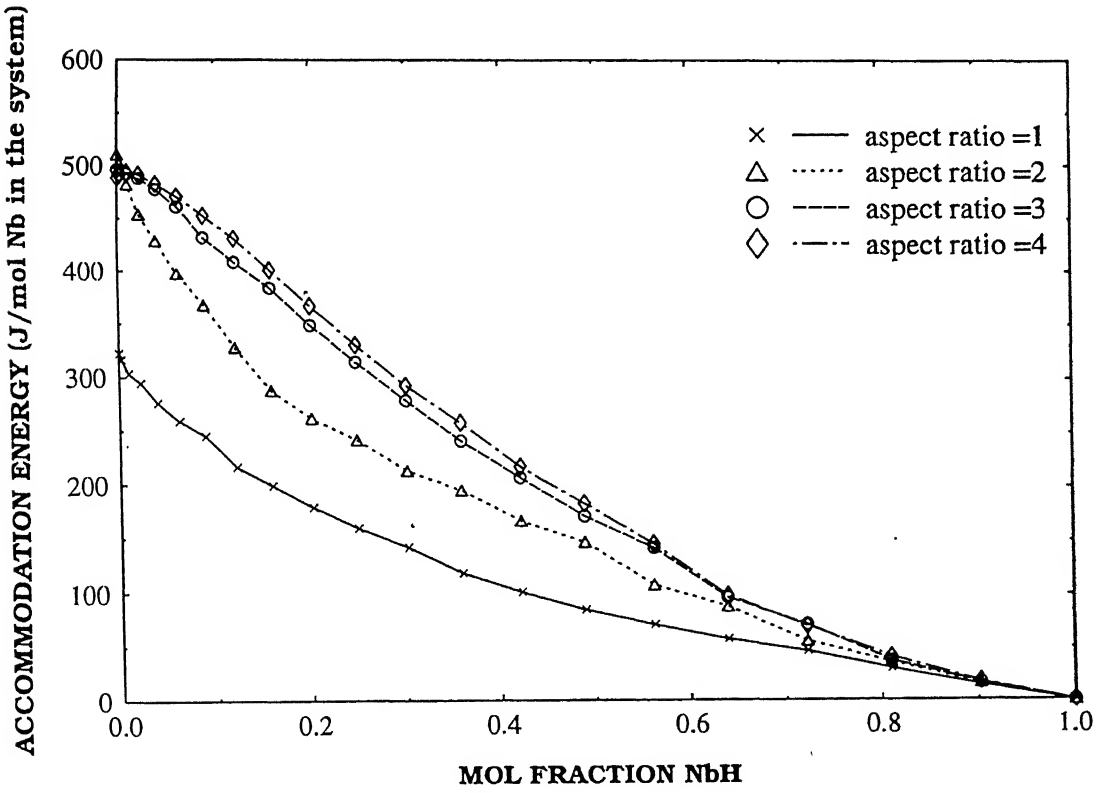

(b) reverse

Figure 34 Variation of system elasto-plastic accommodation energy during (a) forward and (b) reverse transformations through the surface centre path for different aspect ratios of the precipitate using plane stress formulation.

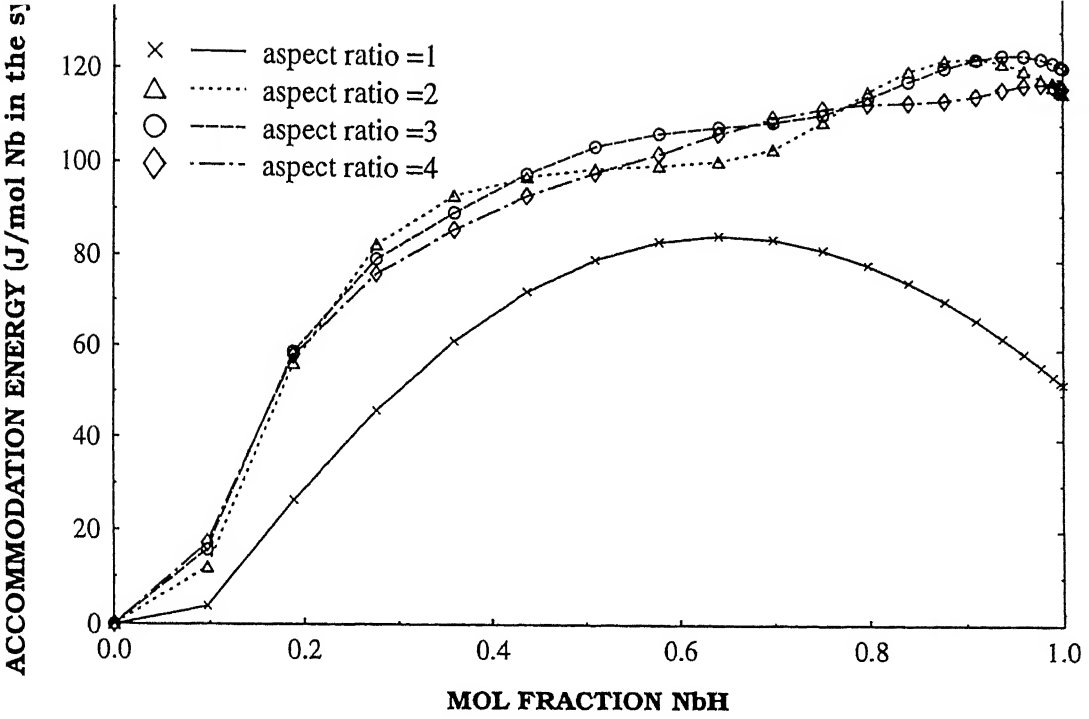

(a) matrix energy

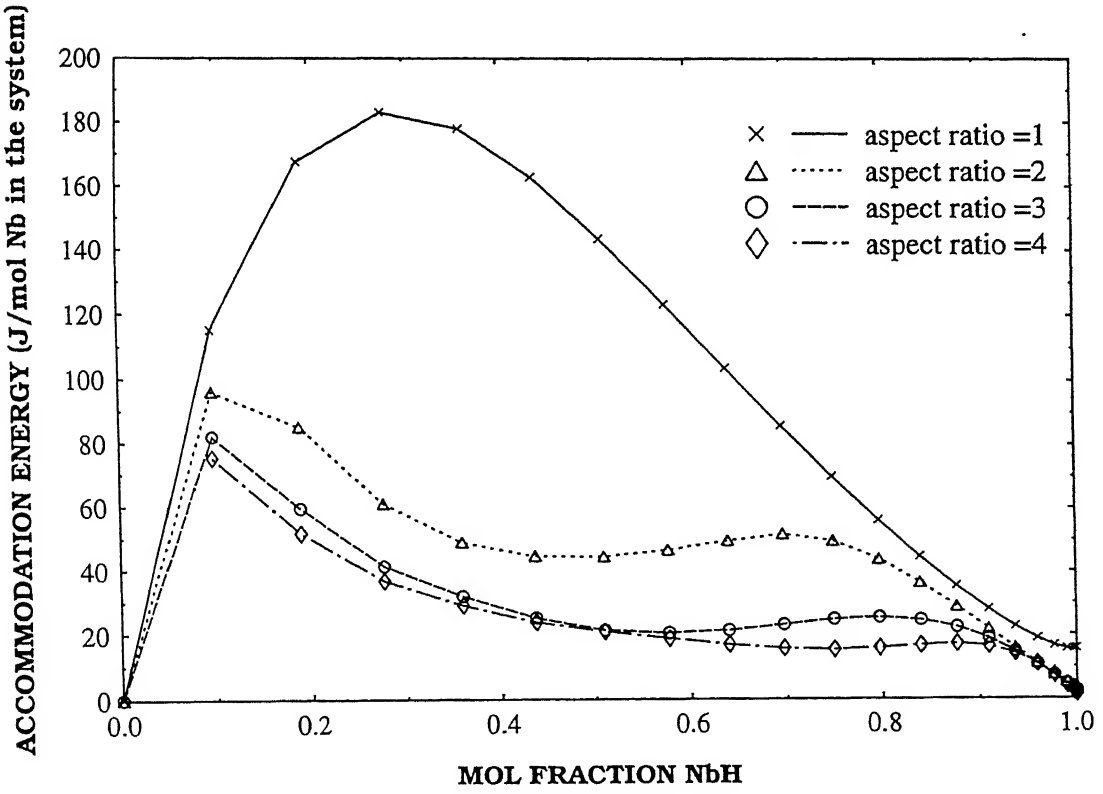

(b) precipitate energy

Figure 35. Variation of elasto-plastic accommodation energy stored in the (a) matrix and (b) precipitate during forward transformation through surface to centre path for different aspect ratios of the precipitate using plane stress formulation

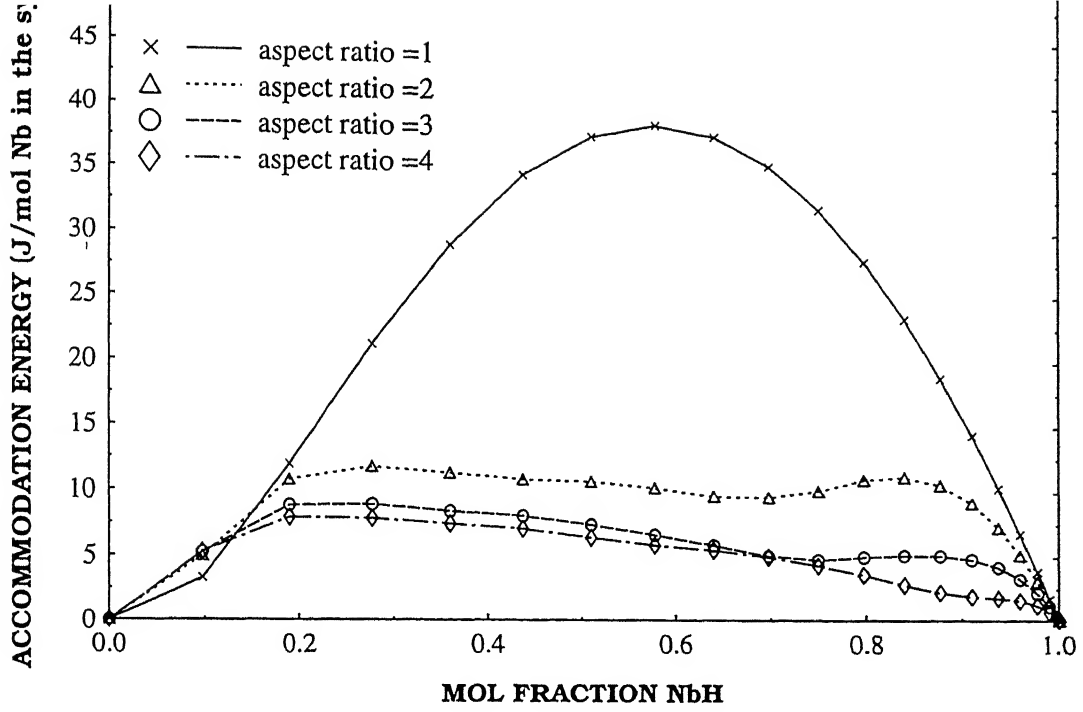

(a) elastic strain energy

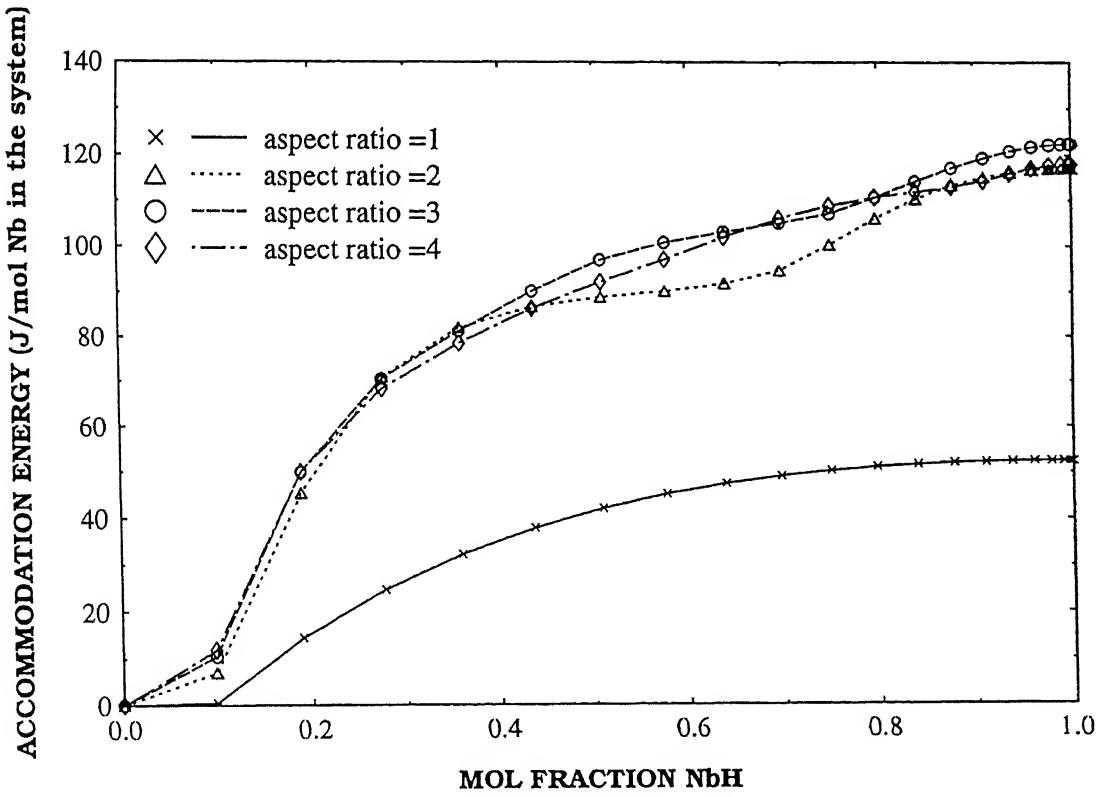

(b) plastic strain energy

Figure 36. Variation of (a) elastic and (b) plastic part of accommodation energy stored in the Nb matrix during forward transformation through the surface to centre path using plane stress formulation.

transformation by the surface to centre path increases with increase in aspect ratio at the initial stages of transformation (Figure 34b). However, at the end of transformation the strain energies are almost same for aspect ratio other than one which is in conformity with the results obtained in axisymmetric analysis.

CHAPTER 5
SUMMARY

5.1 CONCLUSIONS

The salient conclusions of the present finite element study are the following. The initial strain approach of the finite element method (FEM) has been successfully applied in order to evaluate the effect of precipitate aspect ratio on the accommodation energies during solid state hydrogen transformations in the Nb-H system. The transformation was modelled to occur from the surface of the system inwards and also from the centre of the system outwards. One of the main advantages of the FEM model is that finite systems can be modelled. The FEM method was utilized to evaluate the elastic and elasto-plastic accommodation energies during hydrogen transformations for the plane stress and axisymmetric conditions. The individual (elastic and plastic) energies stored in the matrix and precipitate phases can be evaluated by finite element analysis (FEA). The effect of the aspect ratio of the precipitate on the accommodation energy has been primarily addressed.

In the elastic FEA, it was observed that the accommodation energy of the system decreases as the aspect ratio of the precipitate increases, using both the plane stress and

axisymmetric formulations. This was found to be true for both the forward and reverse transformations by the center to surface and surface to centre transformation paths. In all these cases, the accommodation energy stored in the inner phase increases with increasing aspect ratio while the accommodation energy stored in the outer phase decreases with increasing aspect ratio. Therefore, the elastic analysis reveals that most of the energy is accommodated in the phase which surrounds the inner phase.

In the elasto-plastic FEA, the accommodation energies during the course of the transformation are generally lowered compared to that obtained by the elastic analysis. This is due to plastic deformation that occurs in the metallic Nb phase. Residual energies are present at the end of transformation which are essentially due to the irreversible plastic deformation that occurs during the transformation. Exception to the above are when the metallic phase is the inner phase having aspect ratio one in which case the metallic phase does not yield as the state of stress is purely hydrostatic. The accommodation energies at the end of transformation are higher in the case of the transformations in which the final phase is plastically deforming niobium compared to the transformations in which the final phase is niobium hydride. The accommodation energies generally increase with increasing aspect ratio for all the transformation paths considered.

The finite element model has also been applied to obtain

the elasto-plastic accommodation energies for hydrogen transformations in the Pd-H system. The nature of the results are similar to that obtained for the Nb-H system.

5.2 SCOPE FOR FUTURE STUDY

The following aspects could be considered in detail while applying the finite element method to evaluate accommodation energies during solid state transformations:

a) The model applied in the present thesis assumes a single precipitate growing in a single crystal. This could be extended to take into consideration multiple nucleation and growth events (i.e. interacting precipitates) and also a multigrained matrix. In this case, grain boundary effects would also have to be considered and suitably accounted for in the FEM model.

b) The transformation is assumed to progress through a pre-destined transformation path whereas the growth of the precipitate, in practice, would be governed by the stress state in the system, i.e. the precipitate would prefer to grow in the direction where the accommodation energy density is favorable. This should be incorporated into the model.

c) The transformations could be modelled in three dimensions by choosing suitable three dimensional elements (for example, brick or tetrahedral elements).

d) Several other shapes of the precipitate could be modelled by

the FEM technique.

e) It was implicitly assumed that the misfit strain was one third of the volumetric strain for the transformations considered in the present work. However, the misfit strains would be different in different crystallographic directions due to specific orientation relationships between the hydride and matrix. This could be easily incorporated into the present model (when applying for the Zr-H system) as only the input parameters have to be suitably modified.

REFERENCES

1. R. Balasubramaniam, *Acta Metall. Mater.*, **41**, 3341 (1993).
2. J. D. Eshelby, *Proc. R. Soc. London (A)*, **241**, 376 (1957).
3. A. G. Khachaturyan, *Theory of structural transformations in solids*, p. 202,230, John Wiley & Sons, USA, (1983).
4. T.B.Flanagan and J.D.Clewly, *J. less-common Metals* **83**, 127 (1982).
5. C.D.Cann, M.P.Puls, E.E.Saxton and W.G.Hutchings, *J. Nuclear Materials* **126**, 197 (1984).
6. M. A. Pick and R. Bausch, *J. Phys.F, Metal. Phys.*, **6**, 1751 (1976).
7. A. J. Maeland, J. Phys. Chem. **68**, 2197 (1964).
8. J. S. Bradbrook, G. W. Lorimer, and N. Ridley, *J. Nucl. Mater.* **42**, 172 (1972).
9. T. S. Liu and M. A. Steinburg, *Trans. Am. Soc. Metals*, **50**, 455(1958).
10. H.K.Birnbaum, *J. less-common metals* **104**, 31 (1984).
11. T.B.Flanagan, *J. less-common metals* **82**, 385 (1981).
12. S.Sen, R. Balasubramaniam and R. Sethuraman, *Int. J. Hydrogen Energy*, **20**, 567 (1995).
13. S.Sen, R. Balasubramaniam and R. Sethuraman, *Scripta Metall. Mater.*, **33**, 527 (1995).
14. S.Sen, R. Balasubramaniam and R. Sethuraman, *Acta Metall. Mater.*, **44**, 437 (1996).

15. Brian. W. Leitch and Manfred P. Puls, *Metall. Trans.*, **23A**, 797(1992).

16. R. W. Cahn and P. Haasen, *Physical metallurgy : Part 1 (3ed)*, p.484, Elsevier Science Publishing Co., USA (1983).

17. J. K. Lee, D. M. Barnett and H. I. Aaronson, *Metall. Trans.A* **8A**, 963 (1977).

18 A. G. Khachaturyan, *Sov. Phys. Solid State,* **8**, 2163 (1967).

19. S. L. Sass, T.Mura, and J. B. Cohen, *Phil. Mag.*, **16**, 679 (1967).

20. G. Faivre, *Phys. Status Solidi,* **35**, 249 (1969).

21. R. Sankaran and C. Laird, *J. Mech. Phys. Sol.*,**24**, 251 (1976).

22. L. K. Lee and W. C. Johnson, *Phys. Status Solidi,* **46**, 267 (1978).

23. J. K. Lee, Y. Y. Earmme, H. I. Aaranson and K. C. Russell, *Metall. Trans.A* 11A, 1837 (1980).

24. Y. Y. Earmme, W. C. Johnson and J. K. Lee, *Metall.Trans.A* 12A, 1521 (1981).

25. S. Qian and D. O. Northwood, *Int. Jl. Hydrogen Energy,* **13**, 25 (1988).

26. B.Lambert and S. F. Gates, *Proc. R. Soc. A*, **100**, 456 (1925).

27. A. R. Ubbelohde, *Proc. R. Soc. A,* **159**, 295(1937).

28. N.A. Scholtus and W. K. Hall, *J. Chem. Phys.* **39**, 868 (1963).

29. F. A. Kuijpers and H. H. Van Mal, *J. Less-common Metals* **23**, 395(1991).

30. H. K. Birnbaum, M. L. Grossbeck and M. Amano, *J. Less Common Metals* **49**, 357 (1976).

31. T. B. Flanagan, B. S. Bowerman and G.E.Beihl, *Scripta Metall.*, **1414**, 443 (1980).

32. O. C. Zienkiewicz, The Finite Element Method (3 ed), p.24, Tata McGraw Hill, New Delhi, India (1979).

33. D. R. J. Owen and E. Hinton, Finite Elements in Plasticity, p.226, Pineridge Press, Swansea, UK (1980).

34. Tai-Ran Hsu, *The Finite Element Method in Thermomechanics,* Allen and Unwin, Boston, USA (1986).

35. H. E. Boyer, ASM Atlas of Stress-Strain Curves, p. 571, ASM International, Metals Park, USA (1987)

36. S.Sen, R. Balasubramanium and R. Sethuraman, *Trans. Ind. Inst. Met.* **47**, 205 (1994).

37. T. Mura, *Micromechanics of Defects in Solids*, Martinus Nijhoff Publishers, The Nehterlands (1982), Chapter 2.

38. B. J. Makenas and H. K. Birnbaum, *Acta Metall. Mater.*, **28**, 979 (1980).

39. T. Schober and H. Wenzl, *Hydogen in Metals II,* eds. G. Alefeld and J. Volkl, p 11, Springer, Berlin (1978).

APPENDIX A

FEM RESULTS FOR THE Pd-H SYSTEM

Palladium/hydrogen system has been extensively experimentally investigated for the hysteresis behaviour [1]. In terms of practical use, hydrogen is most often associated with palladium because of the wide spread use of the metal as a membrane which permits a rapid penetration of hydrogen and provides a convenient method of separating it out of gaseous mixtures. From an academic stand point, interest in the system has centered primarily around the attempts to provide theoretical explanations in the form of pressure-composition relationship which shows the existence of a hysteresis between absorption and desorption p-c relationship [1]. This appendix presents the elasto-plastic accommodation energies obtained for the hydrogen transformations in palladium-hydrogen system evaluated using the Finite element method.

The FEM model of hydrogen transformation described in chapter 3 is used to model the α-β transformation in the Pd-H system. The mechanical and physical properties of palladium and palladium hydride which were used for the calculation are given in Table A1. The work hardening parameter for the Pd was obtained from the stress-strain curve presented in Ref. [4]. The hardening is almost linear in plastic range. The work hardening parameter H' is obtained from the relation $1 / E_T = 1/ E + 1 / H'$. The misfit strain for the $\alpha \rightarrow \beta$ transformation is 0.03506 and that for $\beta \rightarrow \alpha$ transformation is -0.0317 [2].elasto-plastic accommodation

energies during hydrogen transformation were evaluated assuming the precipitate to be a prolate spheroid. The domain was divided in to 80 isoparametric eight-noded elements. The transformation is modeled to take place in 20 steps. All the transformation paths considered in the case of Nb-H system which are described in chapter 4 were modelled here also. Palladium hydride is assumed to be elastic in all the cases.

The results of the finite element analyses are shown in Figure A1 through Figure A6. The figures show the variation of the accommodation energies as function of the fraction transformed for different aspect ratios of the precipitate. Figure A1 shows the system accommodation energy for (a) forward and (b) reverse transformation through the centre to surface path, while Figure A2 shows the accommodation energies stored in the matrix and the precipitate for the forward transformation and Figure A3 shows the accommodation energies stored in the matrix and precipitate for reverse transformation. The accommodation energies in the case of surface to centre path are shown in Figures A4 through A6. The variation of the accommodation energy with fraction transformed and with aspect ratio of the precipitate are same as that has been previously obtained in the case of Nb-H system, which were presented in chapter 4. However the numerical values of the energies are smaller due to lower value of misfit strain and also due to the difference in the physical and mechanical properties of the two systems.

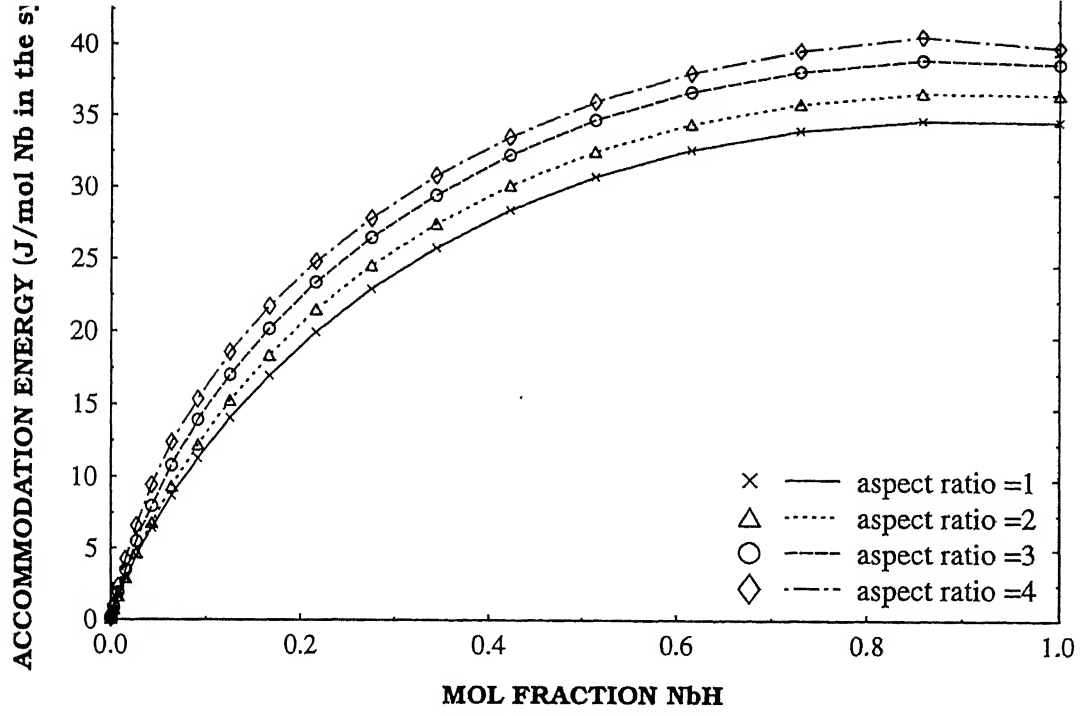

(a) forward transformation

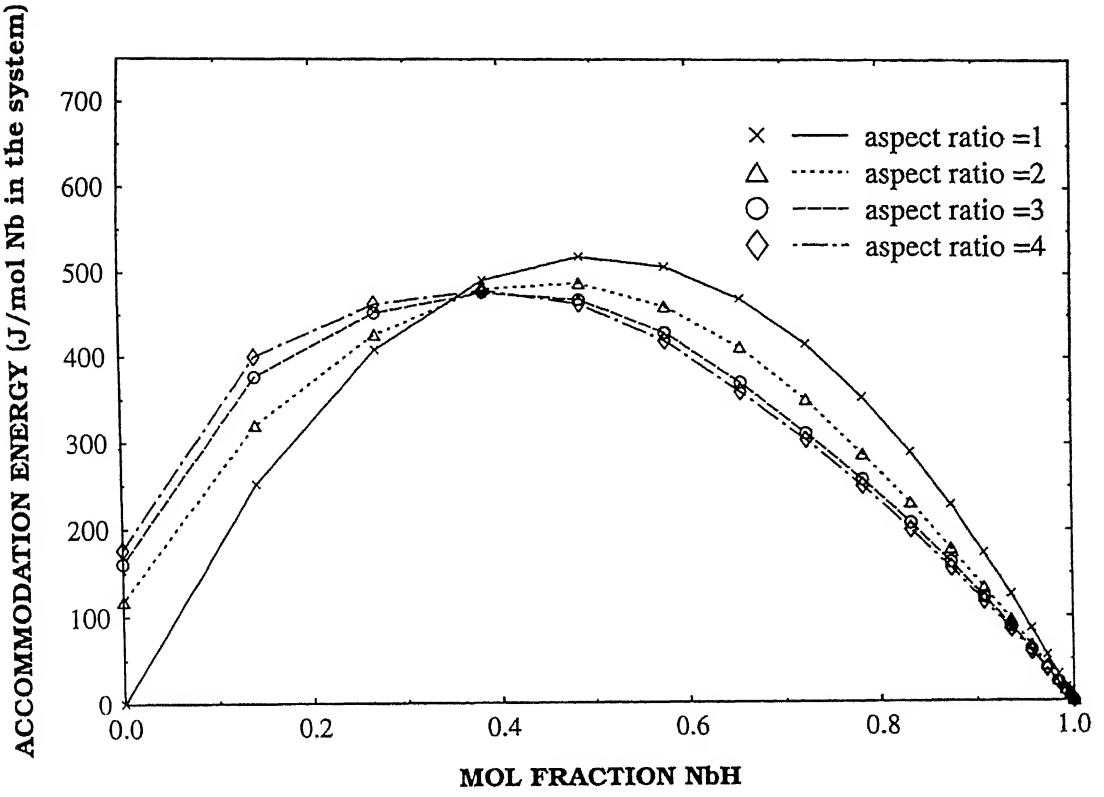

(b) reverse transformation

Figure A1. Variation of system elasto-plastic accommodation energy during (a) forward and (b) reverse transformations through centre to surface path for different aspect ratios of the precipitate using axisymmetric formulation.

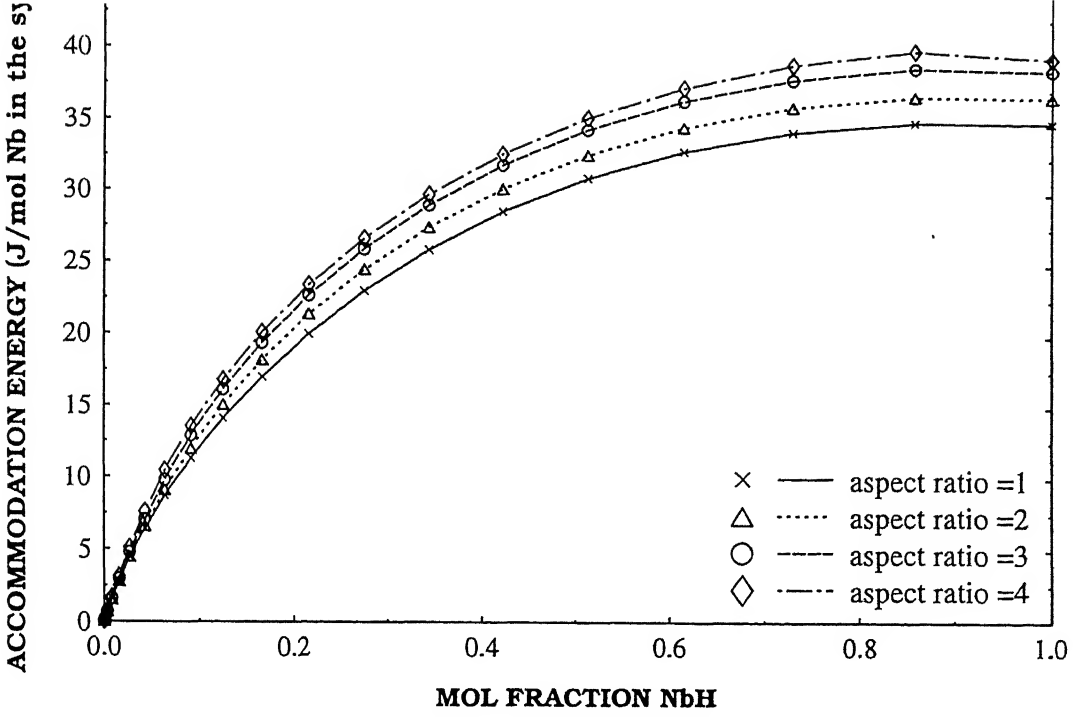

(a) matrix energy

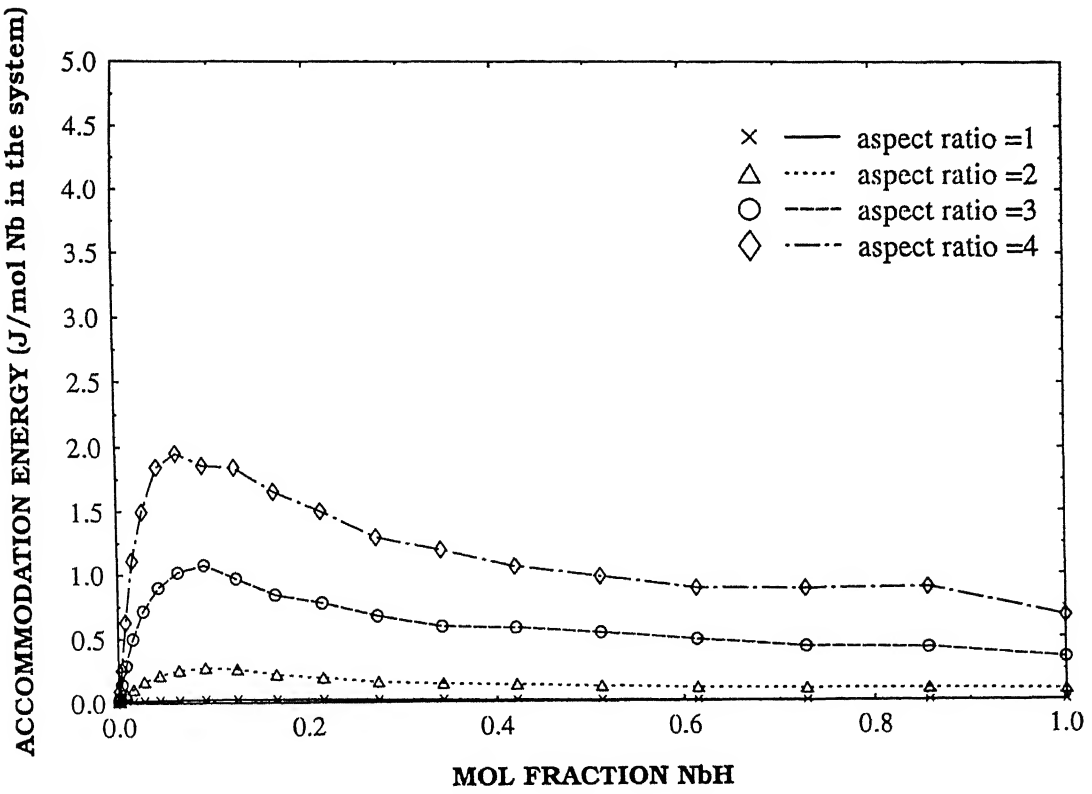

(b) precipitate energy

Figure A2. Variation of elasto-plastic accommodation energy stored in the (a) matrix and (b) precipitate during forward transformation through centre to surface path for different aspect ratios of the precipitate using axisymmetric formulation.

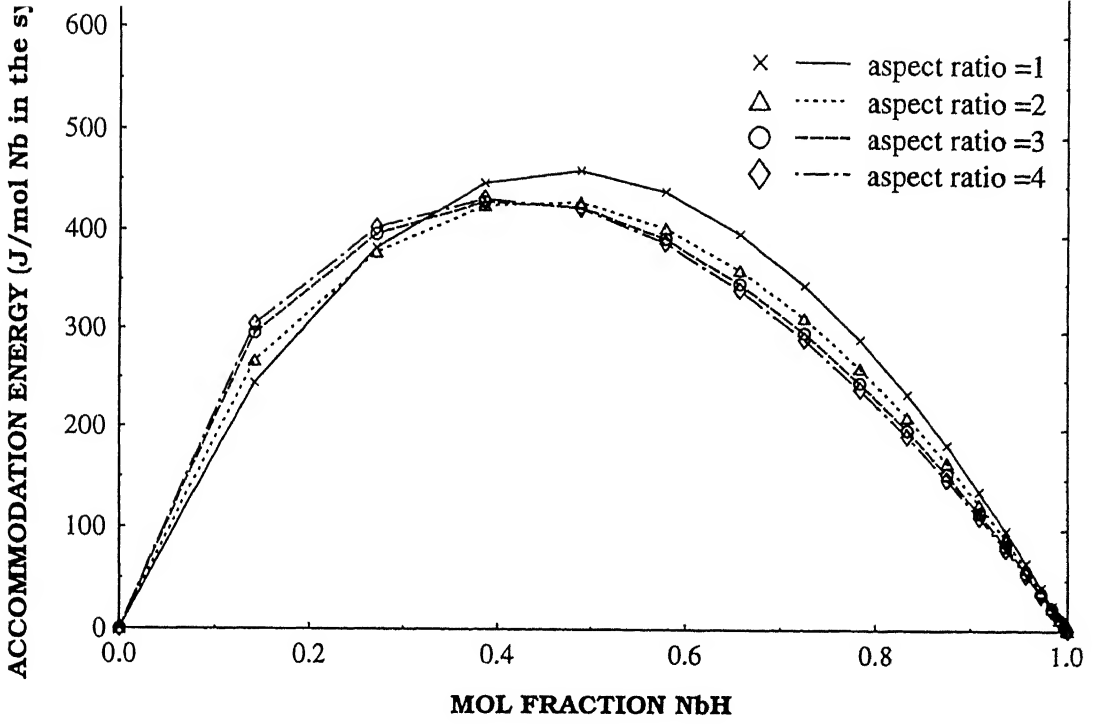

(a) matrix energy

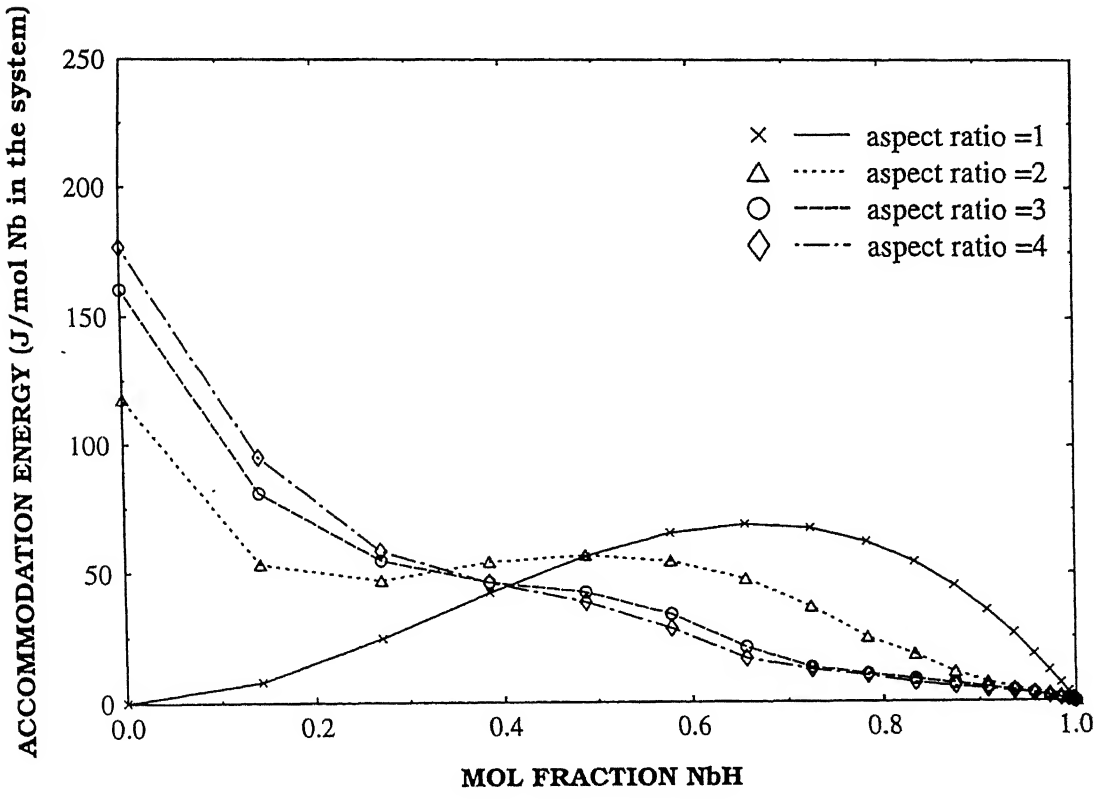

(b) precipitate energy

Figure.A3 Variation of elasto-plastic accommodation energy stored in the (a) matrix and (b) precipitate during reverse transformation through the centre to surface path for different aspect ratios of precipitate using axisymmetric formulation

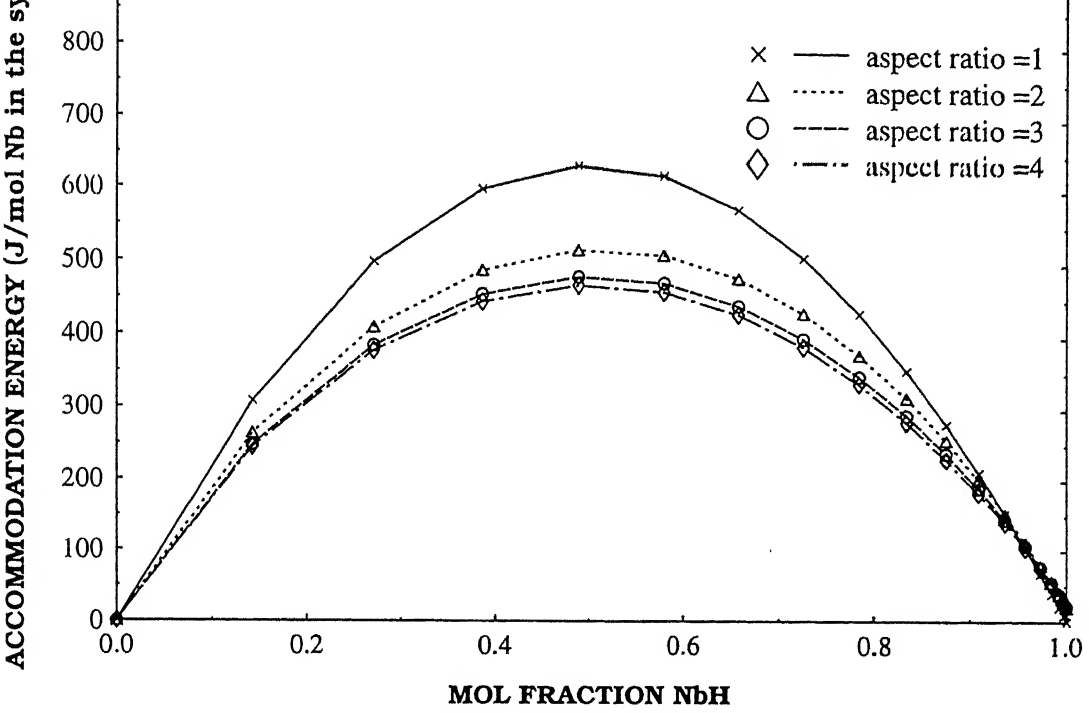

(a) forward transformation

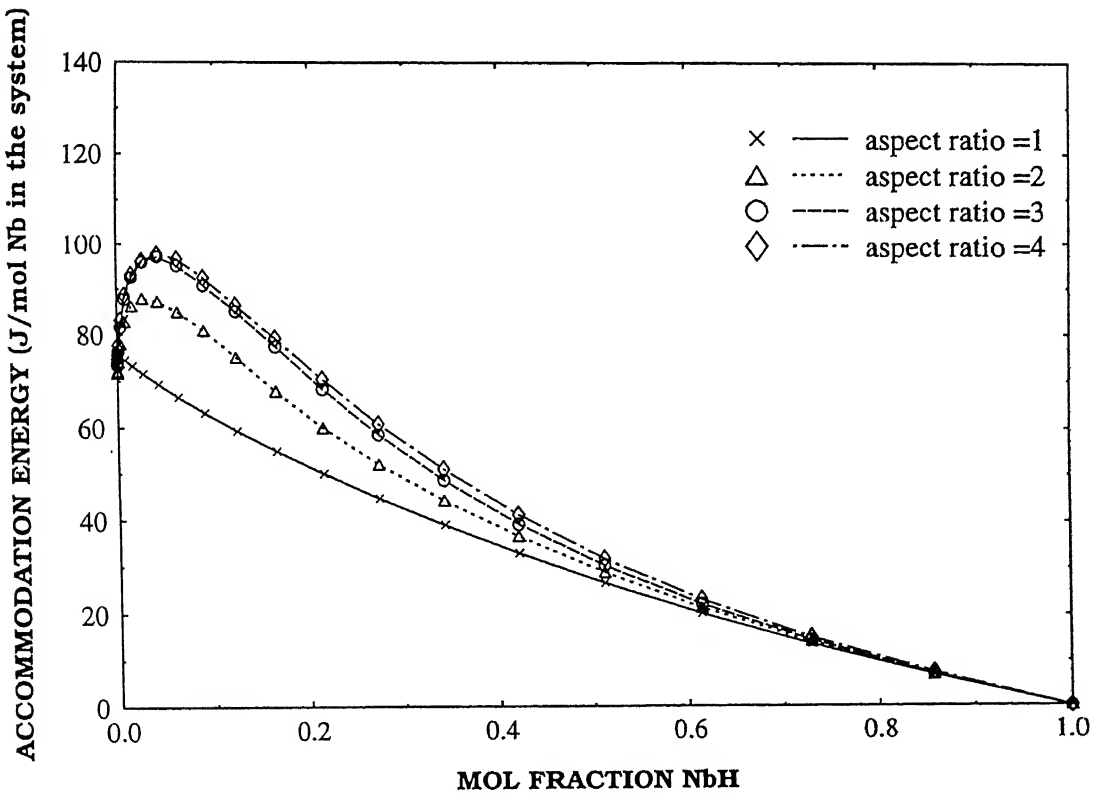

(b) reverse transformation

Figure A4. Variation of system elasto-plastic accommodation energy during (a) forward and (b) reverse transformations through surface to centre path for different aspect ratios of the precipitate using axisymmetric formulation.

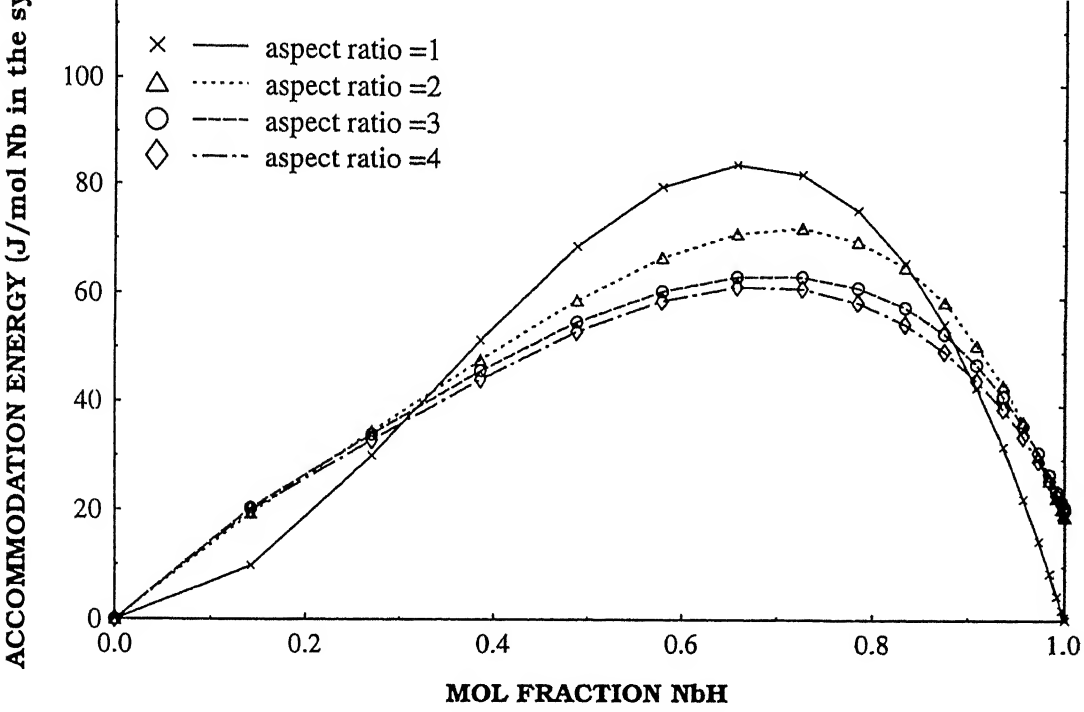

(a) matrix energy

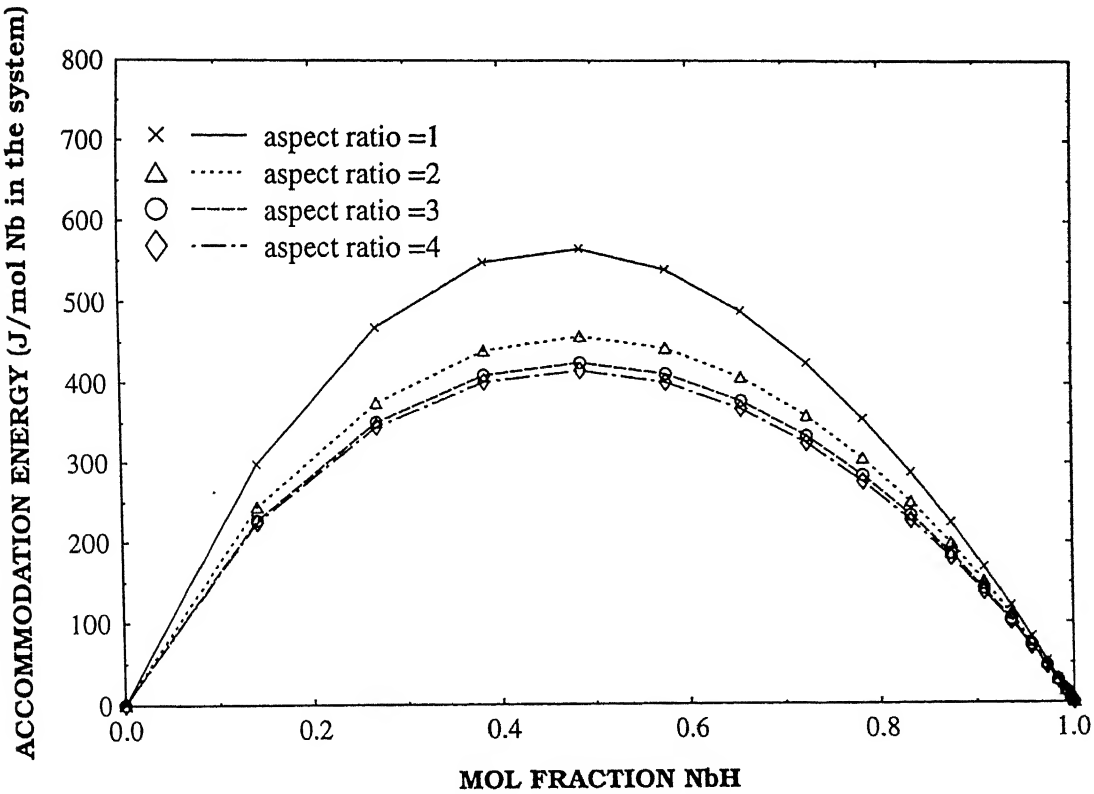

(b) precipitate energy

Figure A5. Variation of elasto-plastic accommodation energy stored in the (a) matrix and (b) precipitate during forward transformation through surface to centre path for different aspect ratios of the precipitate using axisymmetric formulation

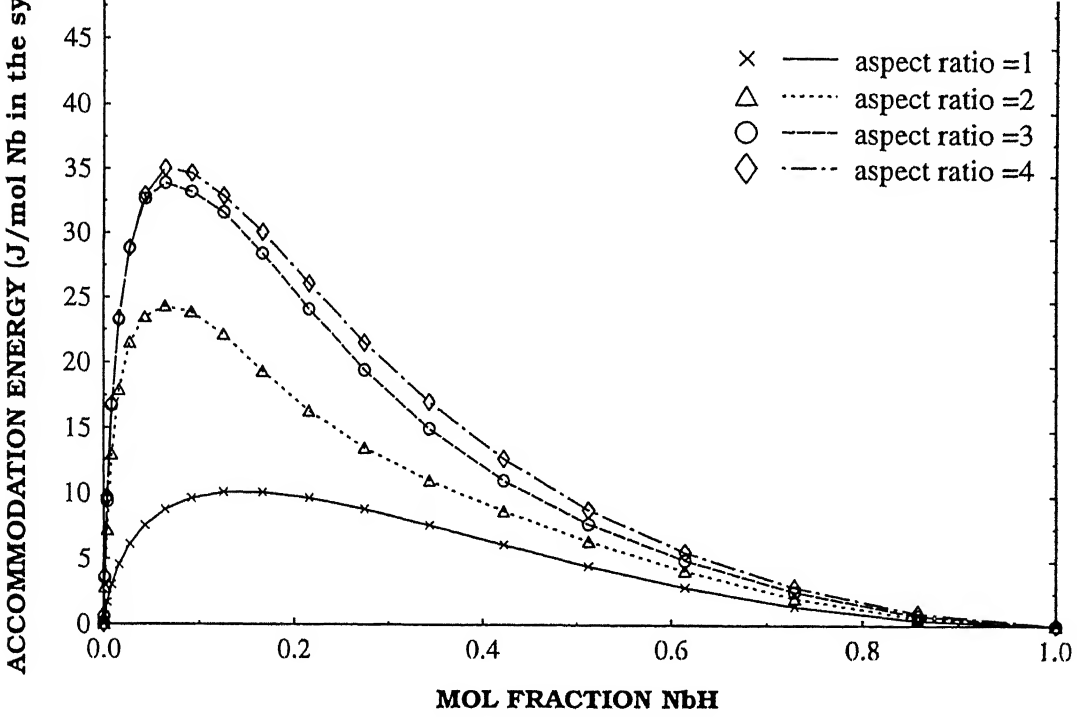

(a) matrix energy

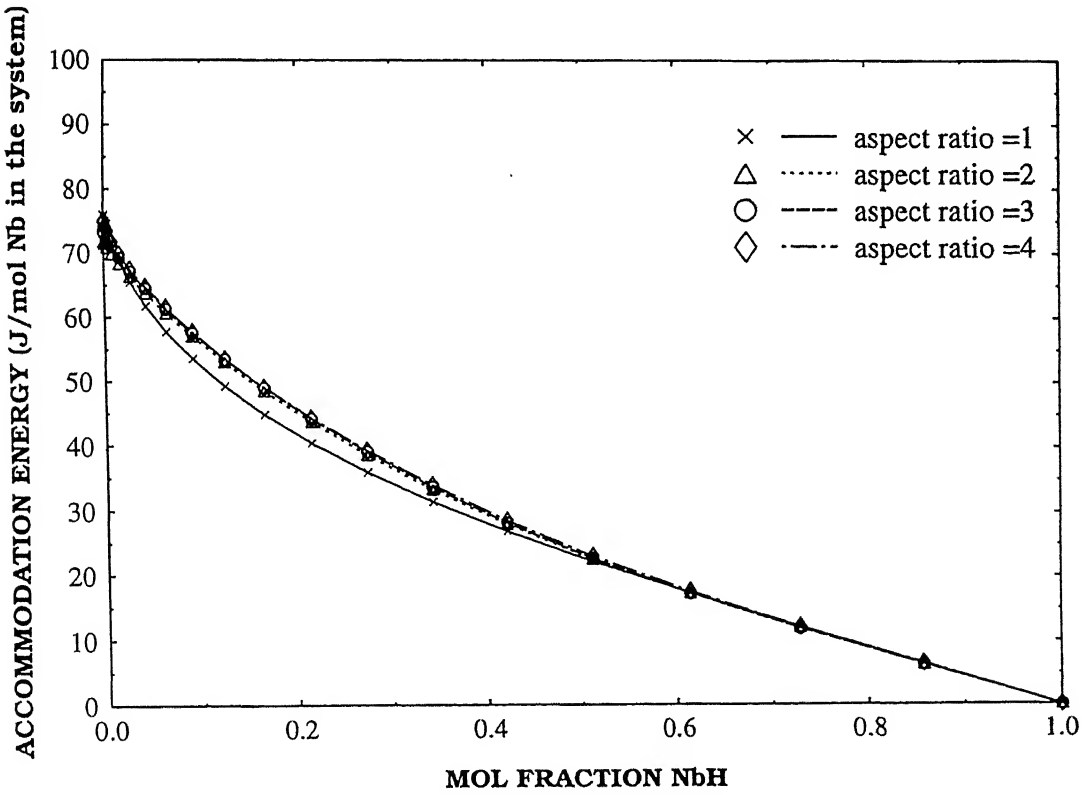

(b) precipitate energy

Figure.A6 Variation of elasto-plastic accommodation energy stored in the (a) matrix and (b) precipitate during reverse transformation through surface to centre path for different aspect ratios of the precipitate using axisymmetric formulation

Table.A1 Physical and mechanical properties of Pd and PdH at room temperature. Reference source is also indicated.

Property	Pd	PdH
Young's Modulus(E) (N/m^2)	$1.25*10^{11}$ [3]	$1.15*10^{11}$ [3]
Poisson's ratio(ν)	0.39 [3]	0.39 [3]
Yield stress (σ_y) (N/m^2)	$0.52*10^{8}$ [5]	$0.52*10^{100}$#
Crystal structure	FCC [2]	FCC [2]
Lattice parameter (Å)	3.894 [2]	4.026 [2]
Work hardening parameter (H') (N/m^2)	$0.12*10^{8}$ [4]	$0.12*10^{100}$#
Molar volume ($\overline{V}$) (m^3mol^{-1})	$8.89079*10^{-6}$ [2]	$9.82594*10^{-6}$ [2]

Value assumed to prevent yielding in PdH

REFERENCES

1. F. A. Lewis, *The Palladium Hydrogen System,* Academic press, New York (1967).
2. W. M. Mueller, J.P. Blackledge and G. P. Libowitz (*Ed*), *Metal Hydrides*, p. 640, Academic press, New York, USA (1968).
3. *Metals Handbook, Vol.* 2 (*9th ed*), p. 699 (1979).
4. D.K.Hsu and R. G. Leisure, *Elastic constants of palladium and β phase palladium hydride between* 4 *and* 300 *K, Physical Review B*, **20,** 1339 (1979).
5. G. W. Nieman, J. R. Weertman and R. W. Siegel, *Tensile strength and creep properties of nanocrystalline palladium, Scripta Metall.*, **24**, 145 (1990).